LONG-TERM STABILITY ANALYSIS OF OPEN PIT MINE SLOPES: A CASE STUDY OF WEARNE MINES IN LIMPOPO

by

RINAE NETSHITHUTHUNI

submitted in accordance with the requirements for
the degree of

MASTER OF ENGINEERING

in the subject

MINING ENGINEERING (ROCK ENGINEERING)

at the

UNIVERSITY OF SOUTH AFRICA

SUPERVISOR: Prof F Mulenga

CO-SUPERVISOR: Prof F Sengani (UL)

(February 2024)

DECLARATION

Name: Rinae Netshithuthuni

Student number: 14803003

Degree: MASTER OF ENGINEERING

Exact wording of the title of the dissertation as appearing on the electronic copy submitted for examination:

Long-term stability analysis of open pit mine slopes: A case study of Wearne mines in Limpopo

I declare that the above dissertation is my own work and that all the sources that I have used or quoted have been indicated and acknowledged by means of complete references.

I further declare that I submitted the dissertation to originality checking software and that it falls within the accepted requirements for originality.

I further declare that I have not previously submitted this work, or part of it, for examination at Unisa for another qualification or at any other higher education institution.

23 February 2024

SIGNATURE DATE

DEDICATION

This study is dedicated primarily to my parents Mr Naledzani Calvin Netshithuthuni and Mrs Kutama Joyce Netshithuthuni who have been nothing short of amazing in terms of their support including emotional and financial support.

I would also like to dedicate this work to my siblings Unarine Netshithuthuni, Thalukanyo Netshithuthuni and Mufhatutshedzwa Netshithuthuni. May this motivate them enough to see that the only limits in life are the ones we set for ourselves.

Acknowledgements

Firstly, I would like to thank the almighty God for his love, protection and wisdom. He kept me going and made it possible for me to study and produce this work.

Special thanks go to the Department of Mining Engineering at the University of South Africa (UNISA) for awarding me an opportunity to pursue Master's degree.

I would also like to express my deepest gratitude to my supervisor Prof Francois Mulenga and my co-supervisor Prof Fhatuwani Sengani. Their guidance, supervision and mentorship are excellent and unmatched. All their inputs made the study interesting.

My family is highly appreciated of their support. My Master's colleagues are also appreciated for their critics during the proposal stage of the study.

Lastly, I would like to give unending thanks to Vhuhwavho Pertunia Mudau, Keabetswe Mmolotsi and Vhutali Carol Netshilaphala for their constant support, motivation, critics and advice throughout.

Abstract

The main objective of the study was to conduct a long-term stability analysis of the slope, which due to blasting and continuous mining activity may deteriorate in its strength and since there is very little slope stability monitoring done, the analysis is warranted. Several methods were applied to achieve the objectives. These methods include Kinematic analysis, Limit equilibrium and Numerical modelling.

The kinematic analysis method made use of the discontinuity orientation and the slope orientation to determine the probability of different types of failures occurring. These failures include planar, wedge and toppling. Limit equilibrium method was used to determine the Factor of safety (FoS) of the slope by analysing the driving forces and the resisting forces of the slope. OPTUM G2 which is a numerical method was then used to simulate the failure of the slope in the presence of different length or depths of discontinuities. Lastly the ROCFALL which is also a numerical model was also used to determine the extent at which the rock will travel down the slope in case of failure.

The results produced by the kinematic analysis showed that the slopes are most likely to experience toppling failure more than planar and wedge failures. The Limit equilibrium results on the other hand showed that the slopes were stable based on its FoS value. OPTUM G2 proved that the increase in the length of discontinuities reduces the strength of the slope. Lastly, the ROCFALL models showed that the slopes geometries are well on balance and the presence of safety berms will prevent the rock rolling to the lower benches.

Keywords: Slope stability; Kinematic analysis; Limit Equilibrium; Numerical modelling; Factor of Safety; Strength Reduction Factor

Table of contents

List of figures

List of tables

List of abbreviations

2D	Two dimensions
3D	Three dimensions
BRM	Bishop’s Rigorous Method
BSM	Bishop’s Simplified Method
CRSP	Colorado Rockfall simulation program
CSIR	Council of Scientific and Industrial Research
DEM	Discrete Element Method
FDM	Finite Difference Method
FEA	Finite Element Analysis
FEM	Finite Element Method
FoS	Factor of Safety
GSI	Geological Strength Index
ISRM	International Society for Rock Mechanics
km	Kilometre
LEM	Limit Equilibrium Method
MPa	Megapascal
NO.	Number
RMR	Rock Mass Rating
RSR	Rock Structure Rating
RQD	Rock Quality Designation
SS	Shear Stress
SRF	Strength Reduction Factor
TBM	Tunnel Boring Machine
UCS	Uniaxial Compressive Strength

List of symbols

°	Degree
%	Percent
>	Greater than
<	Less than
m^3	Cubic meter
N	Newton

Chapter 1: Introduction

1.1 Background of the study

Throughout the course of an open-pit mining operation, slope stability is a critical component (Suman, 2015; Kumar and Parkash, 2015; Bye and Bel, 2001; He et al., 2008; Moses et al., 2020). Slope stability plays a crucial role in ensuring safe access to the resources and reserves of an open pit mine. One could contend that slope stability analysis is an essential component of open-pit mining. Over the past decades, various methods have been proposed to improve the understanding of slope stability (Jin et al., 2023).

Most of the time, the analysis of the stability of a slope or that of any other surface excavation depends on mathematical formulations that represent the geological circumstances and the mechanical properties of the soil and rock formations (Bednarczyk, 2010). Depending on the method chosen (i.e., either traditional or sophisticated), the evaluation may seek to pinpoint areas of the slope that are unstable. The evaluation may also look into possible failure mechanisms or gauge how sensitive the slope is to various triggering factors. Conducting assessments is also necessary to evaluate the effectiveness of various stabilization and support strategies. Above all, slope stability analysis can be utilized to create slopes that are best for economy, safety, and dependability (Moses et al., 2020).

Slope instability continues to be a significant problem for both small and large mining operations, even with the advances in computer-based slope stability analysis (Rocscience, 2021; Llano-Serna et al., 2016). Read and Stacey (2010) also emphasized that the impact of in-situ stresses may need to be taken into consideration when surface mining operations grow larger and deeper.

In addition to this, slopes are said to have an additional weight in them during the rainy times (Hamakareem, 2019). The amount of water in the soil reduces the cohesion which further causes expansion of the rock cracks.

The pore water pressure increases which in turn increases the forces acting on the rock medium. The compounding effects of all these internal phenomena is slope instability and ultimately slope failure. Much attention is therefore to be paid to better describing slope stability and failure. This is especially true because of the proliferation of surface mining operations as the demand for mineral resources increases to support the world's booming population.

There are many tools and methods available today for analysing the slope stability of rock and soil. Eberhardt (2003) states that "these tools and techniques range from the simple planar failure limit equilibrium and infinite slope techniques to sophisticated coupled finite/distinct-element codes." Even with all these advancements, open-pit mines continue to frequently struggle with slope instability. With this in mind, it is suggested that the current study aid in the creation of instruments for the long-term stability analysis of open-pit mines.

1.2 Problem statement

Slope instability remains one of the issues of great concern since it has detrimental effects. This is because slope failure can lead to damage of infrastructure, machinery, casualties and delays in production amongst others. Xiong and Huang (2022) reported that the evaluation of the slope should be treated as a time dependent aspect. This is because over time, the conditions of the slope changes. This is a result of several aspects such as external environmental excitation and internal geotechnical deterioration.

WG Wearne have been operated with the unspoken and undocumented understanding that the rock being mined is strong and assumed that it translates to the overall slope stability. As such little research and constant monitoring of the slopes has been done to understand the general stability of the mine slopes and any possibilities of failures that might occur. Authors such as Chen et al. (2023) believe that it is important for a mine to establish a scientific slope stability analysis for better slope failure prevention.

The continuous drilling and blasting and overall operation as part of the daily activities are contributing towards the disintegrating and fracturing of the rock mass. Since the mine is still in operation, the rocks and the entire slope continue to weaken and compromise the stability of the slope, hence the need to conduct a long-term analysis of the pit. Yand (2005) is of a view that stability problems can be detected and addressed before slope failure occurs. However, for this task to be successful, several disciplines of Science and Engineering have to be brought together in order to understand the mechanisms associated with slope instability.

In recent years, there have been major technological advances that have been applied successfully to the analysis and monitoring of surface slopes. Some, if not most, of these technologies have not been sufficiently applied in the South African context (Bye and Bell, 2001; Wines, 2016; Helsdingen, 2017; Moses et al., 2020; Zondo, 2023).

This is because slope stability analysis does not to end at determining the probability and type of failure to be expected. Moloi and Zvarivadza (2016) argue that it should extend to determining the rockfall control when failure occurs and, better still, to preventing disaster by putting appropriate management methods in place (Zhang et al., 2021). This is only possible when the probability and types of failures can be estimated for the pit under consideration. The problem is that a single method cannot provide a full analysis and description of the rock mass. It is anticipated that this study will reveal some of the factors and properties that will determine the stability of the slope in a long run.

1.3 Research aims and objectives

The aim of this research study is to analyse the long-term stability of pits and their slope due to drilling and blasting operations. Multiple methods from the conventional ones to the more advanced numerical methods are applied to the Wearne open-pit mines as a case study.

The following are specific objectives set out for the research:

- To identify the factors and types of failures associated with slope instability recorded at Wearne open-pit mines.
- To develop a predictive model of slope behaviour at the Wearne open-pit mine allowing for the properties of discontinuities inherent to the rock mass.
- To classify the stability of the slopes based on integrated approaches of Kinematic, Limit Equilibrium, Numerical modelling and provide recommendations with respect to each slope.

The methods selected for this study are anticipated to determine the overall stability of the slopes and through the use of numerical models, a quantified rating can be given, and the stability of the slopes can be extrapolated from this information together with the traditional methods.

1.4 Significance of the study

It is known that the safety of employees is a top priority in the mining industry. Section 24 of the Mine Health and Safety Act (Act no. 29 of 1996) highlights this fact clearly and states that every employee should be familiar with the work-related hazards and risks and the measures that must be taken to eliminate, control and minimize those hazards and risks. This study makes some important contributions to the mine. This is because it provides the factors that may lead to failure along with the probability of failure.

The current study is also anticipated to approach the given problem from a more advanced angle. The advanced angle includes the use of conventional rock mass classification, kinematic analysis, limit equilibrium and numerical simulations. This is because the conventional rock mass classification has limitations which prohibits it from quantifying the probability of failure and the types of failures associated with the slope. This study integrate different methods in order to determine the probability of failure by providing the Factor of Safety (FoS) of the slope through limit

equilibrium, possible modes of failures and the probability of those failures occurring by making use of kinematic analysis. In addition to the prediction of probability of failure, the study goes further to determine and predict the rockfall trajectories and the location where the rock falls may end up.

Furthermore, the numerical methods are said to be flexible. They can allow multiple modelling options such as using different conditions of the slope and rocks to better understand and predict the behaviour of the slope.

1.5 Location of the study area

The study area is located approximately 7km west of Makhado (Louis Trichardt) town. The study area is an open pit quarry mine owned by WG Wearne mines Limited (Figure 1.1).

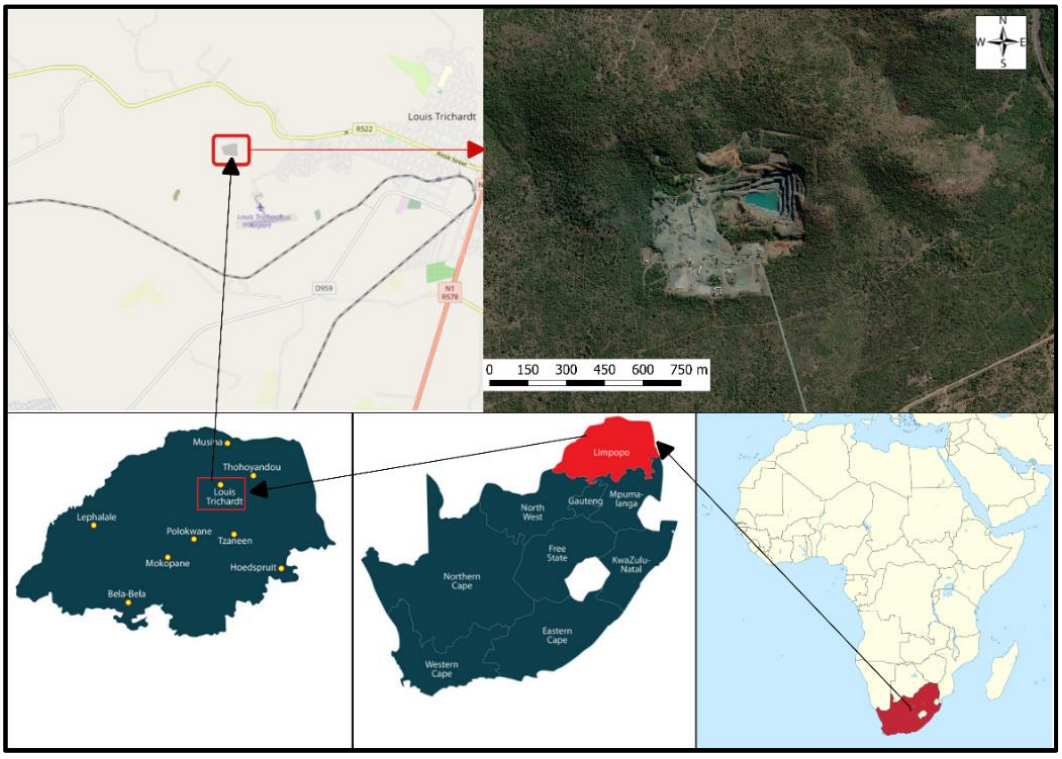

Figure 1.1: The location of WG Wearne open pit mine within South Africa and the province.

The company owns three mining sites in the Limpopo province, with their locations in Tzaneen, Polokwane, and Louis Trichardt. This study focuses

on the Louis Trichardt open pit mine as a case study. The mine is located in the Sibasa formation of the rugged Soutpansberg group. The Sibasa formation comprises the a sequence of cyclically erupted basalts. They are generally dark green in colour, massive and epidotised, but are speckled white in frequently developed amygdoloidal zones.

1.6 Structure of the dissertation

The dissertation is divided into six chapters.

Chapter 1 introduces the background and need for the research study. The problem statement was also discussed while the research objectives were formulated in line with the identified research problem.

Chapter 2 provides a comprehensive review of the parameters that affect slope stability, the methods of collecting data and the analytical method related to slope stability. The case studies in relation to the above-mentioned parameters and methods are also presented in this chapter.

Chapter 3 presents in detail how the Geotechnical data was collected as well as how all the simulation scenarios were carried out. The mapping of discontinuities and the observation of the slopes and rock mass are discussed as part of the field work done. Furthermore, the chapter covers the analytical methods such as kinematic analysis, Limit Equilibrium and numerical modelling for analysis and validation purposes. In closing, the chapter outlines the challenges faced during data collection, slope stability analysis and simulation of the slope conditions.

Chapter 4 provides a summary of the findings from the field observations and rock mass classification. This was done to get a first-hand rating of the slope.

And in Chapter 5, the slope stability analysis was performed using the kinematic analysis, limit equilibrium and numerical modelling methods. These methods were used to analyse the safety of the slopes found at Werne mine. The methods were also used to model the behaviour of the

slopes under the different discontinuities and elongated depths encountered on site.

Finally, Chapter 6 provides the summary of the findings, a conclusion on the work done as well as recommendations for future work.

Chapter 2: Literature review

2.1 Introduction

The slope stability of rocks is one of the most important aspects in the mining industry. According to Wyllie and Mah (2005), the stability of the rock slopes is mostly influenced by structural geology. Structural geology refers to the study of deformed rocks and how they deform in response to the stresses that act upon the rocks in the upper layers of the earth (Suppe,1985).

This study makes use of different methods of determining the stability of the slope. Some of these methods are discussed in this chapter which include kinematic analysis, Limit Equilibrium Methods (LEM) and numerical analysis (Finite Element Method or FEM and Rockfall analysis).

The chapter begins with a discussion of the concept and fundamentals of slope stability along with the factors that affect and influence instability in the slopes. The following section takes a look at the rock mass classification. The discussion of the rock mass classification then follows the discussion of the slope stability analytical methods as outlined above.

2.2 Concept of slope stability

Open pit mines are considered to be amongst the largest geotechnical structures in the world. They are located on surface where ore can be extracted economically (Karam et al., 2015). Open pit mines occur in a series of benches and as such, a huge amount of material is removed from the ground and with each cycle of material removal, this changes the dimensions of the pit (i.e., depth, width and height). This in return causes the destabilization of existing slopes. Destabilizing forces are present within all slopes, and for the forces to cause failure of the slope, it is all dependent on the magnitude of the driving forces against the resisting forces (McColl, 2015).

Slope failure results in land movement downwards which is collectively known as mass wasting. Mass wasting can be divided into different categories which include rockfall and landslide amongst others (Kolapo et al., 2022). Slope stability is considered to be one of the major issues in geotechnical engineering (Kaur and Sharma, 2016). Slope stability analysis was introduced to provide a conceptual basis for understanding the effects of various slope conditions and destabilizing processes. The term “stability” is said to be relative and also refers to a specified time period. This simply means that a stable slope can become unstable over a given time. Sha (2016) argued that gravity is the fain factor in the mass movement. Furthermore, the author pointed out that even though the gravity is the factor, several other factors may lead to slope instability. They can be categorised as internal factors, external factors or environmental factors.

According to Crozier (1986), stability factors are any phenomena that govern or have an impact on the variables that define slope stability. These variables determine the magnitude of the driving and the resisting forces. Certain aspects of stability are fixed and intrinsic to the slope (e.g. Lithology), whereas others might be fleeting and have varying degrees of influence (e.g. joints).

Therefore, the stability of the slopes can be assessed by examining the magnitude of the driving forces against the resisting forces. According to Guadagno (2013), The tendencies for most types of slope failures (with toppling being an exception) are a result of the Shear stresses developed. The reactionary stresses result in the resisting force against the driving forces. This can be considered as the mobilised shear strength with respect to the shear stress (Guadagno, 2013; McColl, 2015). The mobilised strength refers to the stresses that resist movement of the slope. Most often the mobilised strength is referred to total strength of the slope. However, the Mobilised strength should be distinguished from the total slope strength since it is arguably impossible to quantify (McColl, 2015).

For example, the movement of a block prone to sliding failure is influenced by the resistance caused by the friction between the sliding surfaces, and not the internal structure and strength of the block itself. Therefore, in analysing the stability of the block, only the shear strength of the failure surfaces needs to be known.

However, alluding that the sliding slope failure is a result of shear stress alone should be considered an oversight. There are multiple stresses including compressional and tensional stresses involved, mostly at the boundaries of the sliding mass where the mass moves over irregular surfaces. Furthermore, the magnitude of the driving forces against the resisting forces can be represented on a form of a ratio referred to as the Factor of Safety (FoS) given by:

$$FoS = \frac{(c + \sigma \, tan \, \varphi)}{\tau} \qquad (2.1)$$

Where: $c = cohesion$, $\sigma = normal \; stress$,

$\varphi = angle \; of \; internal \; friction$ and $\tau = shear \; stress$

Equation (2.1) can be populated with a wide range of parameters that influence the driving and resisting forces. The choice on which parameters to use is dependent on the problem being analysed, the physical conditions and processes expected on the slope, and the degree of simplicity or complexity sought (Selby, 1993; Norrish and Wyllie, 1996). The stresses and the strength of the slope depending on their interaction with the gravity determines the movement or stability in the slope. The weight of the material can be resolved into stresses acting normally and parallel to contact surfaces as indicated in Figure 2.1.

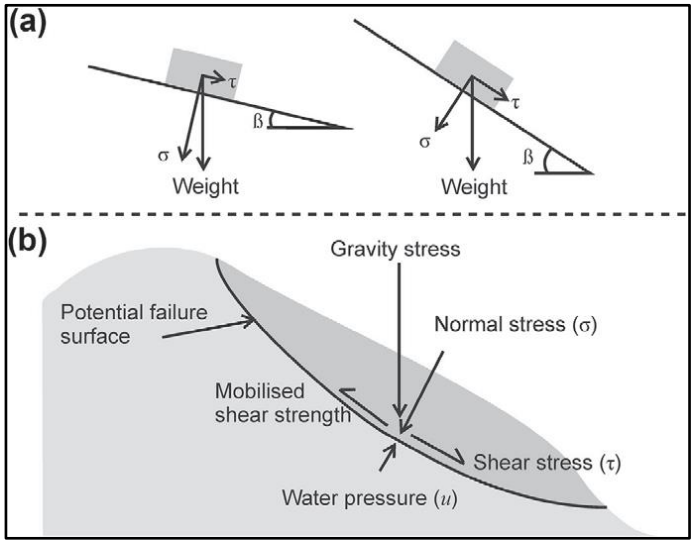

Figure 2.1: (a) Influence of slope angle on the relative magnitudes of shear and normal stress; (b) Stresses acting along a potential failure surface (After Selby, 1993).

Wyllie and Norrish (1996) noted that an increase in the normal stress increases the frictional stress on the sliding surface. This therefore indicates that the relationship between shear and normal stresses is linear governed by Mohr-Coulomb failure criterion. In addition to this, an increase in the stresses acting parallel to the to the failure surface, increases the shear stresses of the slope.

Most of the factors discussed below may influence the stability of the slope directly by altering the shear stress and shear strength. Thus, the relationship between these two stresses should always be kept in mind. Although the term stability can be defined in simple terms, its interpretation can differ depending on the objectives. It often refers to the inherent stability or FoS, as determined by the static physical slope properties; for example, all other stability factors being equal, a high embankment is less stable compared with a low embankment. Landslide susceptibility, which is a measure of the inherent stability of a slope or distribution of slopes, treats the term stability in this way, without any consideration of the likelihood of failure.

Alternatively, slope stability can, more usefully, be a measure of the probability of a failure of an individual slope, which requires consideration of both the stability factors (as discussed above) and the likelihood of a critical failure threshold being exceeded in a given time span (Aki, 1988). Therefore, assessing the stability of the slope requires the knowledge of the potential failure triggers and their likelihood during the time period of interest for each slope. This knowledge includes the probability of the occurrence of a trigger of sufficient (critical) magnitude to induce failure.

2.3 Parameters controlling the stability of the rock mass/slope

The stability of the rock slopes does not only depend on the intrinsic strength of the rocks and as such there are different factors or parameters affecting the stability of the slope in an open pit (Huang et al., 2016). These parameters can either be natural or man-made. The parameters include slope geometry, geological structure and lithology (rock mass characteristics), groundwater, dynamic forces, angle of internal friction, methods of mining and equipment used. However, it should be noted that even though the parameters are present, there is a trigger that sets all into motion. There are natural (e.g. rainfall and earthquakes) as well as man-made (e.g. blasting) events that can trigger slope instability (Huang et al., 2016). Below is a discussion of the major parameters and factors that influence the stability of the slopes.

2.3.1 Slope geometry

The slope geometry generally refers to the basic design parameters of the mine slope which consist of bench width, height, overall slope angle and area of failure surface (Prakash, 2009). Figure 2.2 shows the open-pit bench slope parameters.

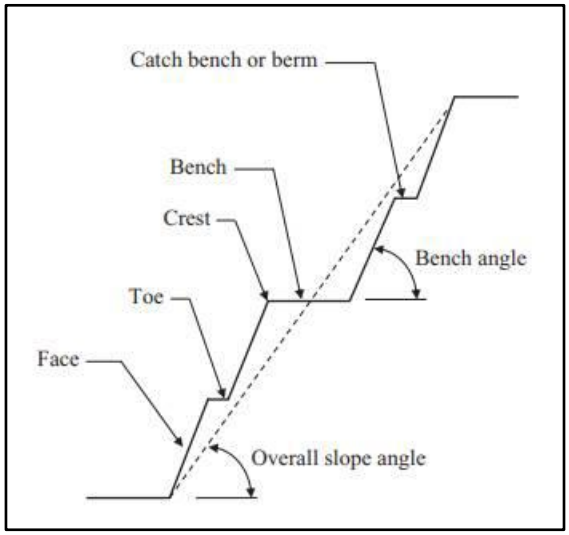

Figure 2.2: Schematic diagram of an open pit mine bench slope parameters (After Chaulya and Prasad, 2016)

Chaulya and Prasad (2016) have observed the stability of the slope decreases with an increasing slope height and angle. Kolapo et al., (2022) alluded that an overall slope angle of 45° is ideal. This angle is thought to be both stable and secure. The curvature of the slope (in addition to slope height and angle) also contributes to its stability (Chakraborty and Goswami, 2016). A convex pit wall also affects the stability of the slope and should be best avoided. Planar failure is most likely to occur in a slope with a convex geometry (Chakraborty and Goswami, 2016).

A slope with a convex geometry is more likely to influence planar failure (Chakraborty and Goswami, 2016). Zhang et al. (2013) added that the curvature usually has a much greater impact on failure on steeper slopes than on gentler ones. The stability of a slope is greatly influenced by the relationship between its height and its curvature. The slope angle should typically be 5-10° steeper than that of conventional slopes if the radius of curvature of a concave slope is smaller than the slope height. According to Chakraborty and Goswami (2016), in situations where the curvature radius is less than the slope height, the slope angle on a convex slope should be 5-10° flatter than on a conventional one.

2.3.2 Rock mass characteristics

A rock mass is composed of rock blocks and discontinuities/structural planes. The rock blocks (which at times are referred to as intact rock) refer to the unfractured rock blocks between discontinuities (Zhang, 2017). Discontinuities are breaks (such as joints, faults and bedding planes) in a rock mass (Pincus, 2003). Discontinuities are said to play a major role in controlling the mechanics and deformation characteristics of the rock mass. Rock mass characteristics include the strength of the intact rock, discontinuities such as joints, bedding planes, faults, foliations and their characteristics such as roughness, discontinuity spacing and infilling material nature (Zhang, 2017; Hussein et al., 2021).

Every slope's stability is contingent upon the material's inherent strength. According to Raghuvanshi (2019) and Keefer (2000), the rock mass properties are one of the factors that aid in determining the height and angle that a slope can sustain against disturbing forces. The spatiotemporal patterns of landslide distributions can be used to infer the effects of the material strength and the geometry on slope stability (Keefer, 2000; Dai et al., 2002). A certain amount of slope failure can be determined using these relationships. Cruden and Martin (2013) stated that the type of failure that may transpire is also influenced by the slope geometry and material type. Consequently, the type of material, the geometry of the slope, and the orientation of the structural elements with respect to the slope aspect are crucial for determining the stability of the slopes.

The structure created by discontinuities or fabric, the apparent cohesiveness given by vegetation, the strength of particles or crystals, and the interparticle contact forces contribute to the strength of the rock mass. The rock masses are typically divided into two categories: rocks and soils. The soils are further divided into cohesive and non-cohesive soils. It is recommended to apply the Mohr-Coulomb failure criterion for describing the strength of the soils and rocks, which takes into discontinuity effects into account (Hoek et al. 2002). When conducting discontinuities mapping, the

quantity, direction and strength of joints, faults, or bedding layers are typically measured. Quantifying the depth orientation, strength and permeability of different compositional units may be appropriate (McColl, 2015).

Discontinuities significantly influence the stability of the slope being excavated. This is because the discontinuities are planes of weakness that occur in a stronger intact rock. As such, they are considered to be one of the most important parameters in determining the stability of the slope. Mostly if they dip out of the slope. Discontinuities arise from the changes in the composition of the rock (Mostly weathering horizons) or structural weaknesses such as cleavage, foliation, fractures, and faults. The compositional changes and structural weaknesses results in two main effects on the slope which are:

1. They provide structural weaknesses below the (intact) strength of the uniform material, which may become preferential failure surfaces, particularly when planar.
2. Discontinuities or changes in the composition can be a pathway for water or create permeability boundaries. Both these can increase the pore water pressure and influence the stresses acting on the slope.

Discontinuities are either formed through natural processes or man-made activities. The natural processes include weathering (Edy Tonnizam et al., 2005). It has been noted that enough evidence exists which links human activities to the instability of slopes with blasting being one of them. Blasting produces vibration waves that will propagate through the rock mass. This rapid transmission of waves leads to the rapture of the rocks and the extension of the structural planes (Fredj, 2021).

2.3.3 Groundwater

Groundwater is said to open up little cracks in a rock mass. This leads to the activation of forces on the rock mass and causes or increases the

instability of the slopes. Water in the cracks increase the pore water pressure which reduces the normal stress across failure planes. The reduction of the normal stresses also reduces the frictional strength on these planes. This leads to an increase in the forces driving failure (driving forces) of the slopes, and this affects the stability of the slope (Kolapo et al., 2022). When water is introduced in the cracks, the spacing between the joints increases, which results in an increase in the depth of the joint and the total force. This in turn results in the failure of rocks subjected to gravitational forces.

2.3.4 Dynamic forces

Blasting and vibrations are said to increase the shear strength of the slope momentarily on the slope. This may cause a dynamic acceleration of the materials in the slope which affects the stability of the slope. Due to slope instability, ground motion and fracturing of rocks then occur. Although blasting primarily governs the slope angles or face angles, it can also cause instability of the very same slopes if poor blasting is executed. This is not only because of blasting-induced vibrations, but by fragmenting the rock behind the slope (Simataa, 2019). The ground vibrations caused by poor blasting lead to the redistribution of the stresses in the slope. As a result, dynamic acceleration of materials on the slope occurs and causes slope instability. (Kolapo et al., 2022).

Similarly, an increase in fractured zone and discontinuities creation can occur caused by poor blasting. The cohesion of the rocks is reduced and then it leads to the water entering the fractured zones and the rock mass continues to loosen (Yin et al., 2018). It should also be noted that in the rock mass, there occur some naturally occurring cracks and fractures and they are extended by additional ground vibrations from blasting. According to Kolapo et al. (2022), the rock mass is continuously weakened by the distribution of seismic waves during the detonation, and this will eventually lead to an unstable slope.

2.3.5 Methods of mining and equipment used

It should always be remembered that deformation in a rock mass develops because of the change in the in-situ stress field. Mining is basically an excavation of the ground and deformation of the face may lead to the reduction of the shear strength of the rock (Sutejo and Gofar, 2015). Therefore, when choosing a mining method and the equipment to be used, the stability should be kept in mind. Similarly, during excavation, consideration should be given to the state of the in-situ stress field, which is characterised by the size and orientation of the principal stress. In open-cast advance, there are four methods of advancement: (a) strike cut with advancing down the dip, (b) strike cut with advancing up the dip, (c) dip cut along the strike, the final and most popular method is (d) open pit working. This method utilizes high-wall slopes, which are more likely to fail due to their steepness and increased height (Prakash, 2009).

Furthermore, a surcharge is created by the movement of heavy equipment used in mining and other operational activities, which intensifies the force that cause the slope to move downward.

2.3.6 Cohesion and angle of internal friction

In the design stage of a mine, cohesion and friction angle, two measures of rock mass strength, are employed to assess the safety factor. One important mechanical property of soil-rock that is relevant to the evaluation of the slope stability is the shear strength. In essence, cohesion is a property of soil or rock that indicates how well it defies gravity's force of deformation. Electrostatic forces in stiff over-consolidated clays are the sources of true cohesion in soils and rocks. On the other hand, negative capillary pressure and pore water pressure are what produces apparent cohesiveness. Rock and loose cohesive soils tend to make a slope less stable.

Conversely, the capacity to tolerate shear stress is determined by the angle of internal friction (Prakash, 2009). On the other hand, internal friction is

influenced by the size of the rock particles, i.e. the angle of internal friction increases with particle sizes. Furthermore, a rock mass strength of cohesiveness is diminished by high water content, undercutting slopes, ground vibrations, and alternating expansions by wetting and contractions by dryness of water (Kolapo et al. 2022).

It is important to remember that the slope's stability decreases with decreasing cohesiveness. Determining the cohesion and angle of internal friction is therefore essential. A triaxial compression test is used in a laboratory setting to determine the parameters of both cohesion and internal friction (Kolapo et al. 2022).

2.4 Types of slope failure

There are basically four main types of slope failure, and they are dependent on the type and degree of structural control. These types of failures are planar, wedge, toppling and circular. The type of failure to occur on a slope is dependent on the orientation of the discontinuities. A full discussion of these failure types follows below. This includes how the orientation of the discontinuities should in relation to the slope for those failures to occur.

2.4.1 Planar rock failure

This type of failure occurs due to the sliding along a single discrete surface that approximates a plane. This means that the discontinuities that lead to planar failure are found striking approximately parallel to the slope face and dipping at a lower angle (Figure 2.3), thereafter intersecting the slope face, which then enables the material above the discontinuity to slide (Prakash, 2009). They are analysed as two-dimensional problems.

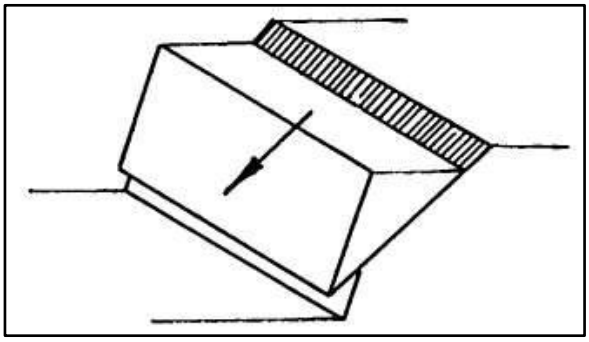

Figure 2.3: Plane failure (after Call et al, 1993)

The size of the planar failure ranges from a few cubic centimetres to large scale landslides that may involve an entire mountain. This was further motivated by a study conducted by Lowell (1990) which involved the study of the K M mountain slide in the state of Washington, and according to the author, the investigated landslide involved an estimated 1.2 to 1.5 million m^3. According to Kolapo et al. (2022), failure does not only occur from a single discontinuity, but it can also be due to a combination of joint sets which form a straight path. The mechanisms of slope failure from stationary to an active moving slope are proof that there is an external force that triggers the slope failure process, or the shear stress is greater than the strength of the ground. It is usually not the case whereby failure is due to a single force, but mostly due to a combination of the forces and factors that may lead to the influence of the failure mechanisms of the slope (Kolapo et al., 2022; Arief et al., 2020).

Slopes with convex designs, where the direction is parallel to the strike of weak planes, are prone to this kind of failure. Kolapo et al. (2022) also demonstrated that planar failure can result from failure that is restricted to one bench, several benches or regions of the pit with unfavourable geometry or structures that strike perpendicular to the slope face. The existence of groundwater is one of the main causes of planar failure, which in turn leads to the slope's instability when there is momentary groundwater pressure, particularly during periods of intense rainfall.

2.4.2 Wedge rock failure

Wedge failure occurs when two or more discontinuities intersect, and this results in a formation of a tetrahedral failure block which is also referred to as a wedge of material (see Figure 2.4). When the angle of inclination between the discontinuities is greater than the internal angle of friction along the discontinuities, a wedge of material may be formed above the discontinuities and may slide out in a direction parallel to the line of intersection of the two discontinuities (Prakash, 2009; Simataa, 2019).

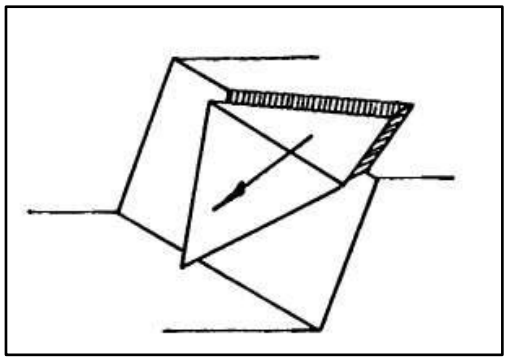

Figure 2.4: Wedge failure (after Hoek and Bray, 1981)

The downward force is a result of the weight of the wedge and the external forces (or surcharges) acting over the whole wedge. According to Goodman and Kieffer (2000), wedge failure is the most commonly experienced type of failure in rock slopes, and as a result, it not only becomes important in designing benches but also in slope stability analysis. The wedge failure, similar to planar can occur from a small scale up to large scales affecting benches or an entire slope.

2.4.3 Failure by Toppling

Toppling failures as defined by Norrish and Wyllie (1996), typically happen in rock masses that are split into a number of slabs created by a series of discontinuities that dip sharply into the face and are parallel to or nearly parallel to the face (see Figure 2.5).

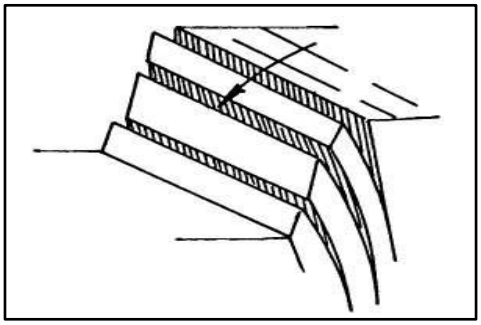

Figure 2.5: Toppling failure (after Prakash, 2009).

Block flexure and rotation cause downslope overturning, which is a characteristic of the failed slope's movement during toppling (Simataa, 2019). As the failure is occurring, the boulders from the top can bounce on other benches and also pose a threat to the lower levels, and according to Kolapo et al. (2022); in areas where toppling failure is likely to occur, the benches should be made wide enough to prevent boulders from falling over the crest to the lower benches. As much as toppling is known to occur on its own in a slope, it can also occur as a secondary failure mode associated with other mechanisms such as block sliding. See Figure 2.6 below which shows toppling occurring as a secondary mechanism.

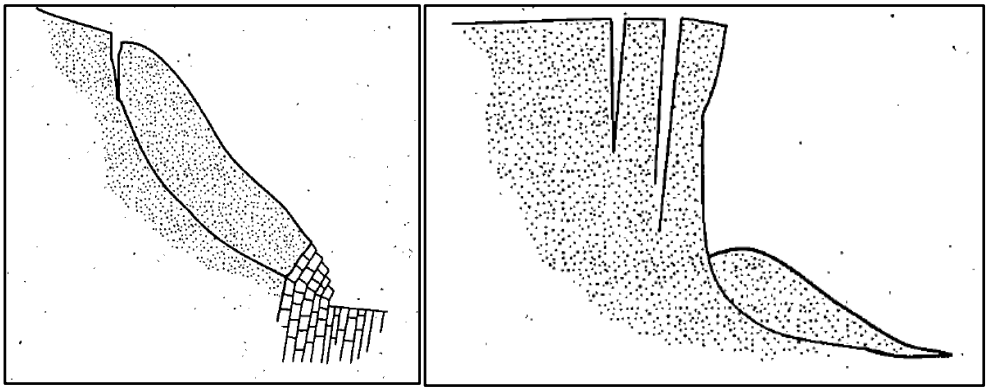

Figure 2.6: (Left) Slide toe toppling when steeply dipping beds of rocks are loaded by instability higher up the slope; (Right) Tension crack toppling in cohesive materials (after Hoek and Bray, 1981).

2.4.4 Circular rock failure

Soils and deeply weathered or closely fractured rocks are the most common places for circular failure. Often resembling the arc of a circle, this kind of failure is not primarily governed by the structural discontinuities (see Figure 2.7 below).

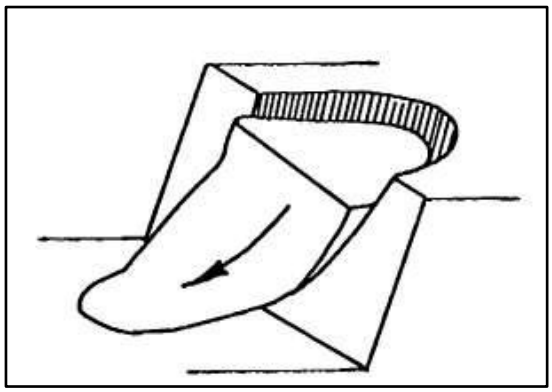

Figure 2.7: Circular failure (after Prakash, 2009).

When the materials of the spoil dump slopes are weak such as soil, heavily jointed, or broken rock mass, the failure is defined by a single discontinuity but will tend to follow a circular path.

2.5 Rock mass investigation

Rock mass investigation involves the full investigation of the rock mass from the collection of rock mass data (discontinuities, rock strength, etc.), followed by the rock mass classification. Traditionally, a geotechnical engineer does the rock mass investigation using the face mapping method. This method measures the required information directly on the exposed face. As described by Russel (2018), a complete face mapping should contain the following:

- Identification, location and size of the exposure/face being mapped.
- A description of rock type, degree of weathering and rock strength.
- Orientation, frequency, persistence and condition of discontinuities.
- Moisture content and seepage.

- Rock mass classification, e.g., RMR.

A sub-section of face mapping called structural face mapping is also carried out with the ultimate goal of obtaining data regarding the discontinuities on the exposed face. The information from the structural mapping is useful when conducting kinematic analysis, limit equilibrium and numerical modelling as input parameters (Read, 2019; McQuillan, 2013).

There are different face mapping techniques which include: Scanline mapping, Cell/Window mapping and digital mapping techniques such as Photogrammetry or laser scanning (McQuillan, 2013).

2.5.1 Face mapping

Face mapping is simply a geological and geotechnical data acquisition method used for determining the rock mass properties. Face mapping can be divided into two techniques which are scanline mapping and window mapping.

Scanline mapping is a face mapping technique whereby a line is drawn over the face of the study area and all the discontinuities that intersect the line are measured and described. Typically, there are several sampling lines which are in different orientations to reduce the sampling bias. During the scanline mapping, measurements taken include orientation of discontinuities, length, roughness, and infilling material in the discontinuities (Simangunson et al., 2004; Wines and Lily, 2003; Bye and Bell, 2001; Call, 1992).

Window mapping is also referred to as cell mapping, and it is a manual face-mapping method that divides the face into cells. The mapping of discontinuities is done in those cells whereby the spacing, persistence, length, orientation and condition of discontinuities are measured. According to Russel (2018), the cell normally constitutes 10 – 25% of the total exposed area of the face. (Read, 2019; Priest, 1993).

2.5.2 Disadvantages of face mapping

In face mapping, as previously mentioned, different parameters from exposed faces are measured and interpreted in order to estimate different parameters related to the rock mass. It should be noted that no method will completely represent the rock mass on the face, hence the disadvantages exist in all the methods (Arief, 2020; Read, 2019). On face mapping, some of the disadvantages arise due to the following:

- Orientation bias: The likelihood that a specific discontinuity will be visible in a mapping face depends on how the discontinuity orientation and face relate to each other (Zhang, 2006). According to Russell (2018), the face mapping process in mining operations is biased toward orientation due to limited exposure of faces that are orthogonal.
- Size bias: Zhang (2006) pointed out that when conducting face mapping, longer discontinuities tend to be favoured more than less persistent discontinuities. The smaller joints are said to be difficult to measure and as a result, they get ignored.
- Censoring bias: The correct length measurements of the discontinuities is difficult to establish at times since some discontinuities extend beyond the scanline or the window being mapped. Zhang (2006) noted that in situations whereby both ends of the discontinuity cannot be seen or extend beyond the window, only a truncated measurement of the joint plane length can be taken.

2.6 Rock mass classification

Assigning a unique description (or number) to a rock mass based on similar properties/characteristics that allow for the prediction of its behaviour is known as rock mass classification (Bieniawski, 1989). This process groups or classes rock masses according to predetermined relationships.

Since a rock mass is essentially an assembly of rock material and its discontinuities, it may be placed under the proper class using a rock mass categorization scheme (Bieniawski, 1993).

Systems for classifying the rock masses are now employed in combination with numerical simulations, particularly in the initial phases of the geotechnical projects, when the data is scarce. Hoek and Diederichs (2006) stated that the strength and deformation parameters can be calculated and applied in numerical simulations to take into account stability, failure pattern, factor of safety, deformations, etc, based on the classification of the rock (Mohr-Coulomb or Hoek-Brown material models). There are several authors such as Gunther et al. (2012), Chakraborti et al. (2012), and Herbst and Konietzky (2012) who have applied the principles of rock mass classification in mining and slope stability analysis. There are several types of classification systems. These categorisation schemes can be classified as either quantitative or qualitative. The geological strength index (GSI), Rock load and Schweizerischer ingenieur-und Architekten-Verein (SIA 199), are examples of qualitative methods (descriptive methods), whereas, the Q, RMR, RSR, and RQD systems are examples of qualitative methods.

The classification systems may also be categorised according to the objective of the rating system. The Q and RMR systems are usually used to evaluate stability. This is a result of the RMR system computing the stand-up time, while the Q system is used to calculate the ground support design (Bolt spacing, linear thickness, etc.). GSI is used to determine the engineering parameters exclusively, while the SIA 199 system is used to identify and determine the excavation class and support classes. However, as one of the most often used techniques for classifying rock masses, the Rock Mass Rating (RMR) method is the primary focus of most studies.

2.6.1 Rock mass failure criteria

One of the fundamental variables needed to forecast the behaviour of rocks and rock masses in geomechanics and geoengineering is said to be the

intact rock strength (Ewy, 1999). Many academics have investigated the failure behaviour of intact rock. According to Coleman and Zoback (2002) and Benz and Schwab (2008), the majority of failure criteria only takes into account the minimum and the maximum stress levels, ignoring intermediate principal stresses. Likewise, a number of researchers have examined the impact of intermediate principal stress on rock mass and discovered a significant relationship.

According to Mehranpour and Kulatilake (2016); there are six major failure criteria used to represent strength of intact rock in Geomechanics. These methods are: (a) Mohr-Coulomb, (b) Hoek-Brown, (c) Modified Lade, (d) Modified Wiebols and cook, (e) Mogi and (f) Drucker-Prager.

Only two of the failure criteria listed above (i.e., Mohr-Coulomb and Hoek-Brown) are common. These techniques are widely used because they are straightforward and may be applied to larger rock masses. Sections 2.6.1.1 and 2.6.1.2 cover the examination of the two failure criteria.

2.6.1.1 Mohr-Coulomb failure criterion

A mathematical model known as the Mohr-Coulomb failure criteria is used to explain how materials react to shear and normal stresses (Labuz and Zang, 2012). Cook (1979) states that Mohr-coulomb uses the primary stresses, major and minor, but ignores the intermediate stresses. Using the normal and shear loads on the plane is another way to understand this. Accordingly, the Mohr-Coulomb failure criterion presupposes that the failure of the evaluated material is contingent upon the major and minor stresses in addition to the failure envelope's form.

This criterion is employed to ascertain the threshold beyond which failure will occur. The critical normal and shear stresses are analyzed in order to achieve this (Coulomb, 1776). A Mohr's circle of states of stress at failure expressed in terms of the lowest and maximum principles of stress can be used to illustrate the Mohr-Coulomb failure criterion. Consequently, the

circle of stages of failure represents the Mohr-Coulomb. As seen in Figure 2.8, this is accomplished by using a straight line that intersects both circles. The Mohr failure criterion is calculated by making use of Equation (2.2) below:

$$\tau = c + \sigma \tan \varphi \quad (2.2)$$

Where: τ is the shear stress

c is the cohesion

σ is the normal stress

$\emptyset$ is the angle of internal friction.

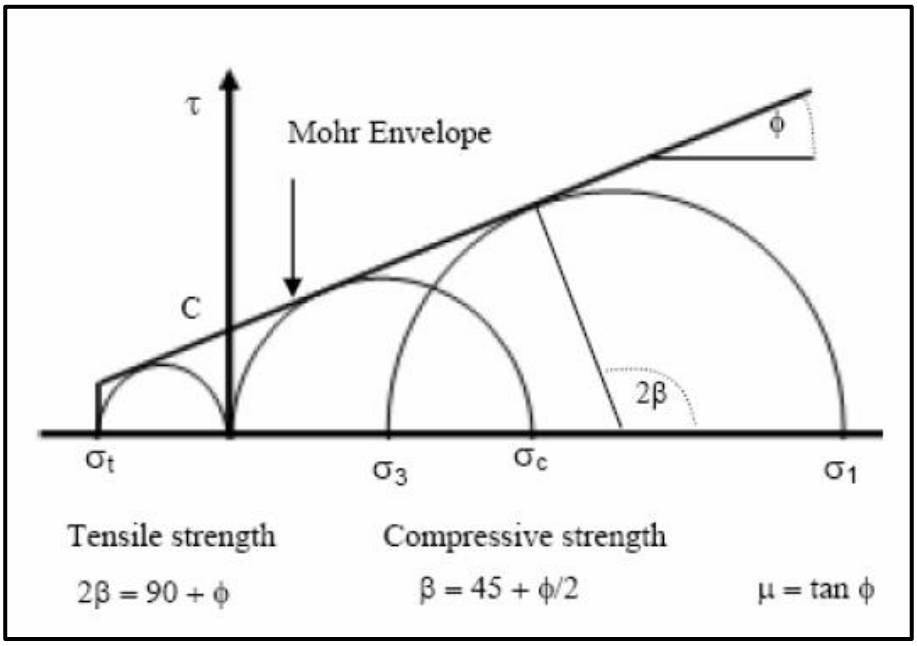

Figure 2.8: Graphical representation of Mohr-Coulomb failure criterion (after Kramadibrata, 2008)

2.6.1.2 Hoek-Brown failure criterion

The generalised Hoek-Brown criterion is a popular name for the Hoek-Brown criterion. Hoek (1994) introduced a tool for estimating the rock mass strength while investigating the brittle failure of intact rock. The formulation of the relationships between shear and normal stress at fracture initiation was based on the experience with brittle rock failure and his use of a

parabolic Mohr envelope derived from Griffith's crack theory (Griffith, 1920, 1924). However, Hoek et al. (1995) expressed the criterion as follows:

$$\sigma_1 = \sigma_3 + \sigma_{ci}\left(mb\frac{\sigma_3}{\sigma_{ci}} + ci\right)^a \quad (2.3)$$

By scaling between the relationship obtained in accordance with the current geological conditions within a rock mass, the Hoek-Brown criteria estimates the strength of the rock mass.

The original formulation of the criterion was based on the experience of Hoek (1968) with brittle failure and his use of a parabolic Mohr envelope to define the relationship between shear and normal stress at fracture initiation, which was derived from Griffith's crack theory (Griffith, 1920 & 1924). Hoek and Brown (1980) developed their criterion by fitting a range of parabolic curves to triaxial test data through trial and error, linking fracture initiation with fracture propagation and rock failure. As a result, the Hoek-Brown criterion is empirical, and there is no fundamental connection between any physical properties of the rock and the constants included in the criterion (Hoek, 1983). A graphical representation of the Hoek-Brown criterion is shown in Figure 2.9 below.

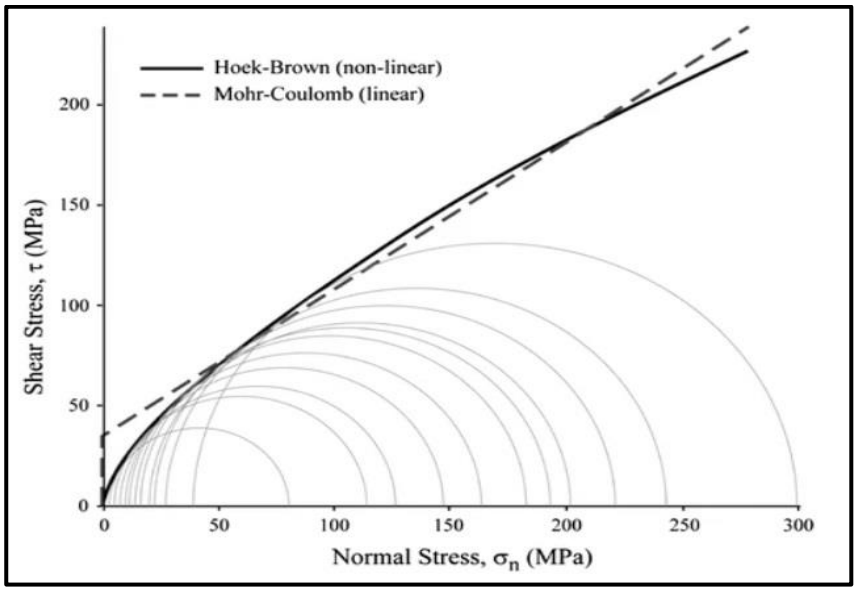

Figure 2.9: Graphical representation of the Hoek-Brown failure criterion (after Eberhardt, 2012).

2.6.2 Rock Mass Rating (RMR)

Developed at the South African Council of Scientific and Industrial Research (CSIR) in 1973, rock mass rating is a geomechanical classification system for rocks. Since then, there have been a number of noteworthy changes to the classification, including the 1975 reduction of the classification parameters from 8 to 6, adjustments to the ratings, and a lowering of the suggested support requirements.

Class boundaries were changed to even multiples of 20 in 1976; the ISRM (1978) rock mass description was adopted in 1979, and so on. As more case studies proved to be viable, these modifications and revisions were made. The most widely used versions are the ones from 1976 and 1989, according to Palmstom (2009). As a result, when RMR values are quoted, it is critical to specify which version is being used. A given site should be divided into a number of geological structural units so that each type of rock mass is represented by a separate geological structural unit in order to apply the geomechanics classification system.

The following six parameters (representing causative factors) are determined for each structural unit:

1. Uniaxial compressive strength (UCS) of intact rock material
2. Rock quality designation (RQD)
3. Joint or discontinuity spacing
4. Joint condition
5. Groundwater condition
6. Joint orientation

The basic RMR in the classification system is represented by the first five parameters mentioned above, as highlighted by Edelbro (2004). Since the influence of orientation varies depending on the engineering application, the final parameter (joint orientation) needs to be addressed separately. A rating is assigned to the parameters, which represents the description of the rock quality. Singh and Goel (2012) did, however, add that ratings for various parameters should be assigned a range rather than a single value in order

to reduce doubts resulting from subjective judgments. Table 2.1 below lists the initial five classification parameters. Different value ranges for parameters have been assigned based on their importance, since different parameters have different significance for the overall classification of rock mass. Note that better rock mass conditions correspond to a higher value for a given rock (Bieniawski, 1989).

1. Uniaxial compressive strength (UCS) of intact rock material

Based on the specific characteristics of the site, rock cores should be used to determine the strength of the complete rock material. Table 2.1 below lists the ratings for the UCS and the point load strength index. Rock lumps at their natural moisture content may be tested for point load strength index to get the UCS value. Numerous rock types would be classified as soil when their compressive strength was less than 1.0 MPa; ISO 14689 redefined these terms.

Table 2.1: Classification RMR system ratings (Bieniawski, 1989). Five basic rock mass classification parameters and their ratings

Parameter			Range of Vaules						
1	Strength of intact rock material	Point load strength index (MPa)	>10	4–10	2–4	1–2	for this low range uniaxial compressive strength is preferred		
		Uniaxial Compressive Strength (MPa)	>250	100–250	50–100	25–50	5–25	1–5	<1
		Rating	15	12	7	4	2	1	0
2	Drill Core Quality RQD (%)		90–100	75–90	50–75	25–50	<25		
	Rating		20	17	13	8	3		
3	Joint Spacing (m)		>2	0.6-2	0.2–0.6	0.06–0.2	<0.06		
	Rating		20	15	10	8	5		
4	Condition of Joints		Not continuous, very rough surfaces, unweathered, no separation	Slightly weathered surfaces, slightly weathered, separation < 1 mm	Slightly rough surfaces, highly weathered, separation < 1 mm	Continuous, slickensided surfaces, or gouge < 5mm thick, or separation 1–5 mm	Continuous joints, soft gouge > 5mm thick, or separation > 5 mm		
	Rating		30	25	20	10	0		
5	Groundwater	Inflow per 10 m tunnel length (1/min)	none	<10	10–25	25–125	>125		
		Joint water pressure / major in situ stress	0	0–0.1	0.1–0.2	0.2–0.5	>0.5		
		General conditions	dry	damp	wet	dripping	flowing		
	Rating		15	10	7	4	0		

2. Rock Quality Designation (RQD)

Rock cores or volumetric joint count which quantify the degree of jointing within a volume of rock mass should be used to calculate RQD (Palmstrom, 1982 – 1986). When calculating the RQD from the core, the formula is as follows: RQD = sum of core samples longer than 100 mm (10 cm) / core length. Since RQD is expressed as a percentage, multiplying the result by 100 is necessary. The recently fractured cores are assembled and counted as a single unit.

In situations where a core cannot be obtained from the research region, a volumetric joint can be used as an additional technique of measuring RQD. The volumetric joint count is utilized in this procedure. The primary input parameters for volumetric joint count, according to Palmstom (1982), are joint frequency and discontinuity spacing. An area (such as 1 m^2) has to be defined in order to determine a volumetric joint. This marked region serves as a stand-in for the whole slope. Table 2.1 provides the specifics of the RQD rating.

3. Spacing of Discontinuities

According to Edelbro's definition released in 2003, discontinuities include small faults, joints, beddings or foliations, shear zones, and other weak spots. The distance between two adjacent discontinuities is known as discontinuities spacing, and it has to be calculated for each set of discontinuities. It is commonly acknowledged that when evaluating a rock mass structure, joint spacing is crucial. The degree to which the strength of a rock mass is reduced by joints is determined by the distance between them. But it is important to remember that if there are many sets of discontinuities and the distance between sets vary, one should take into account the negatively oriented set with the lowest rating when calculating joint spacing (Bieniawski, 1973).

4. Condition of discontinuities

This component takes into account the infilling (gouge) material, weathering of the wall rock or the planes of weakness, length of continuity, and

roughness of discontinuity surfaces. Certain criteria do not apply to each other. For instance, the presence of infilling means that the gouge's influence will overpower any roughness that may be there.

5. Groundwater Condition

Depending on the location of the measurements, different descriptions of the groundwater conditions apply. According to Singh and Goel (2012), a tunnel's overall state can be classified as entirely dry, damp, wet, dripping, or flowing. Alternatively, the rate of groundwater intake should be measured in litres per 10 metres of length. The ratio of the seepage water to the main stress should be mentioned and described in terms of the actual water pressure data, if available. Table 2.1 above displays the ratings based on the water conditions.

Note that the above five parameters are added to obtain the basic rock mass rating RMR_{basic}.

6. Orientation of discontinuities

The strike and dip of the discontinuities are referred to as their orientation. It is necessary to note the strike in relation to magnetic north. The angle formed when the horizontal and discontinuous planes are taken in the dipping direction of the plane is known as the dip angle. It is important to document the foundation alignment, slope face orientation, and tunnel axis orientation. Regarding tunnel drivage direction, slope face orientation, or foundation alignment, the impact of discontinuity strike and dip is taken into account.

Tables 2.2 and 2.3 below offer a quantitative assessment of the key joint orientation impact for tunnels and dam foundations, respectively, and should be consulted in order to determine whether or not the strike and dip are favourable. The total of the joint adjustment rating and the RMR_{basic} may be determined after the rating for the influence of the crucial discontinuity is known, as indicated in Table 2.3. This number is called the “final RMR”.

Table 2.2: Critical joint orientation effects (Bieniawski, 1989).

Strike perpendicular to tunnel axis				Strike parallel to tunnel axis		Irrespective of strike
Drive with dip		*Drive against dip*				
Dip 45°–90°	Dip 20°–45°	Dip 45°–90°	Dip 20°–45°	Dip 20°–45°	Dip 45°–90°	Dip 0°–20°
Very favorable	Favorable	Fair	Unfavorable	Fair	Very unfavorable	Fair

Table 2.3: Sum of joint adjustment ratings (Bieniawski, 1989).

	Dip 10°–30°			
	Dip direction			
Dip 0°–10°	***Upstream***	***Downstream***	**Dip 30°–60°**	**Dip 60°–90°**
Very favorable	Unfavorable	Fair	Favorable	Very unfavorable

Table 2.4 indicates that the impact of orientation in a rough-dilatant joint is less significant in tunnels. For this reason, the Norwegian Geotechnical Institute's Q-system does not take joint orientation into account.

Table 2.4 Adjustment factors for different engineering applications (Bieniawski, 1989).

Joint orientation assessment for	Very favorable	Favorable	Fair	Unfavorable	Very unfavorable
Tunnels	0	−2	−5	−10	−12
Raft foundation	0	−2	−7	−15	−25
Slopes*	0	−5	−25	−50	−60

The influence of joint orientation is particularly critical in rafts. It is particularly significant on rock slopes where slope mass rating (SMR) is advised. The cut slopes of the trench before the tunnel should be designated as SMR rather than RMR or Q.

2.6.3 Estimation of RMR

RMR should be calculated as an algebraic sum of ratings for all of the characteristics listed in Tables 2.1 and 2.4, adjusted for orientation of discontinuities in Tables 2.2 and 2.3. The "rock condition rating," which takes into account the compressive strength of intact rock material and joint orientation, is the total of the ratings for the three parameters (RQD, discontinuities spacing, and discontinuities condition) (Goel et al., 1996). Heavy blasting causes new fractures.

Experience indicates that when tunnel boring machines (TBMs) or road headers are used for tunnel excavation, 10 points should be added to the RMR for undisturbed rock masses. Depending on the quality of the controlled blasting, a further 3 to 5 points may be added. Table 2.5 shows the five classifications into which the rock mass is categorized based on RMR values for a certain engineering structure: very good (RMR 100 – 81), good (80 – 61), fair (60 – 41), bad (40 – 21), and poor (<20).

Table 2. 5: table showing the classes of rock mass classification and description of each rock mass (Bieniawski, 1989).

S. No.	Parameter/ properties of rock mass	RMR (rock class)				
		100–81 (I)	*80–61 (II)*	*60–41 (III)*	*40–21 (IV)*	*<20 (V)*
1	Classification of rock mass	Very good	Good	Fair	Poor	Very poor
2	Average stand-up time	20 years for 15 m span	1 year for 10 m span	1 week for 5 m span	10 hours for 2.5 m span	30 minutes for 1 m span
3	Cohesion of rock mass (MPa)*	>0.4	0.3–0.4	0.2–0.3	0.1–0.2	<0.1
4	Angle of internal friction of rock mass	>45°	35–45°	25–35°	15–25°	<15°
5	Allowable bearing pressure (T/m^2)	600–440	440–280	280–135	135–45	45–30
6	Safe cut slope (°) (Waltham, 2002)	>70	65	55	45	<40

2.7 Slope stability analytical methods

A review of how the structural features influence of affect the stability of a slope was detailed in Section 2.2. This data comes in three dimensions in the real world, and according to Wyllie and Mah (2005), the data needs an appropriate analytical method that turns the data into useful information ready for analysis. The approaches and procedures that may be utilized to assess the stability of the rock slopes are covered in this section.

2.7.1 Stereographic analysis of structural geology

In geology, stereographic projections are used to examine the bearings, angles, and connections between planes and linear structures in order to interpret the intricacies of deformed rock. The two-dimensional representation and analysis of the three-dimensional orientation data is made possible by the stereographic projection (in a circular graph). Points may represent lines, and lines can represent planes, thanks to stereographic presentations that eliminate one dimension from the equation. This entails charting planes and lines on a circular grid or net (refer to Rowland et al., 2007). Stereographic projections have a significant drawback in that they do not depict the location or size of the feature; instead, they consider only the angle connections between lines and planes. Figure 2.10 below shows the stereographic projection, which is made up of a reference sphere with a fixed orientation towards the north and a horizontal equatorial plane.

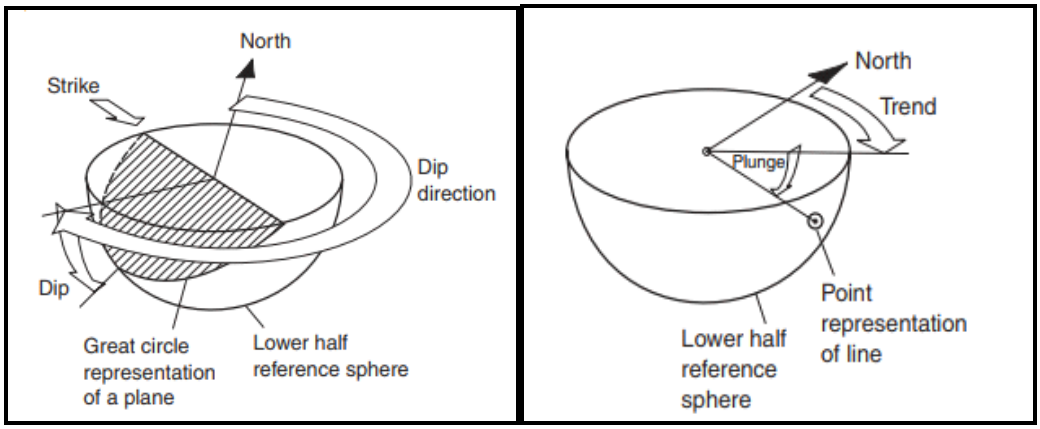

Figure 2. 10: Following Wyllie and Mah (2005), the stereographic depiction of the plane and line on the lower hemisphere of the reference sphere is as follows: (Left) The plane projected as the great circle; (Right) An isometric perspective of the line (plunge and trend).

In order for the axis of the feature to pass through the centre of the reference sphere, planes and lines with a certain plunge and trend are positioned in an imagined sense. A distinct line on the surface of the reference hemisphere is defined by the intersection of the feature with the bottom half of the reference sphere. This intersection between a line and the reference sphere is termed a point for a line, and a great circle for a plane. The intersection with the reference sphere is rotated downward to a horizontal surface at the base of the sphere in order to create a stereographic projection of a plane or line (see Figure 2.11 below).

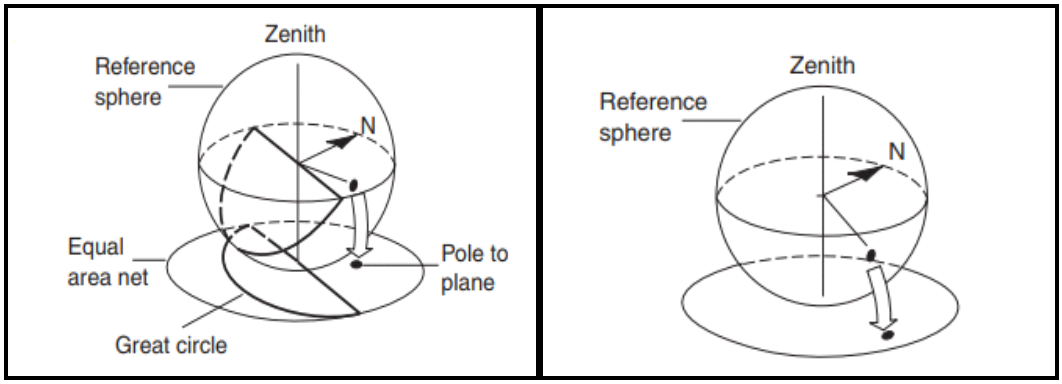

Figure 2.11: Line and plane equal area projections: (Right) Line projected as pole; (Left) Plane projected as a large circle and matching pole (Wyllie and Mah, 2005).

The pole to the plane is an additional way to depict the orientation of a plane. The pole is the location on the surface of the reference sphere where a radial line perforates it in a direction perpendicular to the plane. The ability to represent the whole orientation of a plane with a single point is what makes the pole projection useful. When compared to big circles, the usage of poles makes it easier to analyse a greater number of planes.

For stereographic projections, two common forms of stereonets are used: the Lambert equal-area net and the Wulff net, named for G.V. Wulff who modified the net for use in crystallography. As seen in Figure 2.12 below, there are some differences between these two stereonets. As a result, the two stereonets have different applications; structural geologists mostly utilize the Lambert equal area stereonet, whereas crystallographers primarily employ the Wulff net stereonet.

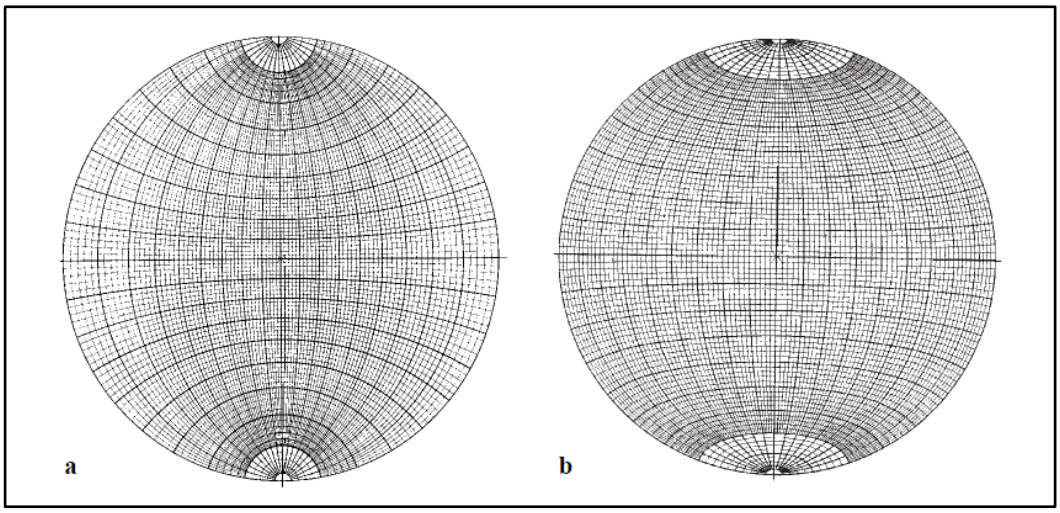

Figure 2.12: Nets used for stereographic projection. (a) Stereographic net or Wulff net and (b) Lambert equal-area net or Schmidt net (Rowland et al., 2007).

This study mainly focuses on the Lambert equal-area net due to its scope.

By having lines for the North, South, East, and West, the Lambert equal area net is built like a globe (Rowland et al., 2007). In contrast to the North-South (also called great circles) lines, which are organized like the longitude lines of the planet, the East-West (also called small circles) lines are similar

to the latitude lines of the globe (Figure 2.13). The perimeter of the net is called the primitive circle.

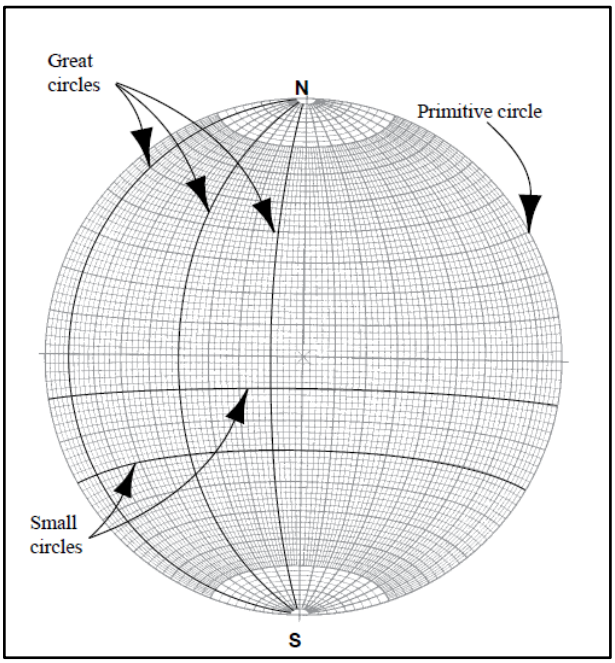

Figure 2.13: Main elements of the equal-area projection (adapted from Rowland et al., 2007)

2.7.2 Kinematic analysis

The branch of mechanics known as "kinematic analysis" explains how things move. Awang et al. (2021), Mohammed et al. (2015), and Admassu (2012) describe it as one of the traditional techniques for analysing slope stability. It is a purely geometric technique that looks at possible failure modes (plane, wedge, and toppling failures) that might arise in jointed rock mass as a result of differently oriented discontinuities.

This is accomplished by applying the stereographic projection method. Kinematic analysis evaluates the connection between the implicated discontinuities and the altitude of the slope (Sigdel and Adhikari, 2020). As seen in Figure 2.14, discontinuity orientation is represented on the stereonet as large circles.

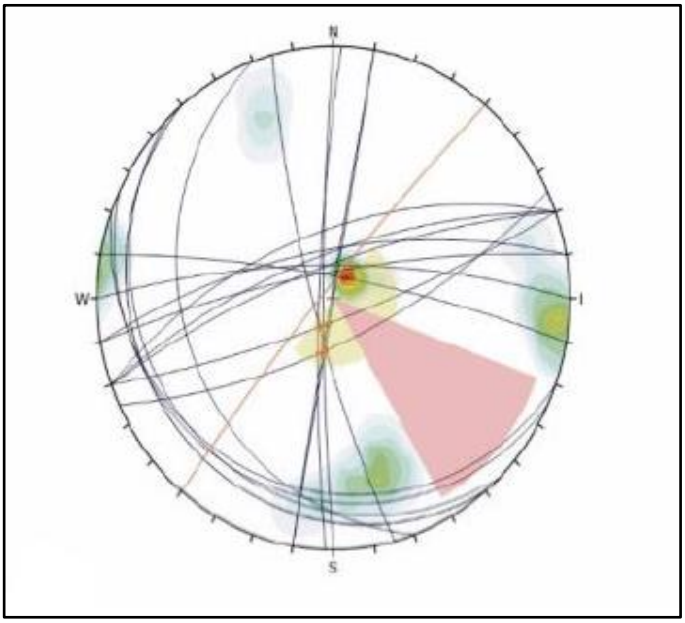

Figure 2. 14: Stereonet showing discontinuity orientation as great circles (Abdullah et al., 2018).

In addition to that, the great circles which represent discontinuities can be shown as poles on the stereonet as shown in Figure 2.15.

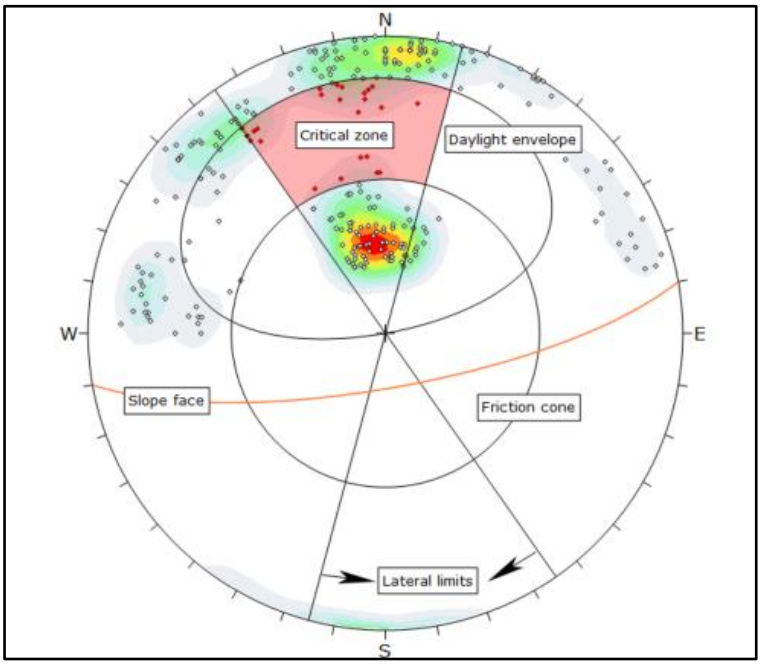

Figure 2. 15: Stereonet showing the discontinuities as poles (Sari, 2019)

The plane-to-pole concept, which is illustrated in Figure 2.11 and explained in Section 2.7.1, describes how a plane may be represented as a point. The

same figure may be used to determine the stability conditions and the direction in which a block will slide after the kind of block failure has been determined on the stereonet. Markland (1972) was the first to propose the common technique in kinematic analysis. Hocking (1976) as well as Hoek and Bray (1981) later redefined it.

Kinematic analysis may be used to detect potential failure modes, such as plane, wedge, and toppling, as was previously described. However, it should be emphasized that specific circumstances must be satisfied for failure to occur, as highlighted by Hoek and Bray (1981) and Goodman (1989). These specifications speak to the orientations of the discontinuities with respect to the slope. Using a rose diagram makes it simple to show the direction of the discontinuities (See below, Figure 2.16).

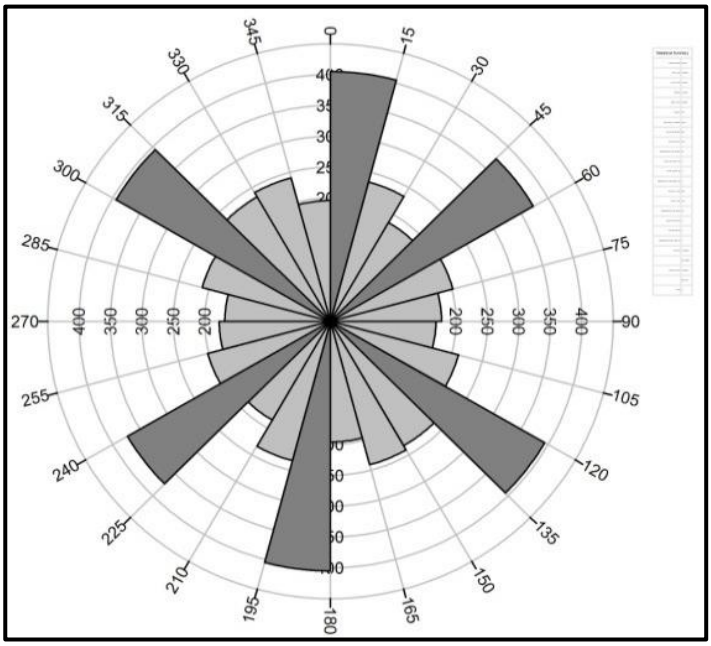

Figure 2.16: An example of a rose diagram (after Lee et al., 2012).

A rose diagram is a circular histogram that indicates the directions of the mapped discontinuities. Different directions of the discontinuities are indicated by a bar. Furthermore, a bar in the stereonet is also a representation of the number of discontinuities.

A rose diagram is mostly used in conjunction with a cardinal compass. Most authors make use of a 16 or 32 cardinal points compass (Figure 2.17) to determine the directions of the discontinuities and discontinuities sets.

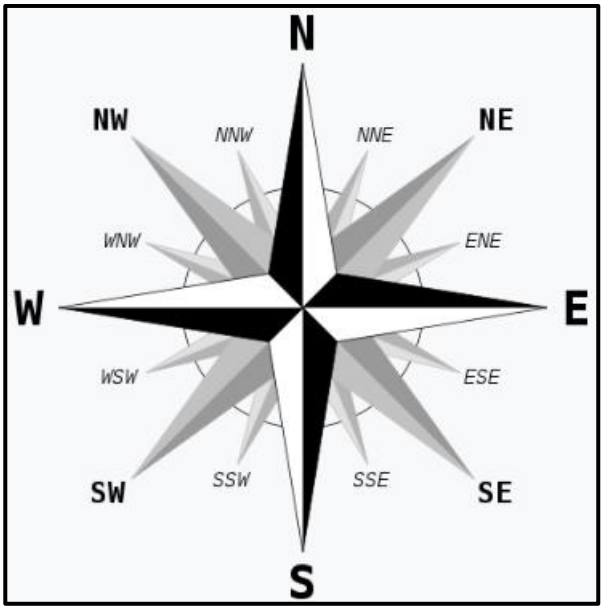

Figure 2.17: 16 points cardinal directions of a compass (after Humphrey and Adams, 2008).

As explained in the previous paragraph, the type of failure that a slope may face is determined by the relationship of the discontinuities and discontinuities sets to the slope. These failure types can be recognized from a stereonet. Below is a discussion of the conditions on how each of the failures occurs.

Planar failure

Markland's test indicates that discontinuity that daylights or dips in the same direction as the slope face (within 20°) and at an angle that is larger than the friction angle along the failure plane, but softer than the slope angle, is likely to result in a plane failure (Hoek and Bray, 1981; Goodman, 1989). As seen in Figure 2.18 below, the discontinuity must fall far inside the shaded region(also referred to as a crucial zone or region) in order for planar failure to be detected on a stereonet.

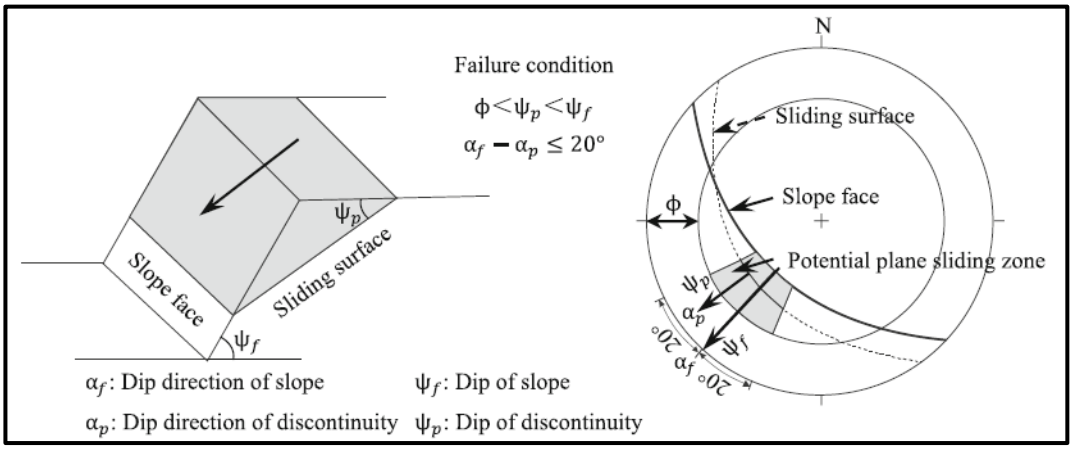

Figure 2.18: Kinematic and geometric conditions for planar failure (Norrish and Wyllie, 1996).

Wedge failure

When the line of intersection of two discontinuities forms a wedge-shaped block and plunges in the same direction as the slope face, a wedge failure on a stereonet may happen. This happens when the plunge angle is greater than the friction angle along the planes of failure, but less than the slope angle (See Figure 2.19).

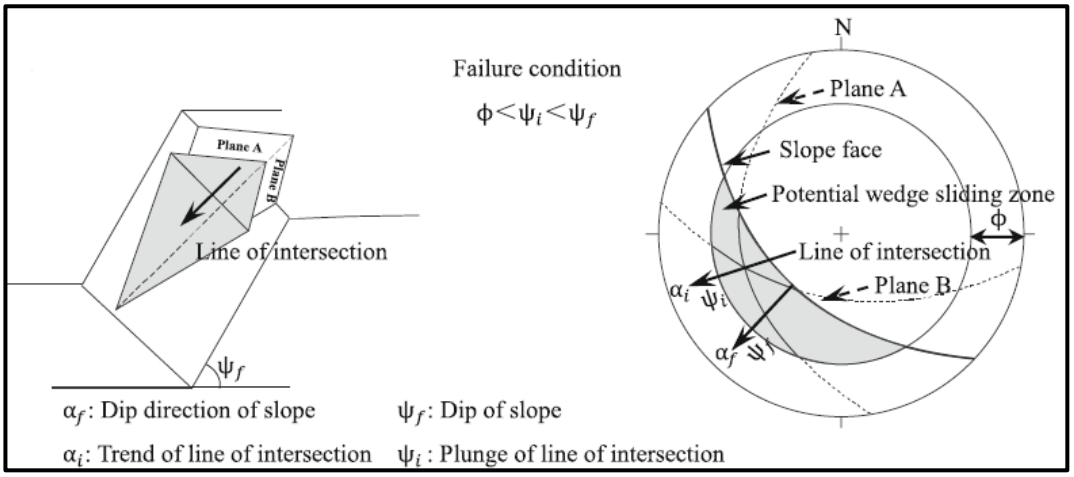

Figure 2.19: Kinematic and geometric conditions for wedge failure (Norrish and Wyllie, 1996).

In contrast to plane failures, wedge failure can occur under a variety of geometric conditions and geologic structures, according to Rusydy et al. (2019). The critical zone of a stereonet can be used to identify the

intersections of discontinuities that may cause wedge failure. The region between the friction angle and the slope angle, which is shaded in grey, is the crucial/critical zone of the stereonet, which is always indicated or shaded (see Figure 2.19). On the slope, wedge failure cannot occur if the discontinuities intersect outside the critical zone.

Toppling failure

According to Wyllie and Mah (2004), the discontinuity toppling failure occurs when the strike of the discontinuity is almost parallel (+/-20°) to the trend of slope, but the discontinuity drops steeply in the opposite direction of the slope, i.e., into the slope.

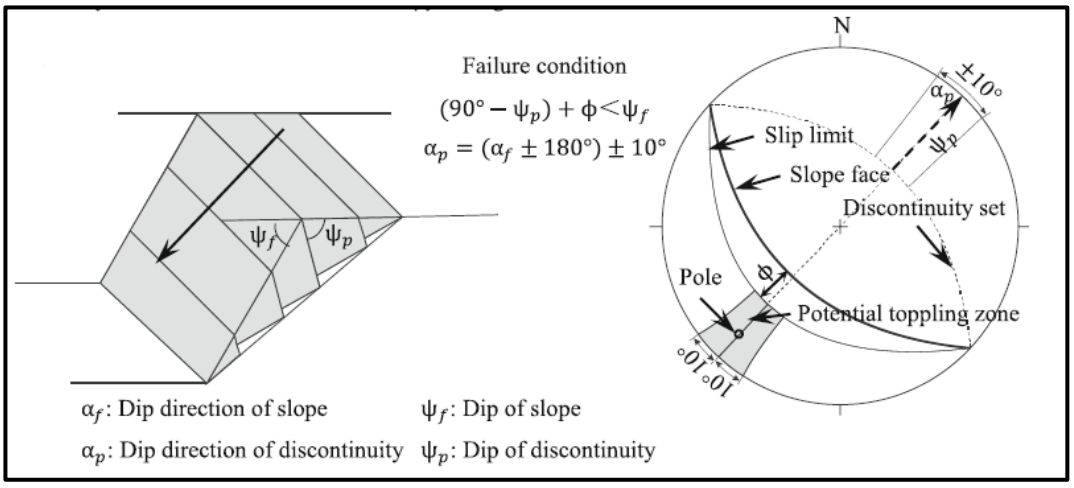

Figure 2.20: Kinematic and geometric conditions for toppling failure (Norrish and Wyllie, 1996)

Furthermore, the dipping angle of the discontinuity must be larger than the friction angle of the slope. Goodman (1989) states that inter-layer slide movement is a factor in toppling failures. According to Sari (2019), the crucial zone on a stereonet is when Toppling failure is discovered. As seen in Figure 2.20, this represents the area over the slip limit. The discontinuities of this region all cause slope failure via toppling mode. This occurs as a result of the discontinuities in the Critical Region being steeper than the slope angle.

In contrast to planar and wedge failures, toppling failure is among the most complicated types of failure. According to Wyllie and Mah (2004), there are three types of toppling failure: direct toppling, or block toppling; flexural toppling; and block-flexure toppling failure. Figures 2.21(a) and (b) show how the direct and flexural toppling may be analysed on the stereonet.

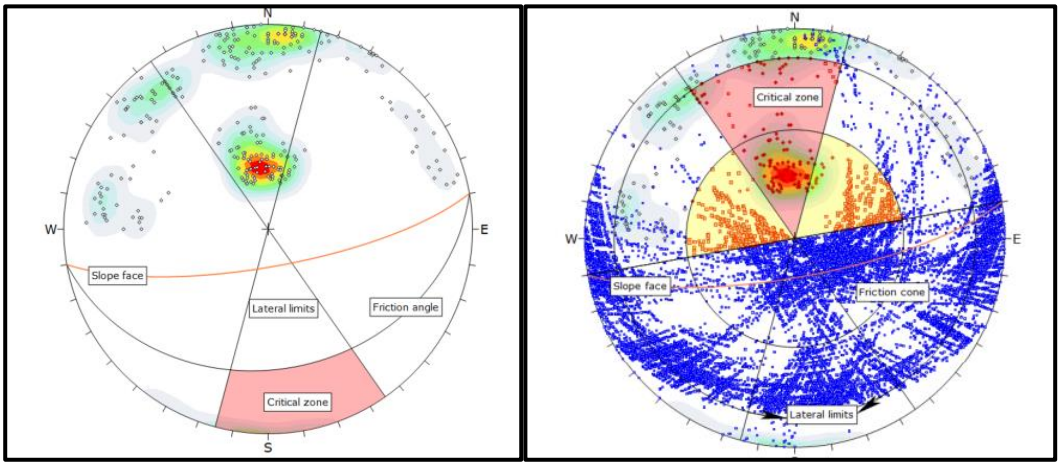

Figure 2.21: Stereonets showing two common types of toppling failures (a) Flexural toppling and (b) Direct toppling (After Sari, 2019).

The possibility of each failure mode—planar, wedge, and toppling—occurring is shown as a percentage during the analysis process. The percentage is obtained by comparing the total number of discontinuities on a given stereonet to the number of poles or junctions in the crucial zone (Awang et al., 2021).

Kinematic analysis is the usual practice for both local geologists and engineering geologists working on rock slopes, according to a review of case studies of engineering geology in Malaysia by Kong (2017). Kinematic analysis was used in many ways, either alone or in combination with other techniques for rock mass analysis.

The kinematic analysis is said to ignore the forces acting on the slope, the strength parameters of the discontinuities, and the rock mass. It is only able to determine the potential for slope failure, not the quantitative slope stability condition (Salmanfarsi et al., 2020). The kinematic analysis is applicable to slopes with structures. Kinematic analysis is still a crucial component in

determining the slope's quality. Kinematic analysis has been advised as the initial step before moving on to other analytical methodologies of slope stability, since it is still crucial for the assessment of structurally controlled rock slopes (Alzo'ubi, 2016; Raghuvanshi, 2019).

2.7.3 Limit equilibrium analysis

The study of limit equilibrium focuses on the moment at which a material reaches its limits of stability and beyond which failure might occur. For all limit equilibrium approaches, the shear strength (τ_f) along the sliding surfaces is found using the Mohr-Coulomb formula. The shear strength of the soil is the shear stress at which the soil collapses under shear. Janbu (1973) states that when the mobilized shear stress (τ) is stated as a percentage of the shear strength, a state of limit equilibrium exists.

According to Nash (1987), when the critical state requirements are met, the shear strength is fully mobilized along the failure surface at the instant of failure. The Mohr-Coulomb linear relationship may so often be used to represent shear strength, where τ_f and τ are defined by:

Shear strength: $$\tau_f = c' + \sigma' tan\theta' or (a - \sigma') tan\emptyset' \quad (2.4)$$

Shear stress: $$\tau = \frac{\tau_f}{F} = \frac{c' + \sigma' tan\emptyset'}{F} \quad (2.5)$$

Where a, c' and $\emptyset'$ are the attraction, cohesion and friction angle respectively in effective stress terms, and F is the factor of safety (FoS).

While mobilized shear is dependent on external forces acting on the soil mass, shear strength is determined by the type of soil and effective normal stress. According to Equation (2.3) above, the FoS is defined as the ratio of the shear strength (τ_f) to the shear stress (τ) in a limit equilibrium analysis.

Calculating the safety factor of the slope is essentially the main duty while analyzing the stability of the slopes.

It is important to remember that there are three definitions of FoS, which are force equilibrium, moment equilibrium, and limit equilibrium (Abramson et al., 2002). Figure 2.22 below does the greatest job of illustrating these concepts. Shear strength is the foundation of the first definition. Either the effective stress technique (α-$\emptyset$ analysis) or the total stress (S_u-analysis) can be used to get this. The kind of soil, the loading circumstances, and the amount of time that has passed since excavation all affect the strength consideration.

Aryal (2006) states that the effective stress method is utilized for long-term issues while the total stress approach is used for short-term circumstances. Moreover, the effective stress method may be used to any situation in which the pore pressure is known. The movement equilibrium and force equilibrium criteria for driving and resisting force and moment components, respectively, serve as the foundation for the second and third definitions.

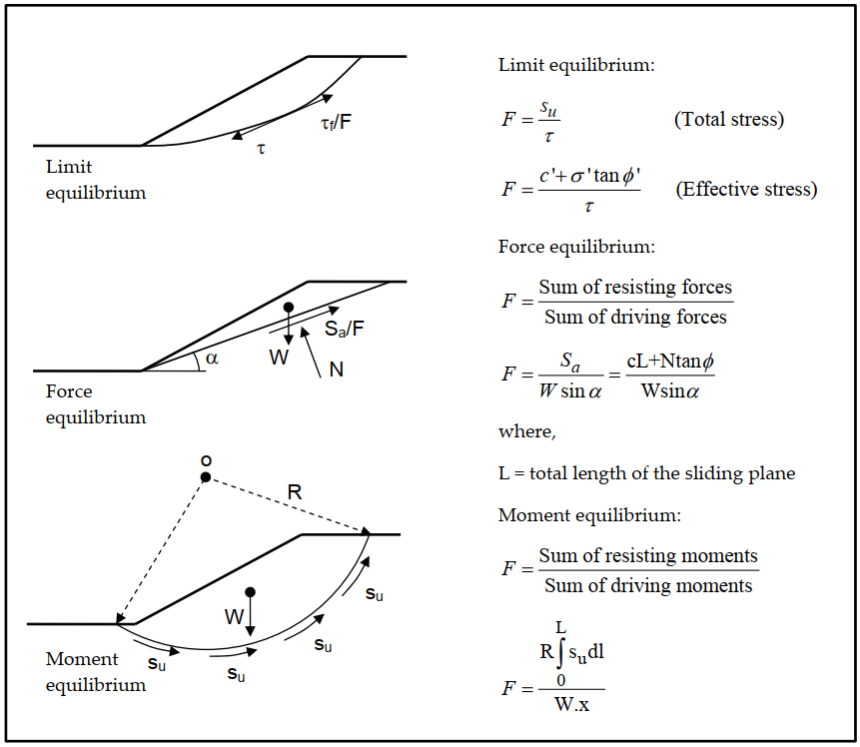

Figure 2.22: Various definitions of the factor of safety (FoS) (after Aryal, 2006).

With reference to reaching Limit Equilibrium, the following assumptions apply: (a) the use of a predefined failure mechanism; (b) the typical 2-D framework analysis which ignores the 3-D impacts (even if slopes are actually three-dimensional); (c) it is assumed that the soil mass moves as a rigid block, moving exclusively along the surface itself; d) it is expected that shear forces are mobilized locally. Shear stresses are often not mobilized equally throughout the whole failure surface. For analytical purposes, though, they are taken to be constant.

2.7.3.1 Approaches to limit equilibrium analysis.

Slope stability analysis can be done through deterministic or probabilistic approaches. These approaches are used for the project to ensure the required minimum security. These methods are discussed below.

Deterministic approaches employ parametric analysis to calculate the FoS of excavated slopes (Goh, 2017). These approaches require simply representative values (often the mean) for each physical and geomechanical parameter concerned. Furthermore, these techniques do not account for the variety and uncertainty of the geostructural and geomechanical properties of joints (Budetta, 2020). Furthermore, (Goh, 2017) said that deterministic FoS approaches or methodologies do not adequately account for the uncertainty of slope materials as well as excavation geometry.

The ratio of the driving forces to the resistance forces is another way that the FoS in the deterministic techniques is expressed. The deterministic approach is applied in different ways using different methodologies with varying degrees of applicability. Janbu's method and Sarma's approach are two instances of deterministic methods. The equilibrium state of the rock mass can be evaluated using these techniques (Janbu, 1973; Sarma, 1979).

The likelihood of slope failure is ascertained using probabilistic techniques (Suchomel and Masi, 2010). Similar to kinetic approaches, these techniques compute the failure probability while accounting for joint orientations, physical characteristics, and shear strength (Budetta, 2010).

Several authors have stated that probabilistic methods can be used to calculate the probability of failure on slopes with uncertain values or measurement errors, such that numerical models provide an inaccurate representation of the actual state of the slope condition (Li and Lo, 1993; Griffiths and Fenton, 2007; Gibson, 2011; Juang et al., 2019).

It is claimed that probabilistic approaches are more useful than deterministic methods for evaluating the stability of designed or artificial slopes when combined with slope risk assessment. Furthermore, probabilistic methods require more computing resources than deterministic methods. Because of this, some techniques, like Monte-Carlo simulations, may require thousands

of calculations to generate the desired amount of output variables (Gibson, 2011; Huang et al., 2016).

It is claimed that the Monte-Carlo approach uses random parameters as input to repeatedly calculate the FoS. Rather than producing a single FoS value, this leads to a distribution of FoS values that accounts for input parameter uncertainty (Tatone and Grasseli, 2010). Keep in mind that the FoS's numerous computations could be costly (Liu et al., 2020). Thus, Huang et al. (2016) noted that more probabilistic approaches may be applied to improve computation efficiency.

2.7.3.2 Limit equilibrium analytical methods

The limit equilibrium method has been the most widely employed strategy for resolving geotechnical engineering issues for many years. Over time, a number of limit equilibrium techniques have been developed. These techniques were created in order to analyse slope stability. According to Beyene (2017), the most popular analysis tools for slope stability issues are traditional limit equilibrium techniques.

Engineers primarily use FoS to determine how far or close a slope is to failing, as previously mentioned. Noroozi (2015) provided further confirmation of this. The practice of slope stability analysis dates back to the early 1900s. Nonetheless, Beyene (2017) pointed out that the Swedish State Railways had the geotechnical commission appointed in 1922 to look into remedies after an expensive slope collapse. The recorded technique was dubbed the Swedish Slip Circle Method. As implied by the name of the method, it is assumed that the slide happens along a circular arc.

Fallenius refined the Swedish Slip Circle technique and in 1936 came up with what is today called the Ordinary technique of slices, or Fellenuis method. The soil mass above the failure surface is divided into vertical slices using the slices technique. The stability of the slope is then determined for every slice. By assuming that the forces acting on the sides of each slice

cancel each other out, the Ordinary Method of Slices simplifies the problem. Despite the fact that these approaches can find the answer, low values for the computed FoS result from incomplete assumptions.

Then, in 1955, the Simplified Bishop's approach was developed as a result of modifications made to the standard method of slicing. By taking into consideration the normal pressures that exist between the slices, the Simplified Bishop's approach was improved. Still, this approach was unable to meet every need for static equilibrium. This is due to the absence of the horizontal force total, which indicates that the equilibrium approach is not complete. Spencer created the "spencer's method," a comprehensive equilibrium technique that fulfils both force and moment equilibrium forces, in 1967.

As a consequence, Spencer (1967) found that this approach was the most accurate in estimating the FoS. The Spencer approach is seen to be helpful as most slope failures do not have circular failure surfaces, even if it may still be modified for non-circular slip surfaces.

Other techniques exist for determining a non-circular failure surface's stability. Janbu (1954) presented two ways for this purpose: the Simplified method and the Rigorous method. While the simpler technique assumes that the interslice forces are zero and provides a correction factor to adjust for them, Janbu's rigorous method takes care of these forces. The Morgenstern-Price Method, created by Morgenstern and Price in 1965, is an additional technique for investigating slope failure for non-circular slopes. All of the static equilibrium equations are satisfied by the Morgenstern-price approach. Below, a few chosen techniques will be covered.

Below is a detailed discussion of the three selected approaches. These three approaches are Janbu's, Spencer's, and Bishop's methodologies. These techniques were picked because, among other things, the geotechnical engineering community views them as the most accurate (Beyene, 2017; Salunkhe et al., 2017).

As was previously mentioned, the Ordinary Method of Slices was modified to create Bishop's simplified method, also known as modified Bishop's method. It has been demonstrated that this technique yields FoS values that are within a few percent of the accurate values (Salunkhe et al., 2017). This approach considers that the moment equilibrium and vertical force equilibrium at the centre of the circular slip surfaces are satisfied, the horizontal force equilibrium is not taken into consideration, and the interslice forces are assumed to be horizontal or to be ignored.

For circular shear surfaces (SS), Bishop's simplified method (BSM) is reported to be widely used in practice. It takes into account the normal forces between the slices but ignores the shear forces between the slices (Abramson et al., 2002). It further satisfies vertical force equilibrium to determine the effective base normal force (N), which is given by:

$$N' = \frac{1}{m_\alpha}\sum(W - \frac{c'lsin\alpha}{F} - ulcos\alpha) \quad (2.6)$$

Where $m_\alpha = cos\alpha(1 + tan\alpha \frac{tan\emptyset'}{F})$ (2.7)

Since the BSM also assumes a circular failure surface, the following formula is used to determine the FoS:

$$F_m = \frac{\sum(c'l+N'tan\emptyset')}{\sum Wsin\alpha} \quad (2.8)$$

$$N' = (Wcos\alpha - ul) \quad (2.9)$$

Where $u =$ pore pressure,

$l =$ slice based length,

$\alpha =$ inclination of slip surface at the middle of slice,

$N' =$ Base normal force,

$W =$ force due to weight,

$c' =$ cohesion,

$\emptyset' =$ friction angle.

Equations (2.8) and (2.9) above were adopted from the ordinary method of slice, since both assume a circular failure surface.

It should be highlighted, therefore, that due to the non-linear connection caused by the FoS appearing on both sides, the computations need to be done iteratively. An overview of the BSM could be found here:

- Satisfies moment equilibrium for FoS,
- Satisfies vertical force equilibrium for N,
- Considers interslice normal force,
- More common in practice, and
- Applies mostly to circular shear surfaces.

The sketch below shows the forces that are used in the BSM method.

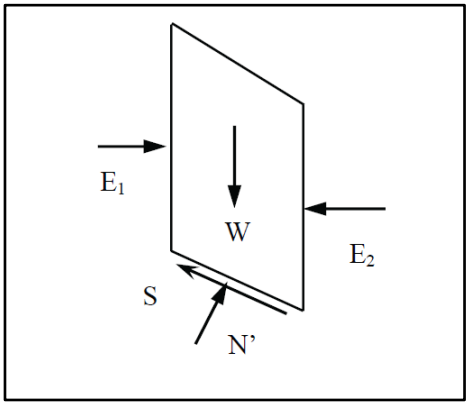

Figure 2.23: Figure showing the forces considered in the BSM (after Aryal, 2006).

Bishop's Rigorous Method (BRM) is an alternative approach to the BSM that takes into account the interslice shear forces (T) in addition to the interslice normal forces (E). Additionally, this technique fulfills the moment equilibrium of each slice and assumes an equal distribution of their resulting forces. An iterative approach determines the FoS and the interslice T and E (Aryal, 2006).

It is well known that Spencer's approach is a variation or expansion of Bishop's method. According to Agam et al. (2016), Spencer's approach was created in 1967. Because it tackles both the force and the moment

equilibrium of the mass failure, Spencer's technique of slices is regarded as one of the rigorous approaches. As a result, it is simple to compute the FoS precisely. One may use Spencer's approach to both circular and non-circular surfaces.

Note that there are simplifications required for all of the slicing approaches. In order to overcome the issue that there are more unknown parameters than those shown in the equations, they take this action. Various techniques disregard the shear forces and/or the interslice normal. That being said, Spencer's approach considers it. A force Q that acts at the midpoint of a slice's base M can be used to replace them in this way. The procedure assumes that the resulting forces have a constant inclination of θ degrees. In Figure 5.24 below, the slice forces taken into account for the Spencer Method are schematically illustrated.

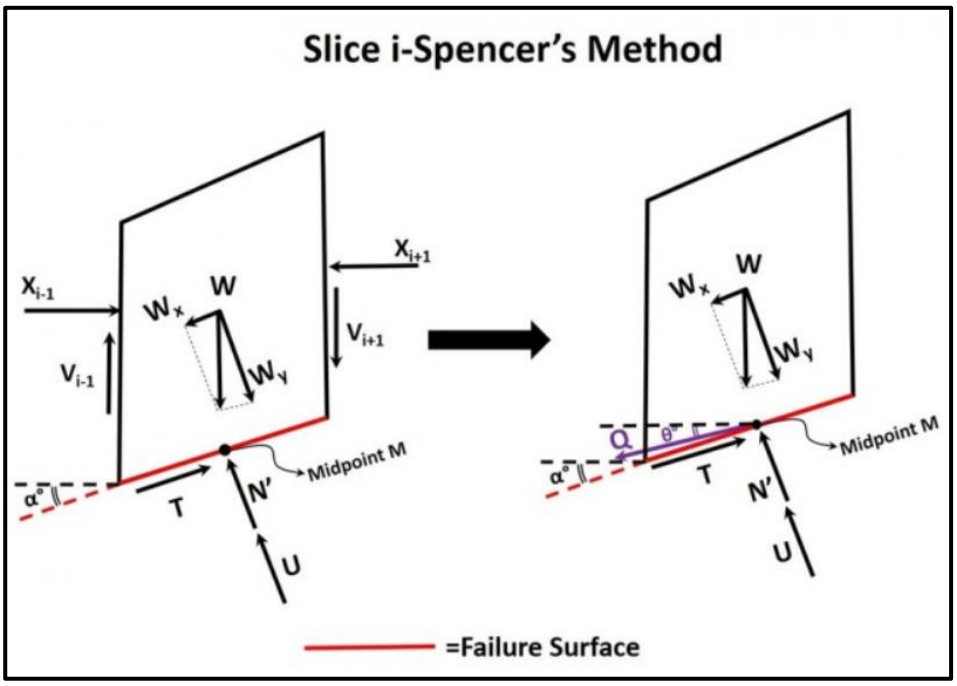

Figure 2.24: Spencer's method of slice and forces considered by the method (after Rabie, 2013).

Left side: Forces acting on a single slice include (a) the weight of the soil above the failure surface *W*; (b) the interslice reactions from the adjacent slices X_{i-1}, X_{i+1}, V_{i-1}, V_{i+1}; (c) the reaction of the stable ground which consists

of a normal effective *N'* and a shear component *T* respectively; and (d) the boundary water force *U*.

Right side: Assumption of Spencer's method in which interslice forces X_{i-1}, X_{i+1}, V_{i-1}, V_{i+1} are replaced by a single force *Q* acting at the midpoint of the base of the slice *M*.

Spencer's method is said to yield better FoS than other methods, hence it is preferred by many. Spencer's method requires six times more time to compute the FoS than the other methods. Therefore, this method is recommended to be used in critical potential failure analysis.

Janbu (1954) developed several methods which include: Simplified, Generalised and Direct methods. However, the generalized methods are considered the most popular method.

For non-circular slip-surfaces (SS), this technique is suitable. Since the shear forces are negligible, the interslice forces are considered to be horizontal. In this method, the FoS is computed by:

$$F = \frac{\sum c'l+(N-ul)tan\emptyset\prime)sec\alpha}{\sum Wtan\alpha+\sum \Delta E} \qquad (2.10)$$

Where $\sum \Delta E = E_2 - E_1 =$ net interslice normal forces (zero if there are no horizontal forces).

Among all of Janbu's approaches, this one is more preferred as it can deal with uneven terrain and slopes. It also does not need to be repeated. This is the first approach that fulfils both the force and moment equilibrium, according to Aryal (2006). Thus, the following formula is used to calculate the FoS:

$$F = \frac{\sum[\{c'l+(N-ul)tan\emptyset\prime\}sec\alpha]}{\sum\{W-(T_2-T_1)\}tan\alpha+\sum(E_2-E_1)} \qquad (2.11)$$

The total base normal forces (N) become a function of the interslice shear forces (T) as:

$$N = \frac{1}{m_\alpha}\left\{W - (T_2 - T_1) - \frac{1}{F}(c'l - ultan\emptyset')sin\alpha\right\} \qquad (2.12)$$

The foundation of this approach is a set of stability charts and dimensionless parameters (Janbu, 1954a). In addition to providing different load circumstances including groundwater, surcharge, and tension fractures, these charts offer a potent tool for doing slope stability analysis. Furthermore, the evaluation of the total and effective stresses may be performed using this approach. One may calculate the FoS for cohesive and frictional soils using the formula (Janbu, 1954a & 1996):

$$F = N_{cf}\frac{c}{P_d}, \quad \lambda_{c\emptyset} = \frac{P_e}{C}tan\emptyset \quad \text{and} \quad P_e = (1 - r_u)Pd \qquad (2.13)$$

Where $P_d = rH$ =total stress; P_e =effective stress; N_{cf} =stability number, which depends on the dimensionless factor ($\lambda_{c\emptyset}$), and $r_u = \frac{u}{\gamma z}$ =pore pressure ratio.

2.7.4 Numerical modelling in slope stability analysis

When analysing the stability of a slope, numerical modelling is a technique that has proven throughout time to be helpful in solving complicated problems with rock slopes. Note that the planning of an open pit mine is a complicated process in and of itself. Thus, adding the idea of geology and the strength of the rock makes it much more difficult (Kolapo et al., 2022).

The Limit Equilibrium approach might not be able to handle these complex and varied situations. Then, complex problems that the Limit Equilibrium approach is unable to resolve are best suited for the numerical approach. In addition to conducting a thorough rock slope research, the numerical modelling approach assists in simulating probable rock collapse processes (Stead et al., 2006; Kolapo et al., 2022).

The last several years have witnessed a significant surge in the development of high computing software tools and technological

advancements. As a result, geotechnical engineers now have access to computational tools that can perform a more thorough and trustworthy slope stability investigation. Suman (2015) states that there are three main categories into which numerical approaches may be categorized: continuum, discontinuum, and hybrid. The finite element and finite difference methods are within the continuum category. The Discrete Element Method and the Distinct Element are part of the Discontinuum category.

According to Fredj et al. (2018), the two most popular numerical techniques are Finite Element Method (FEM) and Finite Difference Method (FDM).

2.7.4.1 Finite Element Method (FEM)

For every given physical phenomenon, Finite Element Analysis (FEA) may be performed numerically using the Finite Element Method (FEM). Numerical mathematics is used to comprehend and describe any physical phenomenon, including thermal, wave, fluid, and structural behaviour (Harish, 2020). Further elaboration was provided by Wanstreet (2007), who stated that in Finite Element Modelling (FEM), discrete points known as finite elements are used to divide the real geometry of a structure. These points may be thought of as tiny portions of the structure.

At locations referred to as nodes, the elements are connected. A mesh is an assembly of nodes and finite elements. To accurately estimate the variables throughout a region of interest, attention must be taken in selecting both the quantity and kind of components. The stability of slopes may be analysed using the aforementioned principle. The FEM may concurrently evaluate the stress, strain, and displacement of the materials that comprise the slope, according to Chen et al. (2019).

In addition to that, FEM is able to determine or identify the critical slip surfaces with no assumptions made (Lu and Lai, 2011). There have been different authors such as Wanstreet (2007), Huo and Zhai (2012), as well

as Lu and Lai (2011) who have applied the FEM in different complex situations. Other authors such as Baba et al. (2012), Wei et al. (2010), Khabbaz et al. (2012), and Potgieter (2016) applied the method in comparison with other methods such as the limit equilibrium methods.

Over the years, several authors made use of the FEM in the analysis of the stability of slopes. As mentioned above, these authors applied the method in different conditions (Fumani, 2021). In order to further understand the processes of failure inside the slope, Wanstreet (2007) used FEM to perform research in which the impact of soil nailing on the FoS was examined. The shear strength reduction (SSR) approach was used to examine the stability of different slopes. Further supporting the claim stated by Huebner et al. (2001) that FEM is applicable in a range of engineering circumstances, the study was carried out on both reinforced and unreinforced slopes.

2.7.4.2 Finite Difference Method (FDM)

One of the older numerical techniques (older than the FEM) is the FDM. This approach is predicated on the claim that finite differences may adequately describe the governing differential equations of the theory of elasticity (Ullah et al., 2020). A multitude of computer programs utilize the FDM coding. One of the programs is the FLACSlope. The shear strength reduction (SSR) approach is used by FLACSlope.

Numerical techniques for calculating the FoS of slopes are made possible by the SSR analysis. While there are alternatives to the traditional LEM, FDM-based SSR often has various benefits for modelling jointed rock mass issues because it can easily integrate slip-along joints with failure through intact material (Dawson et al., 1999; Griffiths and Lane, 1999).

The most advantageous feature of FDM-based SSR analysis is its ability to automatically identify a wide range of failure mechanisms without requiring any prior assumptions about their kind, location, or form (Matsui and San,

1992). By lowering residual shear strength, altering the rock yield strength criterion, computing the stress and strain of the rock slopes, and examining the landslide's displacement, the strength reduction FLAC method has been utilized to assess slope stability (Ming et al., 2006; Yuke, 1999).

The FLAC model has been utilized by authors like Soren et al. (2014) and Mobaraki (2021) to evaluate the deformation of the slope of stresses at critically unstable failure zones, various failure types, and the safe and functional design of excavated slopes. The authors state that the goal of slope stability analysis through numerical modelling is to improve our understanding of the steps involved in identifying unstable zones, looking into possible failure mechanisms, designing the best slopes in terms of safety, dependability, and economy, and possibly creating corrective measures. This is in addition to providing precise values of stress and strain at specific points.

Following an evaluation of the pit slope's stability analysis based on the distribution of stress, displacement, and FoS, the authors concluded that recommendations should be made. Sengani and Mulenga (2020) provided more support for this by determining the FoS using both the FEM and the FDM. The FDM was utilized to illustrate the behaviour of the slope as water pressure increased, the scientists further stated. The displacement of the slope and the FoS were ultimately produced by the model.

2.8 Rockfall analysis

Section 2.3 above explained the types of failures which occur on the slopes. Those failures include planar, wedge, circular and toppling. Kolapo et al. (2022) pointed out that as toppling failure is occurring, the boulders from the top can bounce on other benches posing a threat to the lower benches. E’bayat (2017) emphasized that the rock fall can be assessed by making use of the rock fall simulation.

The rock fall simulations discuss the risks of falling rocks to the lower benches and locate the potential areas that can be affected by the falling rocks and the resting position of the rocks. The boulder falling on the slope may be simulated using a variety of programs. Rocfall and the Colorado Rockfall Simulation Program (CRSP) are a couple of the most popular programs (E'bayat, 2017; Maerz and Youssef, 2005).

2.8.1 Rocfall software

Rocscience has developed a number of geomechanics software packages, including the ROCFALL application. The application simulates rocks tumbling down a hill using statistics. Both two and three dimensions are used to model the rockfalls. According to E'bayat (2017), the program determines the energy, velocity, and bounce height of rocks at the locations of their path's endpoints. It should be mentioned that the user may set the slope geometry, the characteristics of the rock, and the obstacles using this adaptable application.

The degree of flexibility enables for comparisons between the various situations up to the point when the characteristics of the slope can be altered. ROCFALL can also be used to identify the obstacles. Either recently established or predetermined obstacles are in place. This makes it possible to place the barriers in the ideal area to effectively block rocks. Graphs and histograms are the outputs of the ROCFALL software (E'bayat, 2017; Ansari and Singh, 2013; Guzzetti et al., 2003). Figure 2.25 below shows an example of how the findings are presented by the ROCFALL simulation.

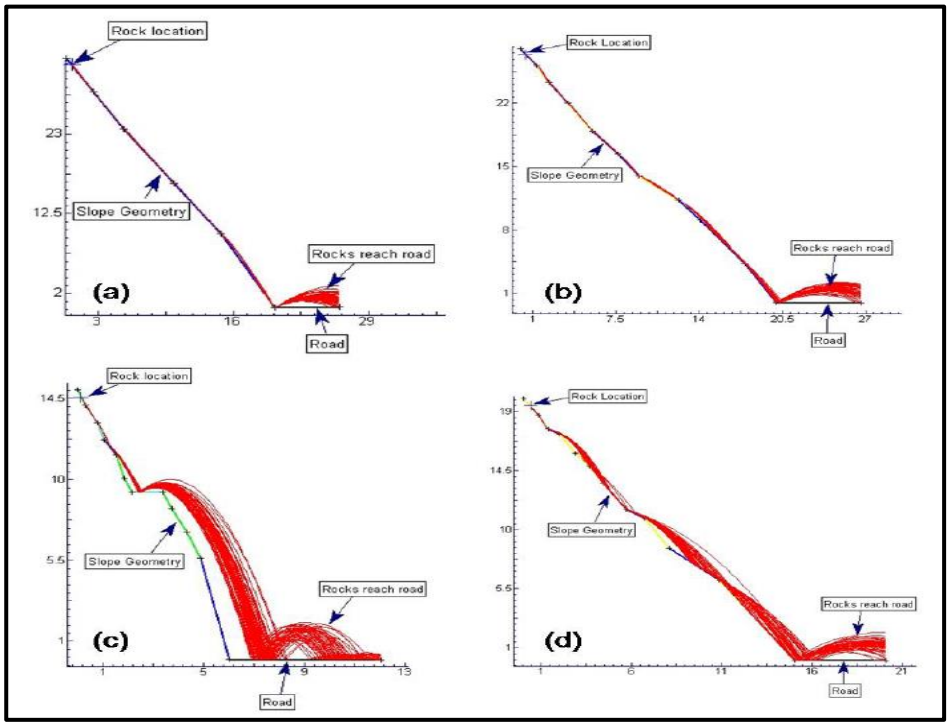

Figure 2.25: Example of how ROCFALL simulation presents the results of rockfall.

2.8.2 Colorado Rockfall Simulation Program (CRSP)

A 2-D numerical algorithm called the Colorado Rockfall Simulation algorithm (CRSP) is utilized to tackle rockfall rollout issues. Timothy J. Pfeiffer first designed the software in 1988 and used it to calculate the bounce height and velocity from the Colorado Department of Transportation. It was reported that the 2-D modelling in CRSP leads to some issues with the interaction and rotation of the slope face with non-spherical rock.

Consequently, depending on velocity, a cylindrical-shaped rock will behave in one of two ways during rollout: (a) it will roll end over end at a high speed, or (b) it will tumble and roll down the long axis at a slower speed. Because cylinder form is not employed in CRSP, it may have an impact on the results and have unintended implications. The CRSP-3D, a three-dimensional simulation of rockfall concerns, was introduced as a result. In modelling the interaction between the rock and slope geometry, CRSP-3D is thought to be more accurate than CRSP-2D.

According to Andrew et al. (2012), the CRSP-3D model helps to simulate several rockfall trajectories on a slope and can simulate the rotating movement of non-spherical boulders since it employs the Discrete Element Model (DEM) for dynamic model simulation utilizing the equations of motion.

2.9 Summary of the chapter

Based on the literature review, it is well established that various methods are used for slope stability, yet most of the scholars do not come clear in terms of the determination of the long-term stability analysis of the open pit. Furthermore, the simplicity methods are dominant in various studies and those methods do not incorporate stress and strain analysis in the determination of stability of the slope. As much as the slope is concerned, stress, strain, and Young's modulus among other parameters should be incorporated. Therefore, this gap allows this current dissertation to explore the long-term stability of the slope based on kinematic and numerical simulation which incorporate stress and strain relationship.

Chapter 3: Data collection and procedures for kinematic analysis, limit equilibrium and numerical simulation

This chapter details the methodology followed when collecting data for this research work. This includes field observations and measurements, kinematic analysis, limit equilibrium and Rockfall trajectory simulation. Field observations and measurements deals with discontinuities mapping, rock condition description and slope orientation measurements. Kinematic analysis is more concerned with the direction of movement of the rocks or slopes. Limit equilibrium analysis on the other hand determines the safety factor of the slope. Lastly, ROCFALL simulation method is then introduced to determine the position where the rocks might land in case of slope failure.

3.1 Introduction

This study made use of the Geotechnical data in order to run slope stability analysis by making use of kinematic analysis, limit equilibrium analysis and rockfall trajectory analysis. Each of the analytical methods uses different data sets, all collected during the Geotechnical investigation stage. The field data was collected at WG Wearne mine in Louis Trichardt (Makhado). Additional information used in this study was collected and estimated in relation to the WG Wearne mine.

Prior to any collection of the Geotechnical data, the first step was to conduct desktop study and reconnaissance survey of the area. This was done in order to plan the data collection in the mine. The reconnaissance survey outlined the number of benches per slope, the number of slopes in the open pit, overall slope orientation and also determine the area within the face of the bench where measurements will be taken from.

The plan for data collection was also outlined after the desktop study and reconnaissance survey. From the information obtained, the study area was divided into three different sections based on where each is facing. These sections are labelled A, B and C, as seen in Figure 3.1.

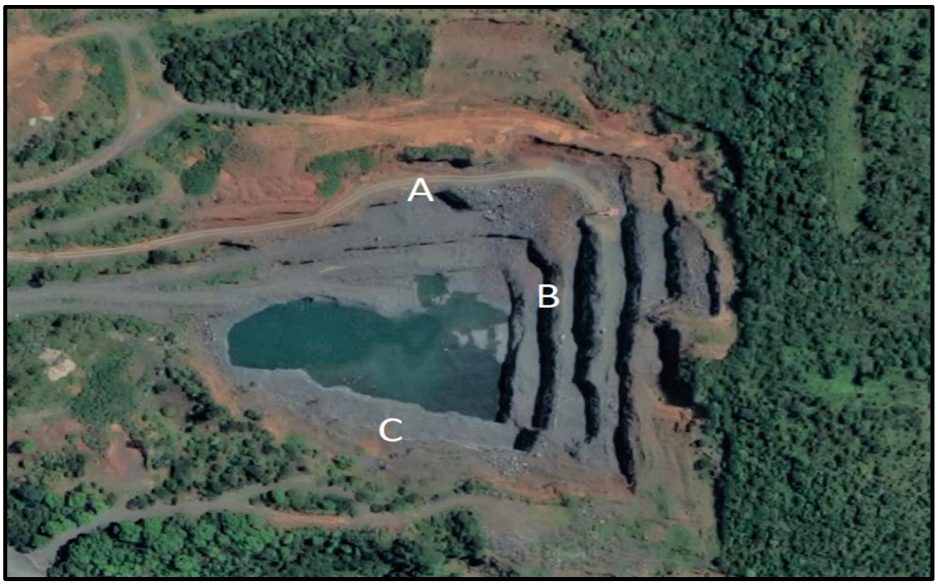

Figure 3.1: WG Wearne open pit showing its layout and different sections: Slope A facing South, slope B facing West and slope C facing North (Source: Google Earth).

The first step was desktop study and reconnaissance survey. This was followed by step 2 which was actual data collection in the field and rock mass properties estimation using a computer program. The field data collection and rock mass properties estimation are discussed in Section 3.2 below.

3.2 Geotechnical investigations

Geotechnical investigations were done in order to determine the mechanisms and types of failures associated with the open pit mine slopes. For this to be achieved, the geotechnical programme was divided into two main parts. The first part entailed field investigations and measurements while the second was stability analysis which was centred on both kinematic, limit equilibrium analysis and numerical modelling.

3.2.1 Field observations and measurements

This section entails the field observation of the study area in general. This included the pit orientation, slopes and bench dimensions. The study area as explained in Section 3.1 was divided into three sections or slopes; namely, slopes A, B and C. Each of these sections have different orientations and number of benches.

Section A had the slope dip and dip direction of 80° and 174° respectively. Additionally, the slope is made up of 5 benches with heights ranging from 6 m to 14 m. Section B had a dip and dip direction of 80° and 268° respectively. Slope B was made up of 6 benches of heights between 7 m and 15 m. Last is Section C which also had a dip of 80°; however, the dip direction of the slope was measured to be 25°. Slope C consisted of 4 benches with heights between 6 m to 12 m.

The height of the benches was measured by making use of a measuring stick which was erected vertically upwards on the face of the bench. A compass on the other hand was used to determine the benches orientations.

The width of the benches around the mine in all sections (A, B and C) were measured from the toe of the bench face to the crest of the bench by making use of a measuring stick. The use of a measuring stick provided enough distance from the toe and the crest of the benches for safety reasons. The measurements of the bench width were at an average of 15 m across all the benches. However, some benches have sections with wider widths than others. This is due to the expansion of the pit. The identified sections wider than the rest of the bench width are shown by the orange arrows on Figure 3.2.

Figure 3.2: Areas in Section A of the open pit mine with wider benches.

The collected information and will be essential when running simulations for slope stability analysis as well as the rockfall analysis. This is because those simulations require the number of benches in a slope amongst other parameters needed for the simulations to be successful.

3.2.2 Rock mass description and condition

The rock mass description and condition give the state of the rock mass which mostly entails geological description of the rock mass. This also included a general description on the weathering of the rock mass as well as the presence of water.

The overall rock mass description was done through classical observation techniques. The on-the-field observation strategy adopted for this research study started with the determination of the rock type. This was performed using the standard geological field mapping principles of rock identification. The geological principles begin off by describing the properties of the rock being observed, thereafter cross referencing them with the known rocks properties in order to give a name to the rock.

The observed rock was seen to be greyish in colour. By making use of a hand-held magnifying glass, the grains were found to be fine. After cross-

referencing the obtained data to the rocks with similar properties, the rock was concluded to be Basalt. In addition to the properties of the rock mass, the condition of the rock mass was observed, and it was found that the rock mass was slightly weathered, see Figure 3.3 below. There are some cracks with reddish colour which is proof of oxidation of the minerals within the rocks. One other aspect that needed to be addressed is the presence or absence of water from the face of the benches. Upon observing the face of the bench, the face was fairly dry, no running water was observed.

3.2.3 Discontinuities mapping

The section at which the mapping process takes place was selected after careful evaluation of the face. The evaluation process included looking for face clear of soil or any materials that can hinder clear mapping of discontinuities. This was done to avoid mapping areas highly damaged by blasting (i.e., crumbling rock) and areas mostly covered by loose materials such as soils. Figure 3.3 shows the area to avoid mapping on the left and the image on the right shows the type of area which was chosen for mapping.

Figure 3.3: Example of an unfavourable site (on the left) and a favourable site (on the right) for face mapping.

For this study, the scanline method was used for discontinuities mapping. The scanline mapping technique was discussed in Section 2.5.1 of the

literature review. Prior to any measurements, the type of discontinuities being measured is identified whether it is a fault or a joint. In order to map the discontinuities, a 30-m long and straight line is drawn horizontally across the face which was measured by making use of a tape measure. All the discontinuities that cut across the line were measured.

The aspects about the discontinuities which were measured included orientation, length, persistence and spacing of the discontinuities. The orientation (which includes dip and dip direction) was measured by making use of a hand-held compass. The lengths of the discontinuities as well as the spacing between the discontinuities were measured by making use of a measuring tape.

The additional information about the discontinuities was collected. This information included the number of joint sets available in the area of measurements, the presence of the infilling material in the discontinuities, persistence and roughness of the discontinuities. It should be noted that the discontinuities were found with no infilling materials in between. This additional information assists in the classification of the rock mass and further assist in determining the stability of the slopes since the stability of the slopes is dependent on the properties of the discontinuities.

Table 3.1 below were completed as part of the onsite collection of geotechnical data.

Table 3.1 Template of the table used during discontinuity mapping.

ROCK MASS RATING GEOTECHNICAL PARAMETERS				
LOCATION:				
Slope				
Slope orientation	Dip			
	Dip direction			
Slope height				
Joint description	Spacing			
	Persistence			

	Roughness			
	Aperture			
	Infilling material			
	Orientation			
Rock mass description	Water presence			

3.2.4 Estimation of additional rock mass properties

After observation and measurements of the data in the field, additional rock mass properties were estimated using the RSData computer program. The additional information collected included UCS of the rock mass, Geological Strength index (GSI), Intact rock constant and the disturbance factor of the rock mass. This will assist in further evaluating the strength of the rock mass.

The procedure for estimating rock mass properties is described below.

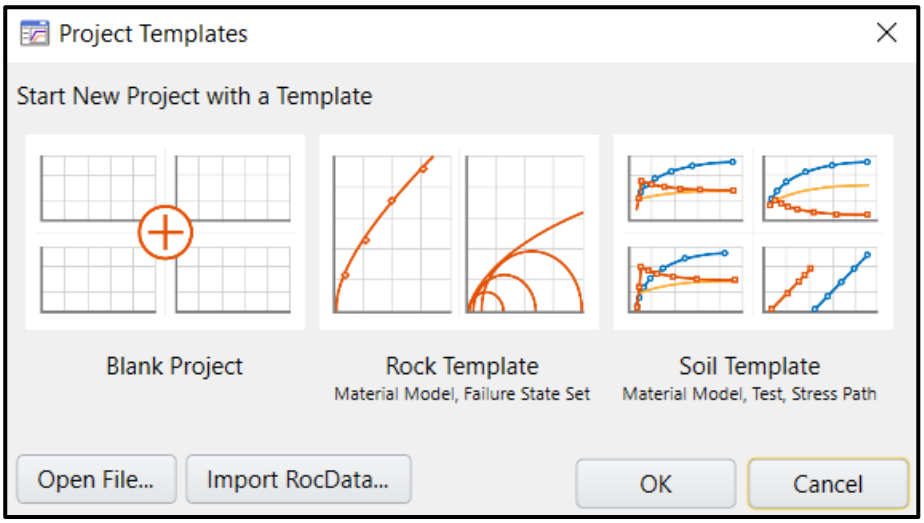

Figure 3.4: Window of the creation of a new file in RSData for the estimation of the rock mass properties.

Upon running the program, three templates (Blank project, Rock template and Soil template) automatically open up and for this study the rock template was selected (see Figure 3.4). After the rock template was selected, a default window (see Figure 3.5) opened up with default failure

states. However, this window also allowed for the rock properties to be adjusted to the study areas rock properties.

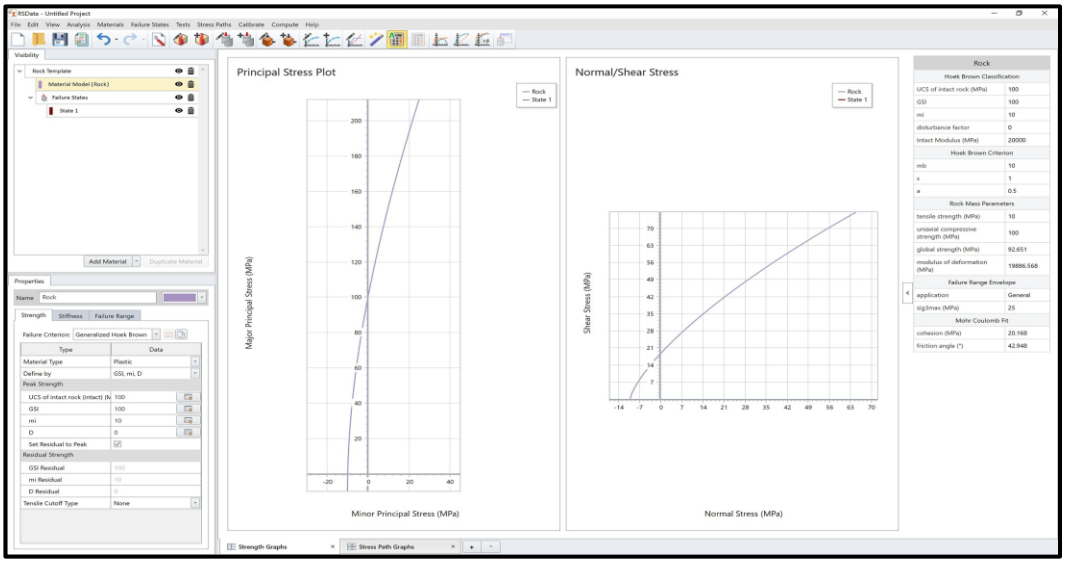

Figure 3.5: Default blank rock failure model in RSData after selecting the create a new file.

On the default window (Figure 3.5), a materials tab is selected in order to define the materials (see Figure 3.6). In the Strength tab, the failure criterion is selected and set to Generalized Hoek-Brown (see Figure 3.6). The Hoek-Brown criterion was chosen because it assumes that the rock mass is characterised by an elastic-brittle-plastic behaviour. Four aspects are used in Generalised Hoek-Brown failure criterion to define the strength of the rock which are UCS (of the intact rock), GSI, Intact Rock constant (mi) and the Disturbance Factor (D).

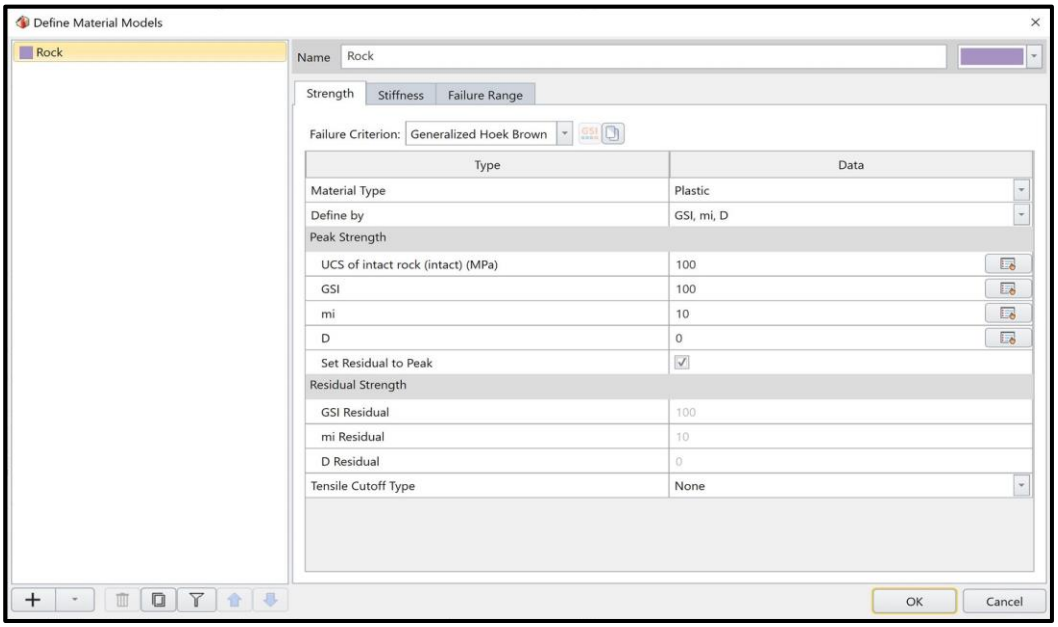

Figure 3.6: Screenshot of the RSData window defining the material properties.

The three aspects (i.e., GSI, mi, and D) were computed by the software through giving a detailed description of the rock mass in the mine. To define the GSI of the rock mass, it is selected under the peak strength tab, thereby opening the GSI picker (see Figure 3.7) window which allows the description of the rock mass in order to compute for GSI. The GSI picker is used as a guideline on how rocks on the slopes on the ground are fractured. The chart on the GSI picker have two major sections, one on the left which shows the structures of the rock mass to choose from and the right section shows the surface conditions which ranges from ‘very good’ to ‘very poor’.

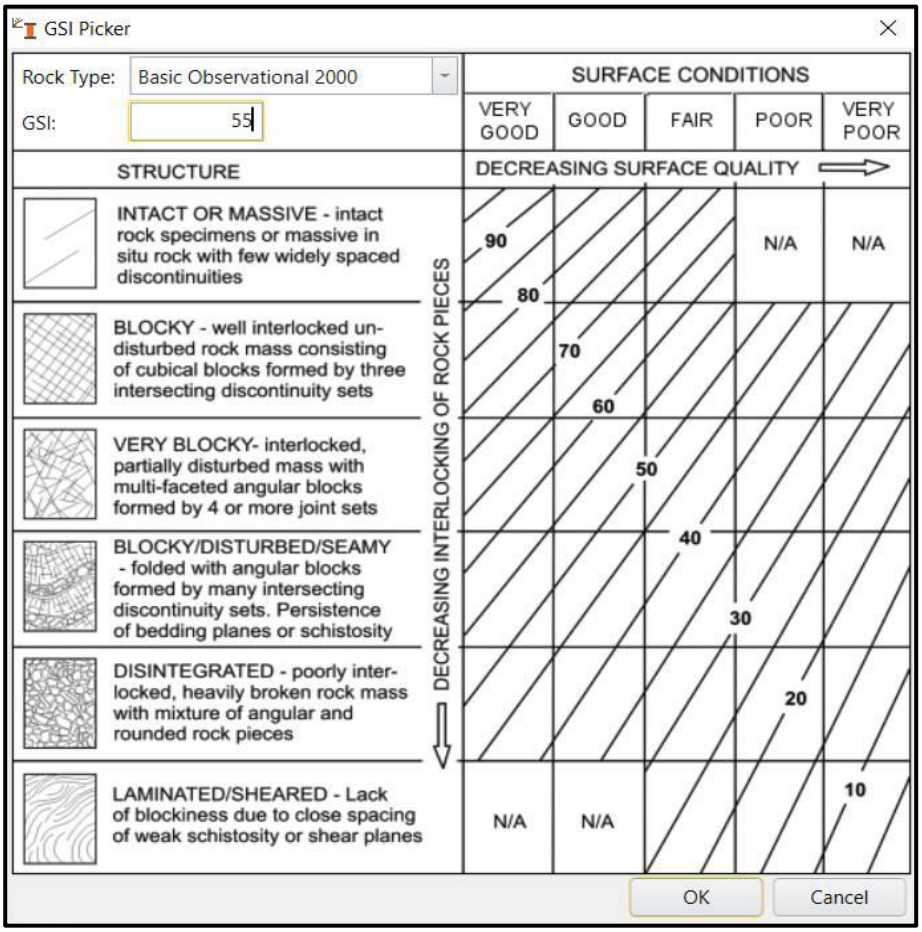

Figure 3.7: Chart used as a guideline in defining the quality of the slope properties, also known as the GSI picker in RSData.

The study area had a blocky structure, and the surface conditions were fairly good. By making use of the values shared in between the surface conditions and structure of the rock mass, the rating of GSI can be obtained. In our study area, it was found that the rock mass is blocky with discontinuities facing multi-directions and have more than four joint sets. As per the GSI picker, the rock mass is categorised as very blocky. In defining the rock mass conditions, Figure 3.8 was used as a guide to categorise the rock mass.

The study area had rough discontinuities with slightly weathered rock, and with some stains which are a result of oxidation of minerals as discussed in Section 3.2.2. By making use of this information and Figure 3.8, the rock

mass was categorised as good. This means the rating of GSI had to be between 50 and 60, therefore an average was calculated to be 55.

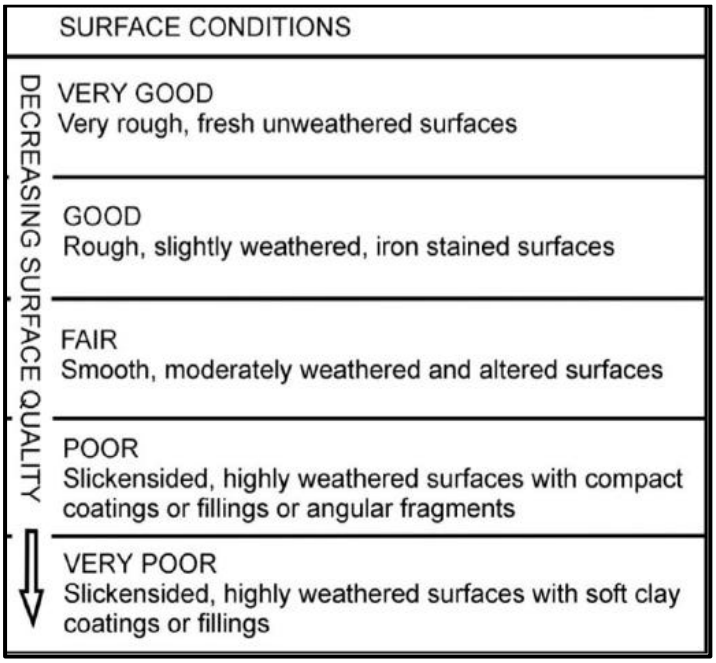

Figure 3.8: Surface conditions description extracted from the GSI picker from the RSData.

Provision for the Intact Rock Constant (mi) was built-in the RSData program. Upon selecting the mi button, different types of rocks appear along with their different values. Aladejare et al. (2022) pointed out that the mi value depends on the frictional characteristics of the component minerals in the intact rock. This in turn has a significant influence on the rock strength. Therefore, every single rock type has its own mi value.

However, the strength of the rock mass found at the WG Wearne mine is deteriorating due to the continuous drilling, blasting and material loading. Demirdogen and Yildirim (2022) stated that the blast damage and stress relief caused by excavation reduce the mechanical properties of the rock mass. This degradation or reduction of the rock mass strength is commonly referred to as a disturbance factor. The disturbance factor was determined from the computer program. Figure 3.9 shows a chart used to determine the disturbance factor for the slopes. At the top of the window for defining the

disturbance factor, the type of environment is selected which in this case a slope was selected.

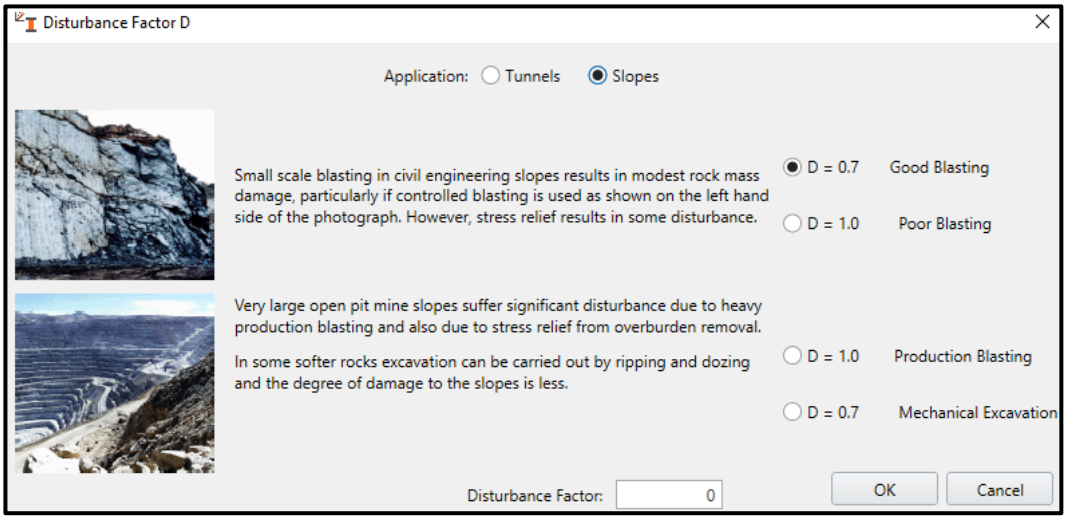

Figure 3.9: Selection of the disturbance factor in the RSData computer program.

The program has two slopes to choose from, one being the small scale and another being the large scale. For this study, small scale blasting was chosen, and the disturbance factor is defined based on whether the blasting of the slope was good or poor. The values are defined already built in the program, meaning no adjustments of the values. The disturbance factor for the slopes in the study was identified to be 0.7. This is based on the damage to the slopes due to blasting. The blasting damage represents the degree of disturbance whereby 0 represents undisturbed and 1 for a very disturbed rock mass. The blasting at the WG Wearne mine was controlled, however, the stress relief is said to cause some damage even though the blasting is controlled (Zhu et al., 2021). After all the parameters were defined, the outcome of the computation could be produced which is an estimation of the rock mass properties which will be presented in Chapter 4.

3.3 Geotechnical assessment of rock slope stability

As discussed in Section 2.7, there are several methods that can be used for the assessment of the stability of slopes. For this research study, three

approaches were used: the kinematic analysis, the limit equilibrium method, and numerical simulations. The implementation of these three approaches is covered in this section.

3.3.1 Kinematic analysis

The kinematic analysis of the rock cuts was conducted for the structurally controlled failure using DIPS computer program. This was done in order to estimate the possibility of failure. Three basic slope failure mechanisms were analysed using the DIPS program: planar, wedge, and toppling.

The data for kinematic analysis was collected during field observation and measurements. As described in Section 3.2.2, this data included discontinuities orientation, spacing, condition, aperture, and infilling materials. This allowed for the kinematic analysis to be executed by inputting the dip and dip direction of the discontinuities as the first step in the DIPS computer program. The dip and dip direction data was collected and recorded in accordance with Table 3.1. The discontinuities data was added to a new file as indicated in Figure 3.10.

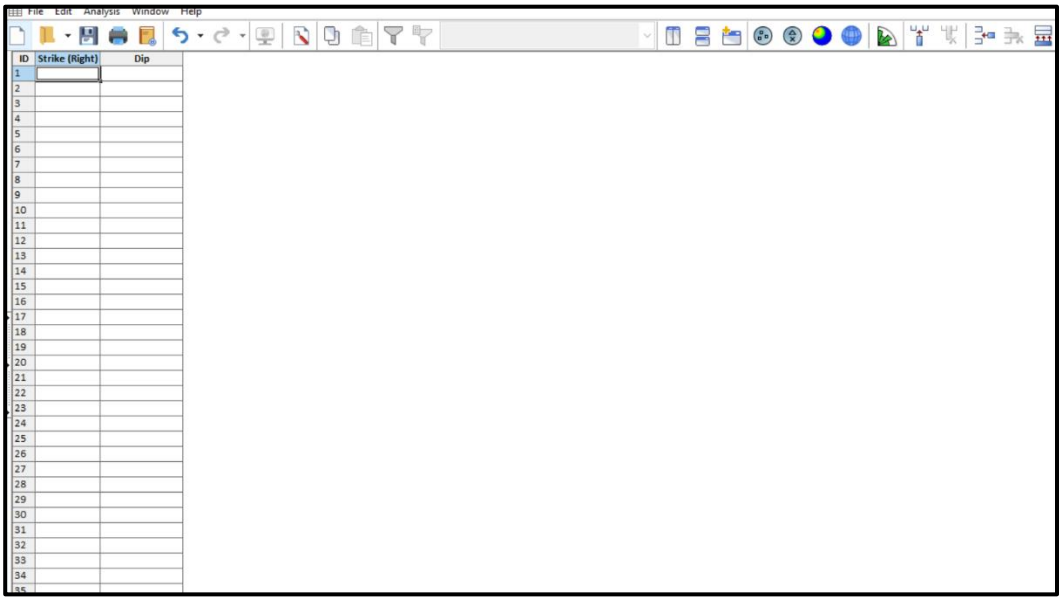

Figure 3.10: A blank window for starting a new project in DIPS.

A contour plot and the pole plot of the data were created with each pole plot representing the orientation of the recorded discontinuities. Afterward, the two were overlain to give a stereonet. Following the production of the pole plot and a contour plot, a rose diagram was then developed to determine the dominant orientations (joint sets) within the plane (the contour plot, pole plot and rose diagram are presented in Chapter 5 which forms part of the results produced).

Then, on the Analysis tab of the program, the Kinematic option was selected in order to analyse and determine the mode of failure of the slopes. It should be noted that the analysis of different modes of failure was done individually. Under the Kinematic Analysis tab, the mode of failure which needs to be analysed is then selected (i.e., Planar, Wedge, or Toppling). All the plots were conducted with a mean friction angle of 22.924°. The friction angle was obtained from estimating the rock mass properties using the RSData computer program (which was discussed in Section 3.2.2 of chapter 3). The results from the rock mass properties estimation are presented in Section 4.3 (Table 4.1). The Slope dip directions were measured using a hand-held compass for slopes A, B and C and the values were found to be 174°, 268°, and 25° for slopes A, B, and C respectively. A summary of the slope orientation data and the friction angle used on this study is presented in Table 3.2 below. Since the study area is divided into three sections, three separate kinematic analysis files were created. They are each presented below in separate sub-sections.

Table 3.2: Summary of the data used in the kinematic analysis.

Slopes	A	B	C
Slope Dip	80°	80°	80°
Dip direction	174°	268°	25°
Friction angle	22.924°	22.924°	22.924°

3.3.1.1 Planar failure

A stereonet analysis was performed for planar failure to indicate the unstable zones and the joint sets that have the same property and behaviour. This was done by selecting the planar option indicated by a red square on the Kinematic Analysis window given in Figure 3.11.

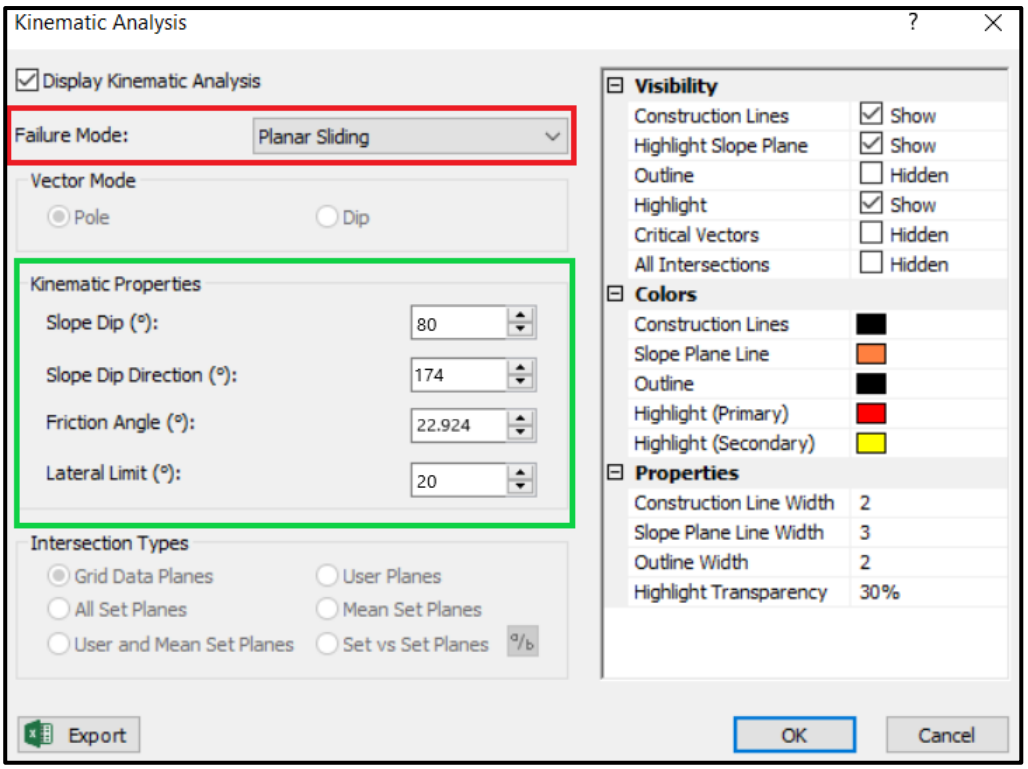

Figure 3.11: Planar failure setup screenshot with the failure mode in a red rectangle and kinematic properties in a green rectangle.

Under the Kinematic Properties section (area with a green rectangle around it on Figure 3.11), the slope dip, slope dip direction and friction angle are inserted. The slope dip angle was measured by making use of a hand-held compass and for slope A, it was measured and found to be 80°. The procedure for determining the slope orientation was detailed in Section 3.2.1. The friction angle was also determined through the use of the RSData computer program explained in Section 3.2.4 and the results were presented in Section 4.3 (Table 4.1). For slope A, the friction angle was found to be 22.924°.

3.3.1.2 Wedge failure

Wedge failure analysis was also conducted in a similar way as the planar failure as presented in the previous section (Section 3.3.1.1). However, on the Failure Mode entry (section with a red rectangle on Figure 3.12), Wedge Sliding was selected.

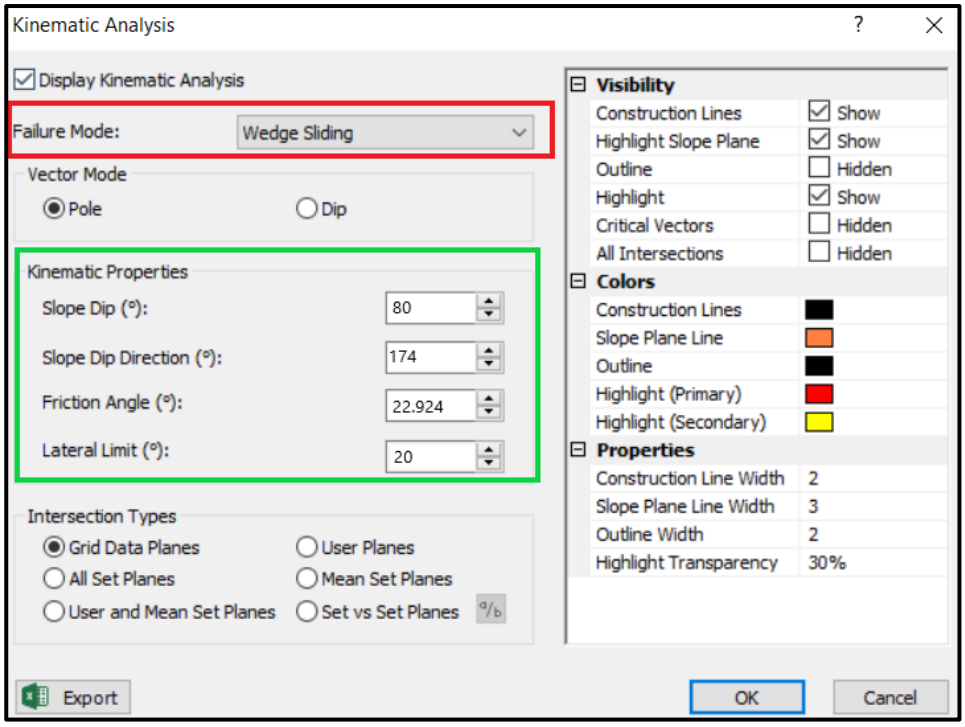

Figure 3.12: Wedge failure setup screenshot with the wedge failure mode selection panel in a green rectangle and the kinematic properties in a green rectangle.

Since wedge failure is being conducted for the very same three slopes, the slope dip angle and slope strike direction should be similar to the ones used for the planar failure analysis. In other words, the slope dip direction and dip angles for slope A should be similar when conducting planar, wedge and toppling failures. The same goes for slopes B and C. The slope orientation and data collection are discussed in Section 3.2.1.

3.3.1.3 Toppling failure

Toppling failure was analysed using the Direct Toppling option shown in Figure 3.13. In terms of the kinematic properties, the slope dip, slope dip direction, and friction angle were entered as per Table 3.2. Here also, toppling failure analysis was conducted on all three slopes, i.e., slopes A, B, and C.

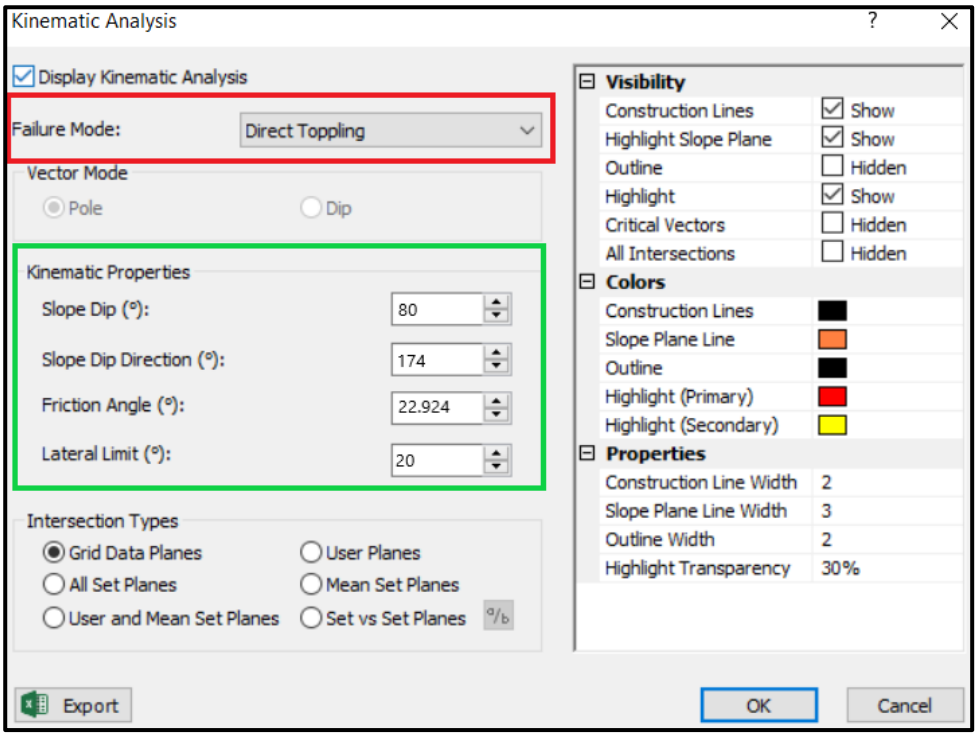

Figure 3.13: Toppling failure setup screenshot with toppling failure mode selection panel in a red rectangle and the kinematic properties in a green rectangle.

After all the analyses are done (Plane, Wedge and Toppling), The number of poles were presented. The discussion on how poles are presented on a stereonet is detailed in Section 2.7.2. DIPS computer program goes further to analyse the discontinuities that can lead to failure. The discontinuities that lead to a specific failure are found in the critical zone of the stereonet. The results of the kinematic analysis are later presented in Section 5.2.

3.3.2 Limit equilibrium analysis with SLIDE2

The limit equilibrium method (LEM) as presented in Section 2.7.3 is considered to be the most widespread method in slope stability analysis. An LEM slope stability software called SLIDE2 is used to assess the probability of failure or safety factor of both circular and non-circular failure surfaces in rocks and soils.

It does so by analysing the slip surface using the vertical slice or non-vertical slice limit equilibrium. In order to achieve this, the SLIDE2 program is opened, and a new project is started. This is then followed by generating limits, project settings, entering boundaries, computing and analysis. These steps are explained in detail below.

As a starting point, Figure 3.14 shows the window that opens up when the new project option is selected.

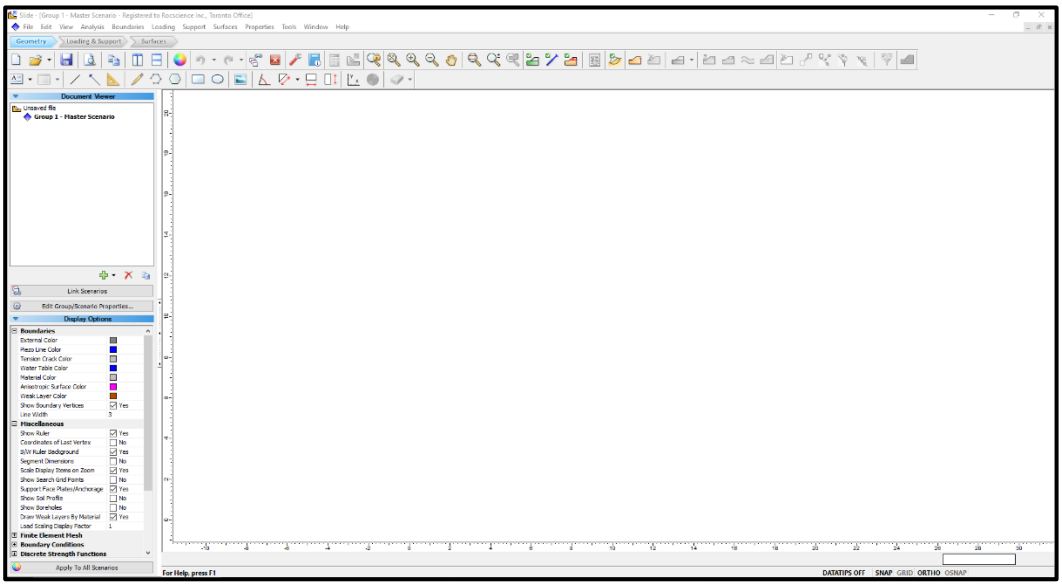

Figure 3.14: New project window opened in SLIDE2.

Following the selection of the new project option, the limits of the model are then generated. This is achieved by selecting the View tab and then Limits on the taskbar. The limits are generated in order to define the limits of the XY coordinates. These coordinates are entered in a dial box as indicated in Figure 3.15.

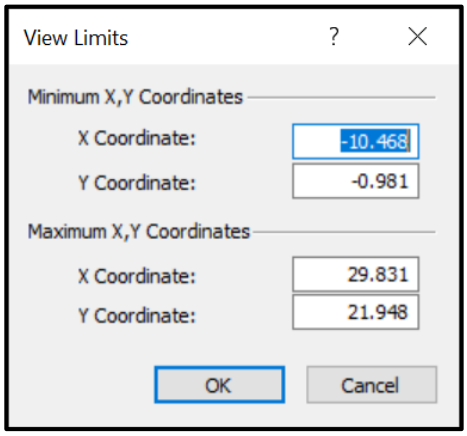

Figure 3.15: Generating limits of the model in SLIDE2.

After generating limits, the next step was to define the project settings (see Figure 3.16). The project settings included the following tabs which needs to be defined: failure direction, units of measurement, methods to be used, and groundwater conditions. On the project settings window, the first tab was the 'General' tab. This tab allowed the project title to be defined. Furthermore, the units of measurements were selected and for this study, the metric system was used as a preferred system of measurement as opposed to the imperial system. In addition to that, the failure direction was chosen. This simply defines how the model to be produced will appear. This means that if the failure is from left to right, the slope failure will be from left to right and vice versa. The chosen failure direction for this study was from right to left.

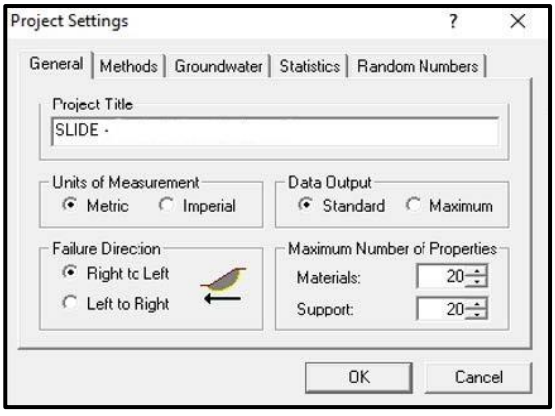

Figure 3.16: Project settings for the SLIDE2 model.

The next tab on the project settings was the methods to be used for Limit Equilibrium analysis (see Figure 3.17). Section 2.7.3 discuses the methods that can be used for Limit Equilibrium analysis. This research study made use of the following LEMs: Bishop's simplified, Janbu's simplified, Morgenstern-price, and Spencer's. These methods were selected as shown in Figure 3.17 to allow for a thorough and improved interpretation of the outputs produced. All the methods included in the analysis have different approaches and each has its own limitations; hence, the use of multiple methods.

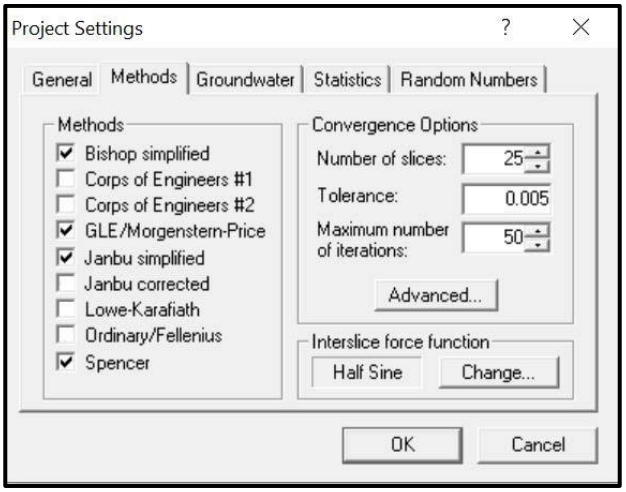

Figure 3.17: Selection of the analytical methods in the SLIDE2 program.

In the context of this research, SLIDE2 was rated according to the standard properties of rocks such as unit weight and hardness amongst others. On the properties tab, the materials are defined (Figure 3.18). The properties defined include cohesion and water presence on the rock mass. The cohesion of the rocks along with other rock mass properties was determined in Section 3.2.4 which discusses the estimation of the rock mass properties. The results of rock mass properties which include the cohesion estimation are presented in Section 4.3 (Table 4.1). Furthermore, the probabilistic Monte-Carlo technique was selected as the analysis tool of choice in this work due to its simplicity. The probabilistic method was chosen over the deterministic methods since they have difficulties in handling the variations and uncertainties of the rock properties. The probabilistic methods have

seen a great increase in applicability from authors such as Sari (2009), Sari et al. (2010), and Cai (2011) since they account for variations and uncertainties in the rocks. A full description of the deterministic and probabilistic methods was given in Section 2.7.3.1 of Chapter 2.

The Monte-Carlo method is a probabilistic method which uses statistical calculations in order to determine the slope stability. During the calculations, this method assigns random variables of the strength parameters of the rock (cohesion and friction angle). The method runs repeated calculations until the values of failure are determined.

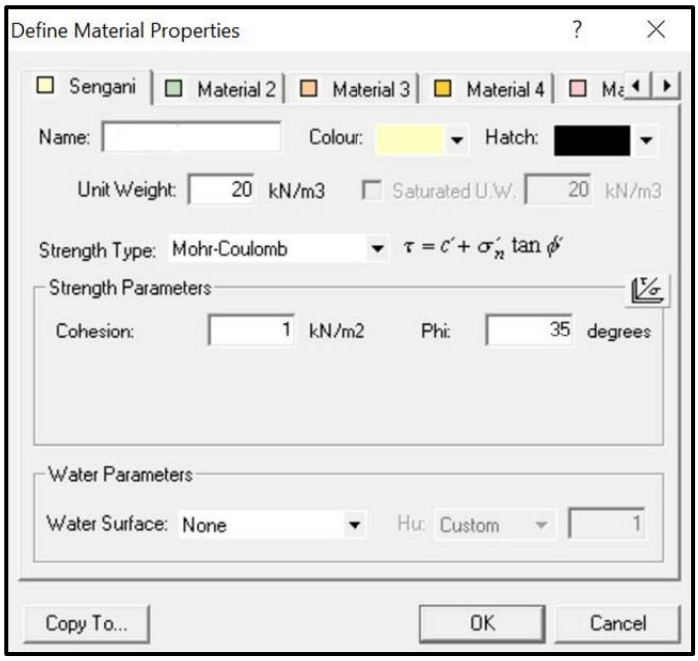

Figure 3.18: Defining the soil and rock mass properties.

After defining the material properties, the next step was to define the boundaries of the pit slope. The boundaries of the pit slope are based on the measurements of the slope benches presented in Section 3.2.1 thereby extrapolating the slope dimensions. After the generation of boundaries, the model will be presented as shown in Figure 3.19.

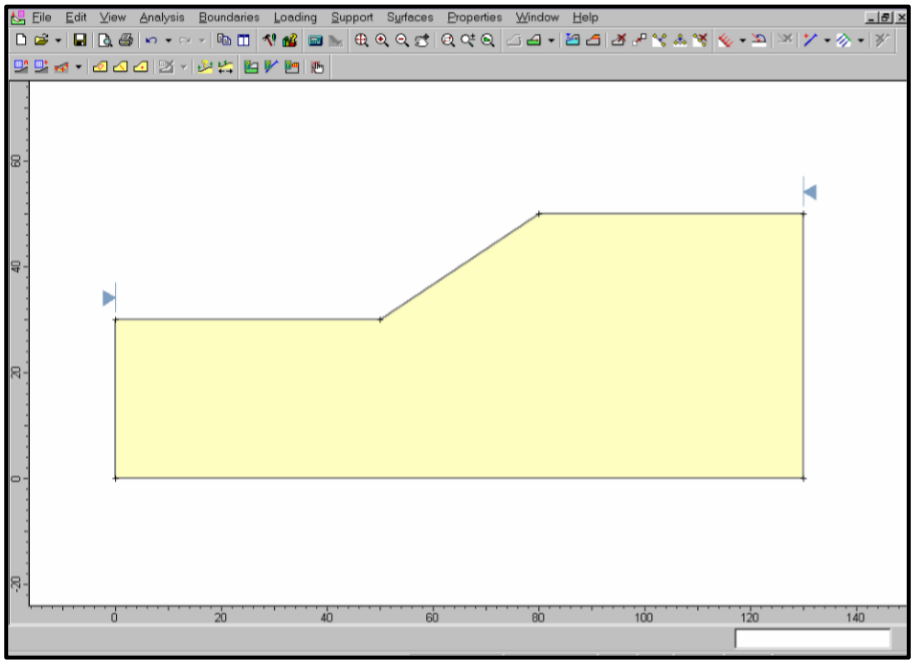

Figure 3.19: Example of SLIDE2 computed slope to display critical slip surface and FoS for circular failure.

Since the model of the slope is generated, the analysis of the slope can be done by selecting the analysis tab and then click the compute icon on the toolbar. In doing so, this will allow the analysis of slope stability to be done. This is done by selecting interpret on the analysis tab, thereafter, select the interpret icon. This will open a window on which the results of the computation will appear. The results are presented in Section 5.3 of Chapter 5.

3.4 Numerical analysis of rock behaviour

As previously explained Section 2.7.4, kinematic analysis and LEMs are said to have limitations in their applicability. Numerical analysis was used to generate complementary data to support the analysis of the slope stability covered in Section 3.3.

In this study, the OPTUM G2 software was used to simulate the behaviour of the slope when discontinuities deepen through the rock mass. Indeed, discontinuities tend to expand when there is disturbance of the ground

which may be due to blasting and the operation of heavy-duty machinery. The frequency of the discontinuities (which is the number of joints per unit area) also increases in the presence of ground disturbance. In addition to OPTUM G2, ROCFALL was used as another numerical tool to simulate the behaviour of the rocks in the events of rockfall.

3.4.1 Slope behaviour analysis using OPTUM G2

OPTUM G2 is a computer program that is based on the Finite Element Analysis (FEA) technique. The software package can be used for the analysis of geotechnical stability and rock mass deformation amongst others. In order to begin the analysis, a new project was started. A window of the new project popped up as shown in Figure 3.20.

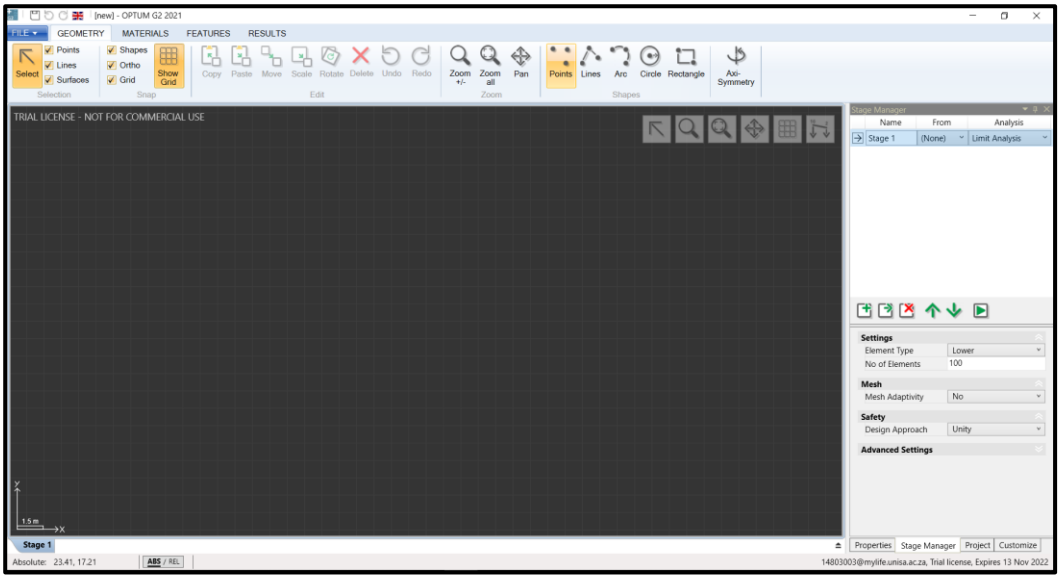

Figure 3.20: New project window in OPTUM G2.

In order to simulate the failure that can occur in the presence of discontinuities, firstly the pit needs to be designed following the number of benches per slope. The information about the number of benches per slope was recorded in section 3.1. On the taskbar of the new project window, a geometry section was selected. The line shape was selected on the shapes section. By making use of the line shape, the pit was designed. As can be seen in Figure 3.21, the working space is made up of a grid. In preparing

the platform and prior to designing the slope, one box in a grid was set to correspond to 1 m^3 on the ground. After the set up was done, the slope was then designed as seen in Figure 3.21.

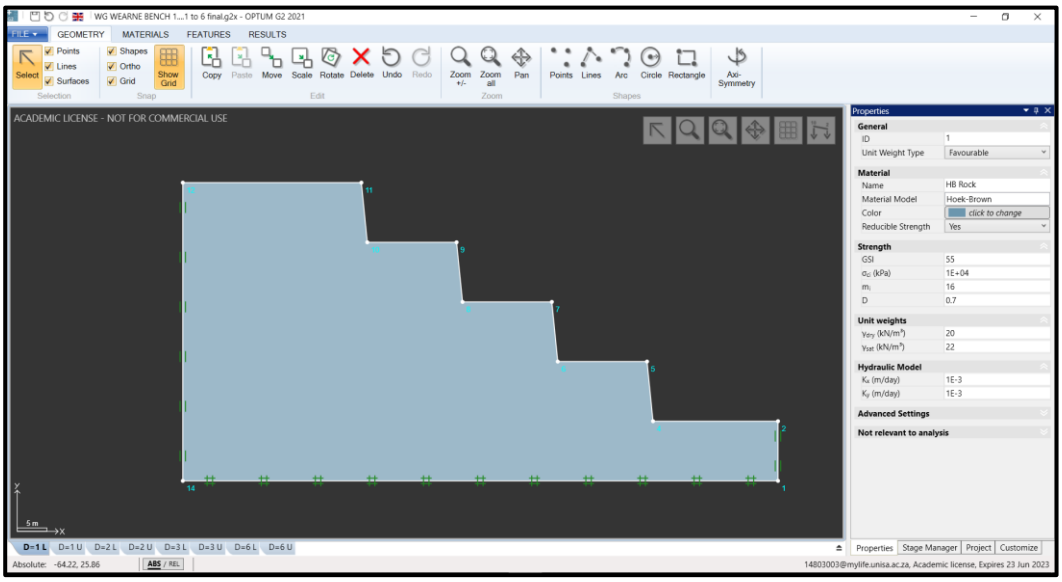

Figure 3.21: Design of the open pit.

It should be noted that the design of the slope was done for all slopes individually (namely, slopes A, B, and C) since they all differ in terms of their dimensions and number of benches. After the design of the slopes, the material properties were defined on the right-hand panel of Figure 3.21. From there, the Hoek-Brown criterion was selected to describe the rock material. Indeed, the Hoek-Brown criterion assumes that the rock mass is characterized by an elastic-brittle-plastic behaviour while the Mohr-Coulomb criterion assumes an elastic-perfectly-plastic behaviour (As explained in section 2.6.2). The Hoek-Brown criterion was used in this work for its reliability and simplicity (Mehranpour and Kulatilake, 2016).

Discontinuities were introduced as indicated in Figure 3.22. The discontinuities were introduced following the statement made by Sun et al., (2022) which clearly stipulates that failure of the slopes is mainly related to the presence of the discontinuities. The OPTUM G2 therefore comes in as a tool to determine the role of the depths at which the discontinuities play in the stability of the slope. Simulations were run with discontinuities 1 m, 2 m,

3 m, and 6 m deep from the slope face. The spacing of the discontinuities was kept constant at 1m apart. This was done in order to analyse the failure pattern in cases where the discontinuities continue to deepen or propagate deep into the slope due to continuous mining activities in the pits. These activities specifically refer to drilling, blasting and machine operation.

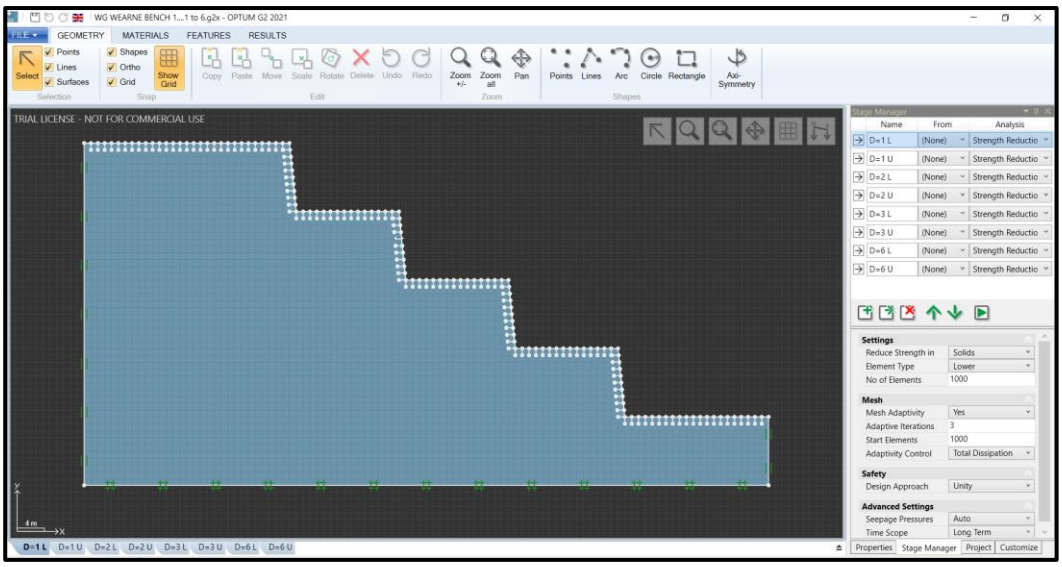

Figure 3. 22: Inclusion of discontinuities on the slope.

The white lines that run from the surface of the slope into the slope represent the discontinuities. These discontinuities were inserted by making use of the line tool on the shapes section of the task bar of the program. Figure 3.22 shows when the discontinuities were at 1-m deep into the slope. In addition to defining the properties of the rocks, on the bottom right corner of the right panel, the Stage Manager option is chosen to further define how the analysis should be run. In this study, the strength reduction analytical method was used to analyse the stability of the slopes. The strength reduction method was chosen because of its advantages since it reduces the cohesion and internal friction angle which are the components of shear strength. As a result, the method determines the factor of safety at which failure might occur. As can be seen in Figure 3.23, several methods of analysis are available; however, in this case, the strength reduction method was used to assume that the strength characteristics of the materials are

reduced by a certain factor until the loss of stability or failure of the structure occurs.

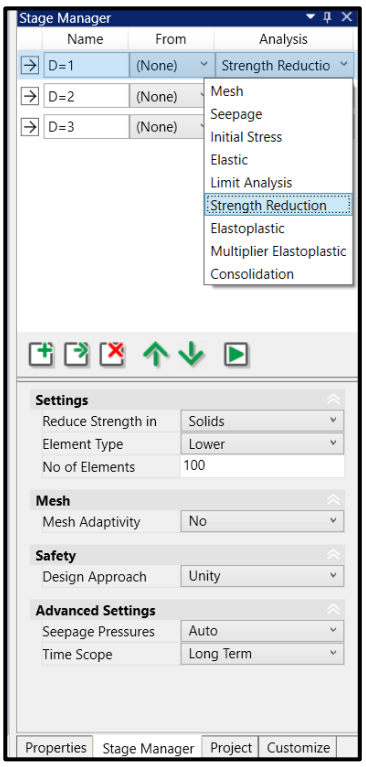

Figure 3. 23: Stage Manager tab and selection of analytical method.

After choosing the analytical method, the time scope of the analysis was chosen and 'long-term' was the one to go for. This was in conjunction with the topic of the study which aims at addressing the long-term stability analysis of the slopes. After all the parameters were well defined and the analytical method chosen, the Analysis tab was run in order to determine the strength reduction factor of that particular slope. The outcome of the analysis is presented later in Chapter 5.

3.4.2 Rockfall behaviour simulation using ROCFALL

As previously stated in Section 2.8 of Chapter 2, slope stability should not only end at determining the probability of failure and the type of failure that might occur on the slope. The scope of slope stability analysis should extend to determining the material control and remedy actions. This is done

in order to prevent or minimize the damage that can be caused by the failure.

This study applied the rockfall trajectory simulation using the ROCFALL computer program. This program simulates the trajectories of the rocks falling from the slope. A ROCFALL simulation begins with the creation of a new project (Figure 2.24).

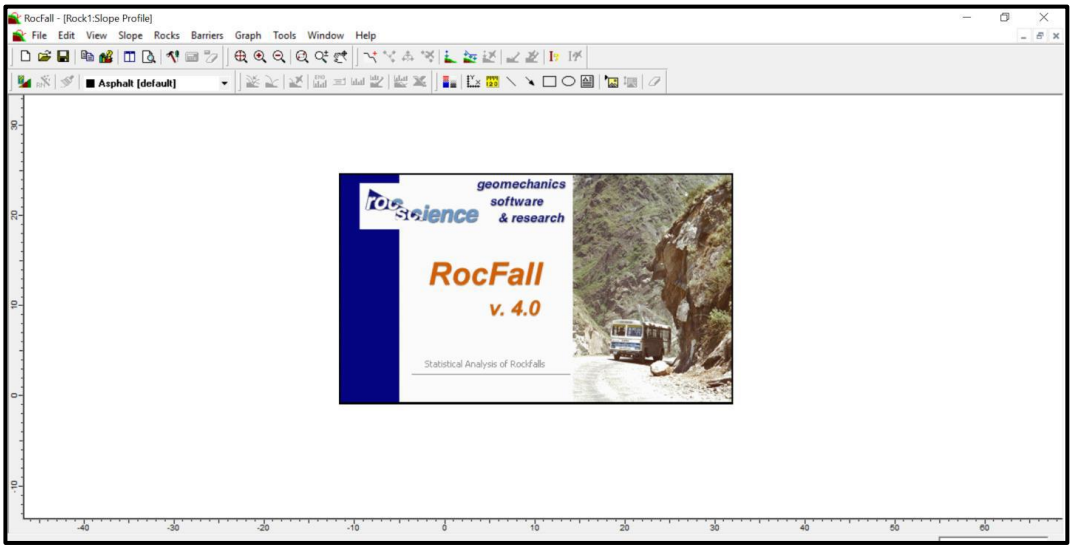

Figure 3.24: new project window in ROCFALL computer program.

The slope is then modelled based on the field data which include slope height, bench height, bench width and the type of rock which also include its properties (see Figure 3.25). These mentioned aspects play a key role in the determination of the final position where the rock will be deposited in case of a rockfall.

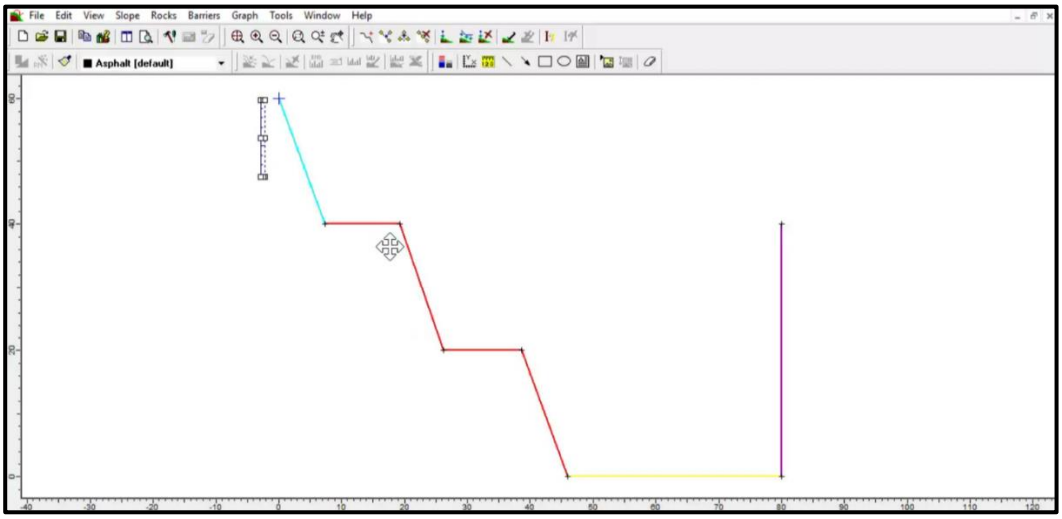

Figure 3.25: Slope modelling for rockfall simulation using ROCFALL program.

After creating the model, the material comprising the slope needs to be defined on the material editor tab. This began by choosing the most appropriate material representing the slopes in study. In this case, Bedrock outcrop was deemed more suitable. Furthermore, the friction angle of the rocks and the roughness of the slope to be entered. The friction angle of the slope was measured in Section 3.2.4 and results presented in Section 4.3 (Table 4.1) and was recorded to be 22.924°.

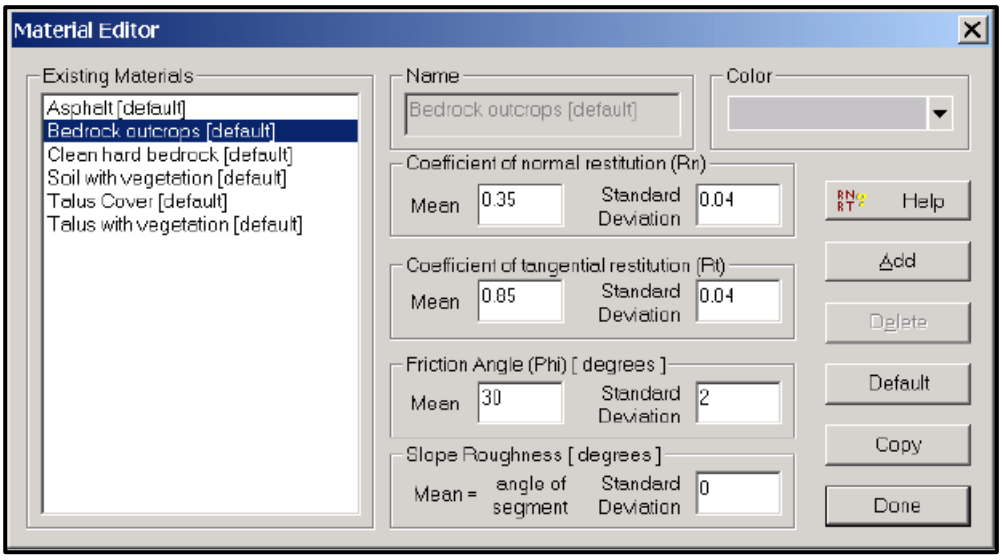

Figure 3.26: Material editor window for defining the material properties of the slopes.

For a rock to move down the slope, an initial force is needed. In order to define the initial condition, the define initial condition tab was selected and the window in Figure 3.27 was shown. On this window, a 1.5 m/s horizontal velocity was selected. The 1.5 m/s velocity was selected to initiate the downward motion of the rock. This was adopted from a study by Sengani (2020). Furthermore, a standard deviation of 0.15 m/s is used. Since the simulation will be run for multiple rocks, each rock will differ by a magnitude of 0.15 m/s on the initial velocity. This will allow for different simulations to be run by the program.

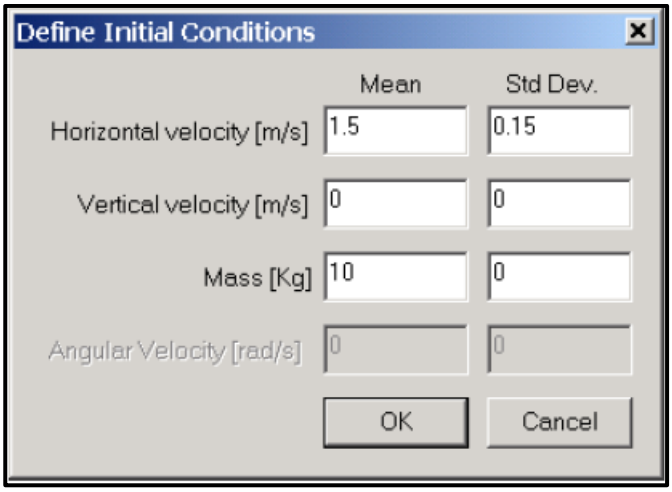

Figure 3.27: Initial conditions window to define the initial vertical and horizontal velocity of the rock.

Additionally, the project settings tab is then selected for additional set up. on this window, a number of rocks to be run for simulation is then selected. For this study, 100 rocks were simulated. After all the parameters are set, a compute option from the toolbar is selected. This will allow simulate the rocks falling from the top of the slope. The results are then presented in Section 5.5 of Chapter 5. From the program, the statistical elements that are in-built are used to compute the probable trajectories, Kinetic energy, Velocity and bounce height of the rocks as they move down the slope.

3.5 Limitations and challenges encountered

one of the limitations encountered in this study is that the analytical methods used could not contemplate for the three-dimensional analysis of the slopes

Secondly, some of the areas within the pit where data was to be collected was inaccessible. This was because the areas were unsafe to go since there was no safety measures near the bench face because the area was cleaned up in preparation for drilling.

Thirdly, the rock strength properties were not obtained from the actual laboratory testing. This was due to time constraints and the budget limits. This led the study to resort to using the computer program to estimate the rock mass properties instead of measuring them in the laboratory.

Lastly, some of the computer programs could not be used since they are expensive to purchase. Therefore, those that could be used were used at a limited timeframe during trial period.

Chapter 4: Field observation results and empirical rock mass rating

4.1 Introduction

As presented in Chapter 3, the study area was located at the Wearne open pit mine in Limpopo, South Africa. The identified area was divided into three sections denoted A, B and C (see Figure 3.1 for reference).

Relevant information was collected from the mining site by resorting to field observations coupled with appropriate measurements of various properties. The data collection methodology adopted for the purpose was followed as discussed in Chapter 3.

Upon collecting the necessary field observation and measurement data, the next step was to conduct rock mass classification. This was aimed to give a qualitative assessment of the strength of the slopes. It is in this light that results and relevant findings from the field observation and rock mass classification are presented in this chapter.

4.2 Open pit slopes observations and measurements

During the initial walkaround in the WG Wearne pit, the rock was identified on the field. This was done following the geological rock identification principles as discussed in Section 3.2.2 of Chapter 3. The discontinuities were also observed and measured. From the observations, it was established that the dominating discontinuities on the face were joints (see Figure 4.1 below).

This section presents the data collected in the field. This includes the results of the slopes orientation, benches measurements, bench width, and safety berms put in place in each bench.

4.2.1 Slope A observations and measurements

As discussed in Section 3.2 of Chapter 3, slope A is made up of 5 benches. The bench heights on this slope range from 6 to 12 m with the bottom bench (bench 1) with the lowest height, i.e., 6 m. The width of the benches was measured and found to be at an average of 15 m. Figure 4.1 shows the benches in Slope A.

The geological structures observed on slope A were joints as can be seen in Figure 4.1. These joints exhibited a slight weathering; however, additional conditions of the joints are discussed further later in Section 4.4. Visual inspection suggested that slope A did not have any other structures present.

Figure 4.1: Slope A benches and dominant discontinuities on the slope.

In addition to the observed and measured discontinuities, the slope showed a few hanging rocks by the crest of the slope. The hanging rocks are on observed to be on the verge of being dislodged from the face. This can be seen as evidence of possibility of toppling failure to occur on the slope.

4.2.2 Slope B observations and measurements

Like on slope A, slope B also had 6 benches with bench 1 on the slope having the shortest height of 6 m. In contrast, benches 2, 3, 4, 5, and 6 were 13, 14, 11, 10, and 8 high respectively. The widths of the benches on this slope were measured and found that it was kept at an average width of 15 m on all benches of slope B.

Similar to slope A, slope B is made up of basalt as the only rock type. Additionally, the discontinuities identified on the slope were joints as seen in Figure 4.2. Suffice it to say at this point in time that these discontinuities were slightly weathered while a full description of the joint conditions is covered later in Section 4.3.

Figure 4. 2: Slope B benches layout and dominant discontinuities.

One important point is that areas with evidence of dislodged rocks were apparent along the slope. The dislodged rocks were assumed to have experienced one of the three failures. Upon further observation, it was safe to assume that the rocks faced toppling failure. There are also some discontinuities that created a wedge; however, the rock is still hanging on the face. This shows that there is a probability of failure to occur. The probability of different types of failures is discussed further in Section 5.2 in Chapter 5.

4.2.3 Slope C observations and measurements

Slope C has the smallest number of benches which is 4 benches. However, just like on slopes A and B, bench 1 is the shortest at 6 m from the pit floor. The other benches are of heights 8 m, 9 m and 12 m for benches 2, 3 and 4 respectively. Just like in slope A and B, the width of the benches was measured and found to have an average of roughly 15 m. The discontinuities observed on slope C are also joints as captured in Figure

4.3. There is an indication of slight weathering on the face of the slope which may be a consequence of the infiltration of water down the fractures of the rock. The discussion on the joint conditions is detailed in Section 4.3.

Figure 4. 3: Slope C benches layout and evidence of water accumulated at the pit floor.

From the observations of the slope properties, it was noticed that the entire pit is made up of one type of a rock. The identified rock was identified as basalt. Furthermore, the degree of weathering, type of discontinuities observed, and overall conditions of the slopes were found to be similar.

In addition to the properties of the rock mass, It should be noted that on all slopes (namely, slopes A, B and C), a width of 3 m from the crest of the bench was reserved for the berm wall to prevent people and machinery from rolling off to the bottom benches (see Figure 4.4). Three-metre width from the toe of the bench was also reserved for a catchment berm used for catching loose rocks that may fall from the face of the bench.

Since the observations and measurements are being done for the entire pit, it should be noted that WG Wearne pit has water accumulated at the bottom. (see Figure 4.4). The water was accumulated from precipitation. Therefore, since the pit bottom is made up of a rock mass with very little porosity, the water is stored there. The water is mainly used in the crushing plant and haulage ways for dust suppression.

Figure 4.4: catchment berms of the open pit indicated by yellow arrows.

4.3 Estimation of rock mass properties

On-the-field observation and measurements provides an insight on the quality of the rock mass. However, the properties associated with the rock mass remain unknown. This is where the estimation of rock mass properties becomes important as these properties cannot readily be captured by observation and measurements.

The RSData computer program was used to assist with estimating the rock mass properties. The procedure for estimating the rock mass properties is presented in Section 3.2.2. The estimates are based on the assessment of the open pit mine slopes and the condition of the rock mass. Diamantis and Migiros (2018) as well as Brown (2018) explained that the estimation of rock mass properties is of utmost importance in the analysis and design of slopes, foundations and underground structures in rocks. The WG Wearne open pit mine slopes were assessed in order to estimate the rock mass properties. The results of the endeavour are presented in Table 4.1 below.

Table 4.1: Rock mass properties estimated with the help of the RSData computer program.

Rock	
Hoek Brown Classification	
UCS of intact rock (MPa)	175
GSI	55
mi	16
disturbance factor	0.7
Intact Modulus (MPa)	20000
Hoek Brown Criterion	
mb	0.643
s	0.000553
a	0.504

Rock Mass Parameters	
tensile strength (MPa)	0.151
uniaxial compressive strength (MPa)	3.993
global strength (MPa)	18.566
modulus of deformation (MPa)	1796.522
Failure Range Envelope	
application	General
sig3max (MPa)	43.75
Mohr Coulomb Fit	
cohesion (MPa)	6.153
friction angle (°)	22.924

Note from Table 4.1 that the estimated UCS of the rock mass is 175 MPa. The significance of this value is discussed later in Section 4.4. The estimated value of GSI is also reported to be 55. Section 3.2.2 and Figure 3.8 of Chapter 3 describe how the GSI value was obtained from the tools built into the RSData program.

GSI as an indicator puts emphasis on the geological observation of the rock mass characteristics. The chart in Figure 3.7 was used to allocate the GSI value to a rock mass based on observed features. It should be noted that GSI is qualitative in nature; however, the quantification process was introduced because of the inclination to numbers characteristic of engineering disciplines (Cai et al., 2004). The values are based on quantification of the rock mass by making use of Figure 3.7. This chart has GSI rating from 10 all the way to 90. These values represent the strength of the strength of the rock with the rating of 90 representing a very good rock with perfect surface conditions and strength. Additionally, the rating of 10 represents a very weak rock with extremely poor surface conditions. The rating of 55 on this study is a representation of the rock present which was observed. The rock mass was blocky with discontinuities interlocking. Furthermore, the rock was slightly weathered with some iron stains on the surface of the joints.

Other estimated rock mass parameters are cohesion and friction angle. These two parameters are widely used to characterize the shear strength of the materials. In RSData, cohesion and friction angle were estimated based on the Mohr-Coulomb failure criterion. The estimated cohesion and friction angle for the study area was found to be 6.153 MPa and 22.924° respectively.

4.4 Rock mass classification

This section is devoted to the classification of the rock mass found at the WG Wearne open pit mine. According to Abbas and Habil (2017), rock mass classification is all about grouping the rock mass and assigning a unique description (or number). This is done in order to predict the behaviour of the rock mass. As discussed in Section 2.6 of Chapter 2, rock mass classification is a preliminary technique for the assessment of slope stability. The RMR classification system was used for this stud. As previously explained (Section 3.1 of Chapter 3), the study area comprised three slopes whereby the RMR was calculated per slope. Several parameters were used to quantify the description of the rock including UCS, RQD, discontinuity spacing, discontinuity condition and groundwater. Table 4.2 was used as a guide in order to assign a certain value to the description of the rock mass parameters.

Table 4.2: Classification parameters and their ratings (after Bieniawski, 1973).

Strength of intact rock	Uniaxial compressive strength, MPa	> 250	100–250	50–100	25–50	5–25	1–5	< 1
1.	Rating	15	12	7	4	2	1	0
	RQD, %	90–100		75–90	50–75	25–50		< 25
2.	Rating	20		17	13	8		3
	Spacing of discontinuities, m	> 2		0.6–2	0.2–0.6	0.06–0.2		< 0.06
3.	Rating	20		15	10	8		5
	Condition of discontinuities	Very rough, Discontinuous, No separation, Unweathered		Rough walls, separation < 0.1 mm, Slightly weathered	Slightly rough, separation < 1 mm, Highly weathered	Slickenslides or Gouge < 5 mm thick or continuous separation 1–5 mm		Soft Gouge > 5 mm thick Or Separation > 5 mm continuous, decomposed wall rock
4.	Rating	30		25	20	10		0
Ground Water	General conditions	Completely dry		Damp	Wet	Dripping		Flowing
5.	Rating	15		10	7	4		0

When using RMR technique, five basic parameters are used which are uniaxial compressive strength, RQD, spacing of discontinuities, condition of discontinuities, and groundwater (see Section 2.6.2 of Chapter 2). In order to get the ratings of each parameter, the computations or observation is done for the rock mass. The value of computation or the result of the observation is checked against Table 4.2 in order to determine its rating. The slope is rated out of 100. Therefore, by making use of Table 2.5 (of Chapter 2), the rock mass is then classified as good or as poor based on the total rating obtained. The computations done in order to obtain the description for each parameter are discussed in Sections 4.4.1 – 4.4.5 below.

4.4.1 Strength of the intact rock

Starting off with the strength of the intact rock which is also known as the uniaxial compressive strength (UCS). As explained in Section 3.1 of chapter 3, the study area was divided into three sections. Therefore, the strength of the intact rock was determined for the three slopes individually. By making use of the RSData computer program, the rock mass properties were entered for each slope (refer to Section 3.2.2 of Chapter 3) and the values were all found to be 175 for all slopes (i.e., slopes A, B and C). According

to Table 4.2, the UCS rating for all slopes was therefore found to be 12. This is primarily due to the similarity of the rock mass properties. This means that the entire pit is made up of the similar rock type.

4.4.2 Discontinuities spacing

The procedure for determining the spacing of discontinuities was detailed in Section 3.2.2 of Chapter 3. In Section 3.2.2, different discontinuities sets were established (one set of discontinuities refers to discontinuities with the closely related orientation). Therefore, the spacing of discontinuities is done for one set at a time. This means that the spacing of discontinuities is done for those with similar orientation at a time. Thereafter, the average spacing for the slope is calculated by taking an average from spacing of different sets. The spacing of the discontinuities in a particular set is calculated by making use of Equation (4.1).

Below are the steps taken to derive estimates of the joint spacings and the average joint spacing for slopes A, B, and C.

Equation (4.1) was used to calculate the spacing of the discontinuities in a particular set (Palmstrom, 1982):

$$J_{S1} = \frac{S1+S2+S3+\cdots+Sn}{n} \qquad (4.1)$$

Where J_{S1} is the spacing of discontinuities in joint set 1,

$S1 + S2 + S3 + \cdots + Sn$ is the spacing between the joints,

n is the number of joints in a set.

The same formula was applied in determining the spacing in joint set 2, joint set 3, and the rest of the joint sets which are presented in Table 4.3.

After the spacing in each joint set has been determined, the average spacing in the joint sets was then calculated as follows (Palmstrom, 1982):

$$J_{Sa} = \frac{J_{S1}+J_{S2}+J_{S3}+\ldots+J_{Sn}}{n} \qquad (4.2)$$

Where J_{Sa} is the average joint set in the rock mass,

J_{S1}, J_{S2}, J_{S3}, …J_{Sn} are the joint spacings of different sets,

n is the number of joint sets.

It should be noted that the joint sets were determined by the kinematic analysis rose diagram as explained in Section 3.3.1 of Chapter 3.

Note that Equations (4.1) and (4.2) were applied to all three slopes (i.e., slope A, B and C) individually. Results are summarised in Table 4.3.

Table 4.3: Measurements of the discontinuity spacings done along with the mean spacings per square metre.

A		B		C	
Joint set	Spacing (m)	Joint set	Spacing (m)	Joint set	Spacing (m)
1	0.38	1	0.25	1	0.12
2	0.44	2	0.34	2	0.28
3	0.54	3	0.41	3	0.46
4	0.59	4	0.64		
5	0.68	5	0.69		
Mean	0.526	Mean	0.466	Mean	0.287

Table 4.3 summarises the results of discontinuities spacing. The top row written A, B and C represents the slopes of the mine as discussed in Section 3.2 of Chapter 3. Below each slope, there are columns for joint set and spacing in that particular slope. Thereafter, the bottom row represents the mean spacing of the slopes. It was found that the mean spacing for Slope A was 0.526, for Slope B was 0.466 and for Slope C was 0.287. It should be noted that the mean discontinuities spacing also translates to the frequency of the discontinuities. The lower the mean spacing of discontinuities, the higher the discontinuities frequency, and vice versa. Although the spacing of the discontinuities is one of the parameters for rock mass classification, it can also be used on its own to assume but not

conclude the stability of the slopes. If the frequency of discontinuities is high, the stability is assumed to have decreased.

4.4.3 Condition of discontinuities

Table 4.3, introduced by Dyke (2006), captures the rating of the condition of discontinuities. The condition of discontinuities refers to the roughness of discontinuity surfaces, their length, separation, infilling material and weathering of the wall rock.

Table 4.4: Guidelines for classification of discontinuity conditions (after Dyke, 2006).

E. GUIDELINES FOR CLASSIFICATION OF DISCONTINUITY CONDITIONS					
Discontinuity Length (Persistence)	<1m	1-3m	3-10m	10-20m	>20m
Rating	6	4	2	1	0
Separation (Aperture)	None	<0.1mm	0.1-1.0mm	1-5mm	>5mm
Rating	6	5	4	1	0
Roughness	Very Rough	Rough	Slightly Rough	Smooth	Slickensided
Rating	6	5	3	1	O
Infilling (Gouge)	None	Hard Filing <5mm	Hard Filling >5mm	Soft Filling <5mm	Soft Filling >5mm
Rating	6	4	2	2	0
Weathering	Unweathered	Slightly Weathered	Moderately Weathered	Highly Weathered	Decomposed
Rating	6	5	3	1	0

All the data pertaining to the conditions of the discontinuities was collected during the field investigation stage (see Section 3.2). The discontinuities conditions were collected and rated one slope at a time. To attain the rating of discontinuities conditions, a mean of the parameters rating has to be added together in accordance with Table 4.3. The properties of the parameters used to rate the conditions of the discontinuities are summarised in Table 4.6. According to the data presented in Table 4.6, the lengths of discontinuities was measured by making use of a measuring tape. Therefore, a measure of the maximum length of the discontinuities was used to give a rating as per Table 4.4. The separation of the discontinuities

is a measure of the space in between one joint or discontinuity. The measurements revealed that the discontinuities spacing was found to be between 1mm and 5mm. The rating of the separation was found to be 1. As per the field observations discussed in detail in Section 3.2.2 of Chapter 3, the rock mass discontinuities were found to be rough and slightly weathered with no infilling in the spaces between the joints. The abovementioned properties belonged to slope A. Therefore, the same rating was conducted for slopes B and C. The properties of the discontinuities used are summarised in Table 4.6.

Table 4.3 above shows the rating of the conditions of the discontinuities shaded in red. After the addition of all the ratings, it was then found that the conditions of discontinuities have a total rating of 21 (i.e., 4 + 1 + 5 + 6 + 5).

4.4.4 Groundwater presence on the face

In addition to the conditions of the discontinuities, the groundwater on the slopes was also determined through observations of the slope. Through the field work presented in Section 3.2.2 of Chapter 3. The presence of groundwater was investigated through observation. It was observed that the face of the slope was completely dry. In reference to Table 4.2, the rating of the groundwater availability was given as 15 which correspond to a completely dry face.

4.4.5 Rock quality designation

The Rock Quality Designation or RQD of the slopes was calculated as follows (Palmstrom,1982):

$$RQD = 115 - 3.3(J_V) \quad (4.3)$$

In Equation (4.3), J_V is the volumetric joint count. This is simply a measure of degree of jointing in a unit volume of the rock mass. In this case, joint set spacings are used. The formula for volumetric joint count is given by (Palmstrom, 1982):

$$J_V = \frac{1}{S_1} + \frac{1}{S_2} + \frac{1}{S_3} + \ \ldots\ldots\ldots + \ \frac{1}{S_n} \qquad (4.4)$$

Where S_1, S_2, S_3, and S_n are the joint set spacings.

The calculations of the volumetric joint counts are summarized below.

Table 4.3 has presented the spacing of discontinuities sets used in the calculation of the volumetric joint count. According to Fumani (2021), if $J_V < 4.5$, it implies that the RQD is 100% and if the $J_V > 30$, the RQD is equal to 0.

By applying Equation (4.4) to slope A, the following was obtained:

$J_V = \frac{1}{0.38} + \frac{1}{0.44} + \frac{1}{0.54} + \frac{1}{0.59} + \frac{1}{0.68}$ or $J_V = 9.92$.

Therefore, the RQD value was determined as follows: $RQD = 115 - 3.3(J_V)$ or $RQD = 115 - 3.3\ (9.92)$ which gives $RQD = 82.26\%$.

The rating according to Table 4.2 (i.e., Bieniawski's RMR) is therefore 17. It should be remembered that RQD is a measure of the degree of jointing or fracture in a rock mass measured in percentage. The RQD is measured in percentage and according to Table 4.2, the rating of 17 shows a good quality hard rock.

For slope B, $J_V = \frac{1}{0.25} + \frac{1}{0.34} + \frac{1}{0.41} + \frac{1}{0.64} + \frac{1}{0.69}$ which gives $J_V = 12.39$.

Here, RQD is $RQD = 115 - 3.3\ (12.39)$ which gives $RQD = 74.39\%$.

From Table 4.2, the RQD rating in this case is 13.

Using the same procedure for slope C, $J_V = \frac{1}{0.12} + \frac{1}{0.28} + \frac{1}{0.46} = 14.51$ which when used in calculating RQD leads to $RQD = 115 - 3.3\ (14.51) = 67.12\%$.

Referring to Table 4.2, RQD is found to be 13.

After analysing the RQD values of the three slopes, it is clear that slope C has the highest degree of jointing.

The properties of the slope, rock mass and joints are summarised in Table 4.5. The table summarises the results of discontinuities mapping in terms of orientation, description and rock mass properties. The information in table 4.5 was used in the classification of the rock mass of the slopes.

Table 4.5: summary of the slope, rock mass and joints properties.

WG Wearne Rock mass properties				
Location: WG Wearne (Louis Trichardt)				
SLOPES		A	B	C
Slope description	No. of joint sets	05	05	03
	Dip	80	80	80
	Dip direction	174°	268°	25°
Joint description	Joint spacing (mean)	0.526	0.466	0.287
	Persistence (m)	1-3	1-3	1-3
	UCS	175MPa	175MPa	175MPa
	RQD	82.26%	74.39%	67.12%
	Roughness	Rough	Rough	Rough
	Infilling type	None	None	None
	Aperture (mm)	1-5	1-5	1-5
Rock mass description	Rock type	Basalt	Basalt	Basalt
	Weathering degree	Slightly weathered	Slightly weathered	Slightly weathered
	Geological structures	Joints and fractures	Joints and fractures	Joints and fractures
	Water presence	Dry	Dry	Dry

4.5 RMR calculation

The calculation of RMR is based on adding the ratings of all the parameters. These parameters were listed in Table 4.2. Equation (4.5) was used to

calculate the rock mass RMR for each slope. After the computation of RMR, Table 2.5 was used to classify and rate the stability of the slopes.

$$RMR = R_1 + R_2 + R_3 + R_4 + R_5 \quad (4.5)$$

Table 4.6: Summary of the RMR calculations per slope.

	$RMR = R_1 + R_2 + R_3 + R_4 + R_5$
Slope A	$RMR = 12 + 10 + 21 + 15 + 17 = 75$
Slope B	$RMR = 12 + 10 + 21 + 15 + 13 = 71$
Slope C	$RMR = 12 + 10 + 21 + 15 + 13 = 71$

As per table 4.7, the RMR values of the slope are then given meaning. The values signifies if the slope condition is good or not. This then translates to the stability of the slope.

Table 4. 7: Five classes of rock quality as per the ISRM guide (adapted from Ferarri et al., 2014)

RMR value	**Rating**
>80	Excellent
60-80	Good
40-60	Fair
20-40	Scarce
0-20	Poor

4.6 Significance of the findings

The results presented in this chapter have shown that the slopes of the entire pit are made up of a similar rock type which was identified as a Basalt rock. Upon observation of the slopes (A, B and C), the dominant discontinuities were joints and fractures. The rock mass was assessed through visual observation and measurements. This led to the rock mass properties to be determined. However, more rock mass properties were estimated by making use of the RSData computer program.

The rock mass properties and conditions description were used to classify it. The ratings of slope A, B and C are found to be 75, 71 and 71 respectively.

Based on the rating classification (see Table 4.5), the RMR value shows that the rock mass quality is good. This implies that the rock is stable enough. Since the RMR value is not 100, it shows that there is deterioration in the rock strength. It is assumed that the slope strength will deteriorate further due to blasting that continuously happens, which sends seismic waves throughout the rock mass. Further analysis of the slope stability is presented in Chapter 5.

Chapter 5: Empirical and numerical analysis of slope stability at Wearne mine

5.1 Introduction

Slope failure has and still is one of the major concerns in the mining industry. A mine remains in operation provided there are sufficient resources in the ground that can be extracted economically. Owing to that, the slopes should always be assessed and monitored to ensure safe working conditions (Suman, 2014; Kumar and Parkash, 2015; Moses et al., 2020).

There has been a number of methods developed over the years for slope stability analysis. Each method has got strengths and limitations, but none stands out as the best (Albataineh, 2006; Kwofel, 2021). That is why engineers relied mostly on their experience and engineering judgment which can be subjective and biased. This study however opted to use toe combination of selected analysis methods and produce a verdict on the stability of slopes. Conventional methods (i.e., kinematic analysis and limit equilibrium) and numerical methods have both been applied to help in the analysis of slope stability. Applying all these methods is expected to provide a better confidence in the FoS produced. This is unlike when using one method to determine the FoS, the confidence that the method produced accurate results is low. Furthermore, a better description of the probability of failure, the probable mode of failure and the behaviour of materials in failure is anticipated. It is in light with the above that the selected analysis methods (i.e., kinematic analysis, limit equilibrium and numerical modelling) are presented in this chapter.

5.2 Kinematic analysis

The kinematic analysis of the study area was conducted in order to determine the potential mode of failure of the slopes. As indicated in Section 3.3.1 of Chapter 3, the area was divided into three sections or slopes. This

means that the kinematic analysis was performed for all three sections separately. The kinematic analysis started off with the development of discontinuities sets. This was followed by developing a rose diagram which is also known as a Rosette diagram. This was followed by the development of the stereonets which represents the distribution of the discontinuities on the slope. Lastly, the analysis of the stereonets was done. This was to determine the probability of each of the three modes of failure (i.e., planar, wedge, and toppling) occurring on the slopes.

5.2.1 Presentation of discontinuity orientation through a Rose diagram

As discussed in Section 2.3.2 of Chapter 2, the presence of joints and their orientations play a major role in the stability of slopes. Furthermore, authors such as Madun and Omar (2001), Mote et al. (2004) and Sun et al. (2022) explained that discontinuity sets have the ability to interact with each other and affect the slope stability. The orientation of these discontinuities and discontinuities sets influences the mode of failure that may occur on the slope.

It is clear from the above paragraph that discontinuity sets play a key role in slope stability. In this research study, a rose diagram was used to determine the joint sets. A rose diagram is a circular histogram plot that displays the orientation of the discontinuities. It further shows the distribution of discontinuities from the dominant to the least dominant on the slope (Otoo, 2012). This type of diagram was relied upon to determine the dominating orientations of discontinuities for slopes A, B and C. As previously explained in Section 2.4 of Chapter 2, the mode of failure is dependent on the orientation of the discontinuities. A rose diagram (see Figure 5.1) was used as a primary analytical tool. The orientation of discontinuities is analysed in relation to the slope orientation. By using the stereonet, this (orientation of discontinuities) can serve as a tool to understand the probability of failure from the three modes. A rose diagram was created using the DIPS

computer program. The method of generating a rose diagram is detailed in Section 3.3.1 of Chapter 3.

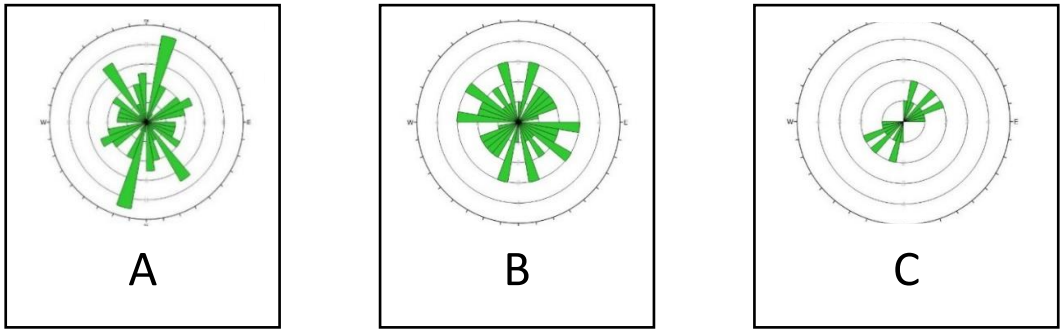

Figure 5.1: Rose diagrams showing the dominant directions of discontinuities on slopes A, B and C respectively.

The green bars represent discontinuity sets with one bar corresponding to one discontinuity set. A long bar represents a high number of discontinuities while a short bar implies that there are fewer discontinuities in that set. The identified discontinuity sets were extracted from the rose diagram. By making use of a 16-point cardinal compass (Figure 2.17), the directions of the discontinuities were extrapolated. This was done through aligning the orientations of the discontinuities with the 16 cardinal point compass. Slopes A and B were found to have five (5) major joint sets each whereas slope C only had three (3) major joint sets. The joint sets orientations obtained from rose diagrams are summarised in Table 5.1.

Table 5.1: Dominating joint sets on the slopes and their orientations.

	SLOPE A	**SLOPE B**	**SLOPE C**
Slope dip direction	174°	268°	25°
Slope strike direction	264°	358°	115°
Joint sets	NNE-SSW	ESE-WNW	NNE-SSW
	NW-SE	SE-NW	ENE-WSW
	ENE-WSW	NNE-SSW	NE-SW
	NNW-SSE	NNW-SSE	
	ESE-WNW	NE-SW	

The discontinuities sets identified in Table 5.1 were scrutinised in order to determine which joint set is responsible for the failure of the slopes. Three modes of failure were investigated on the slopes: planar, wedge and toppling failure. The orientation of discontinuities controls the mode of failure on the slope. The modes of failures are investigated using the stereonets. According to Sarkar et al. (2021), the stereonets provides the probable failure modes and zones of failure for the slopes in question. The probability of failures is presented in sections 5.2.2 – 5.2.4 below.

5.2.2 Planar failure

The conditions for and principles behind planar failure are discussed in Section 2.7.2.1 of Chapter 2. These are embedded in the DIPS software and are used to determine the possibility of planar failure to occur. The software is capable of constructing stereonets associated with the probable planar failure for analysis.

In Section 5.2.1, slope A was reported to consist of 5 joint sets, with the NNE-SSW oriented discontinuities being the dominant one. During the determination of the rock mass properties (Section 3.2.2 of Chapter 3), the friction angle was found to be 22.924°. For planar failure to occur, the discontinuity should dip at an angle greater than the friction angle but lower than the slope angle. Furthermore, the discontinuity should have a strike almost parallel to the strike of the slope within a 20° margin (Norrish and Wyllie, 1996). This principle, extensively discussed in Section 2.7.2 of Chapter 2, was used to create a critical zone shaded in red on DIPS-generated stereonets. Any point/pole found in this critical zone was deemed likely to lead to planar failure. That is why Raghuvanshi (2019) refers to the critical area as the sliding envelope.

From the stereonets produced (Figure 5.2), there is a section shaded in red called a critical region. This region is demarcated by two lines. As discussed in the previous paragraph, the failure should occur almost parallel to the

strike within a 20° margin. These lines define the extent of the critical zone which ranges from parallel of the slope to 20° from parallel of the slope. It should be noted that surrounding the critical region is an oval area. This is known as the daylight cone. The discontinuities in the daylight cone are those that daylight (exposed) on the slope. However, only the discontinuities found in the critical region are the ones that can potentially lead to planar failure.

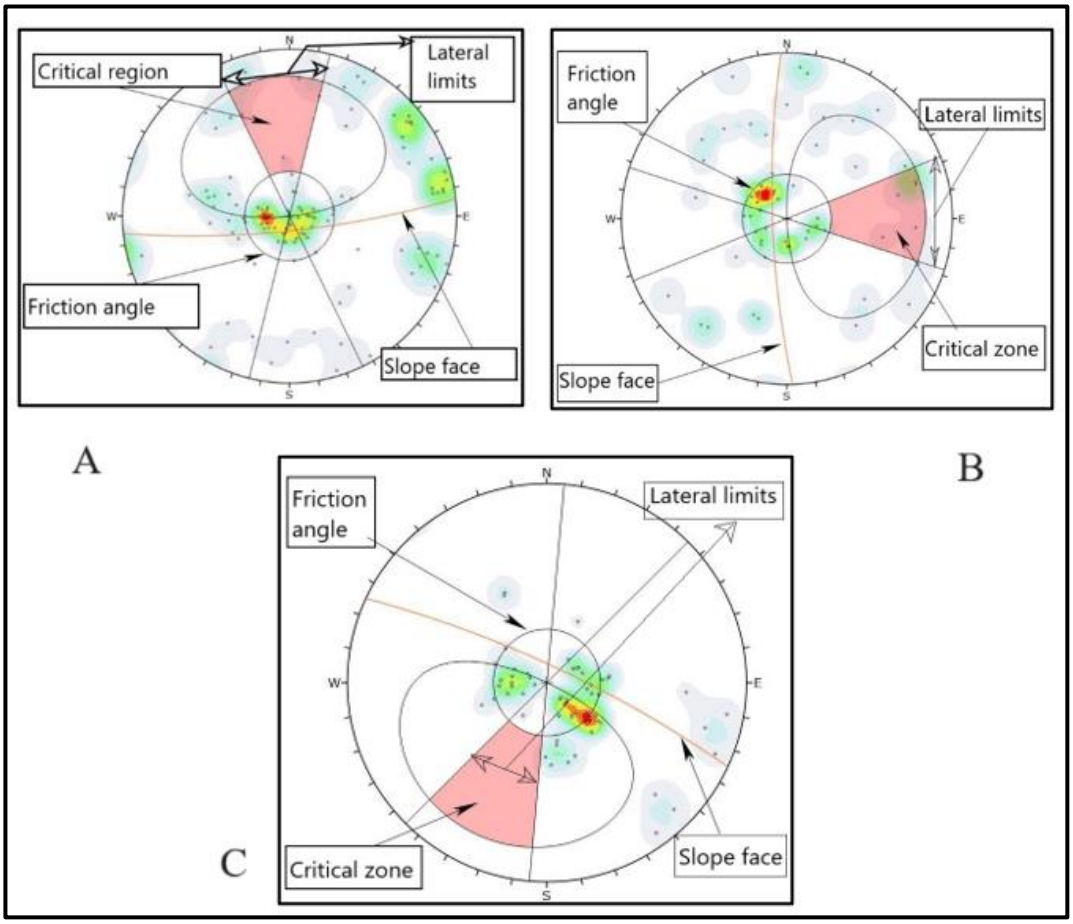

Figure 5.2: Stereonets showing the planar failures of the different slopes (A, B, and C).

Sigdel and Adhikari (2020) as well as Park et al. (2016) noted that kinematic analysis involved determining the relationship between the orientation of the discontinuities and the orientation of the slope. It should be noted that the stereonets interpretation is done in conjunction with the fisher concentration presented in Figure 5.3. The Fisher concentration highlights the information

presented on the stereonets. This information includes the slope orientation, friction angle, total number of discontinuities mapped on the slope along with the number of discontinuities that satisfies the criteria for failure to occur. Additionally, the fisher concentration also provides the probability of failure occurring on the slope. Moses et al. (2020) conducted a similar study whereby the stability analysis of the slope included kinematic analysis. The author indicated that the probability of failure can clearly be analysed through the information provided in the Fisher concentration.

The kinematic analysis was done for all three slopes (namely A, B and C). Slope A has dip direction of 174° (strike direction = 264°). Therefore, the discontinuities that falls within the 20° margin from the slope parallel point, were identified from the stereonet and the rose diagram. The discontinuities that satisfied the conditions for planar failure on Slope A have the ENE-WSW and ESE-WNW orientations. These discontinuities have strike directions ranging from 244° and 284°.

Slope B has a strike direction of 268° (strike direction = 358°). The discontinuities that can lead to planar failure on Slope B have the NNW-SSE and NNE-SSW orientations. These discontinuities have the have strike directions ranging from 338° to 378°.

Slope C on the other hand have a strike direction of 25°. Upon analysing the stereonets, the slope had no discontinuities that satisfies the conditions for planar failure to occur. However, the discontinuities that could have led to planar failure on Slope C should have the strike directions between 5° and 45°.

Upon analysis of the Fischer concentration, the probabilities of failures of slopes A, B and C were presented. The probabilities of failures were found to be 5.13%, 8.33% and 0% for slope A, B and C respectively. The probability of planar failure was calculated as a percentage of the number of discontinuities found in the critical region of the stereonet to the total number of discontinuities measured on the slope.

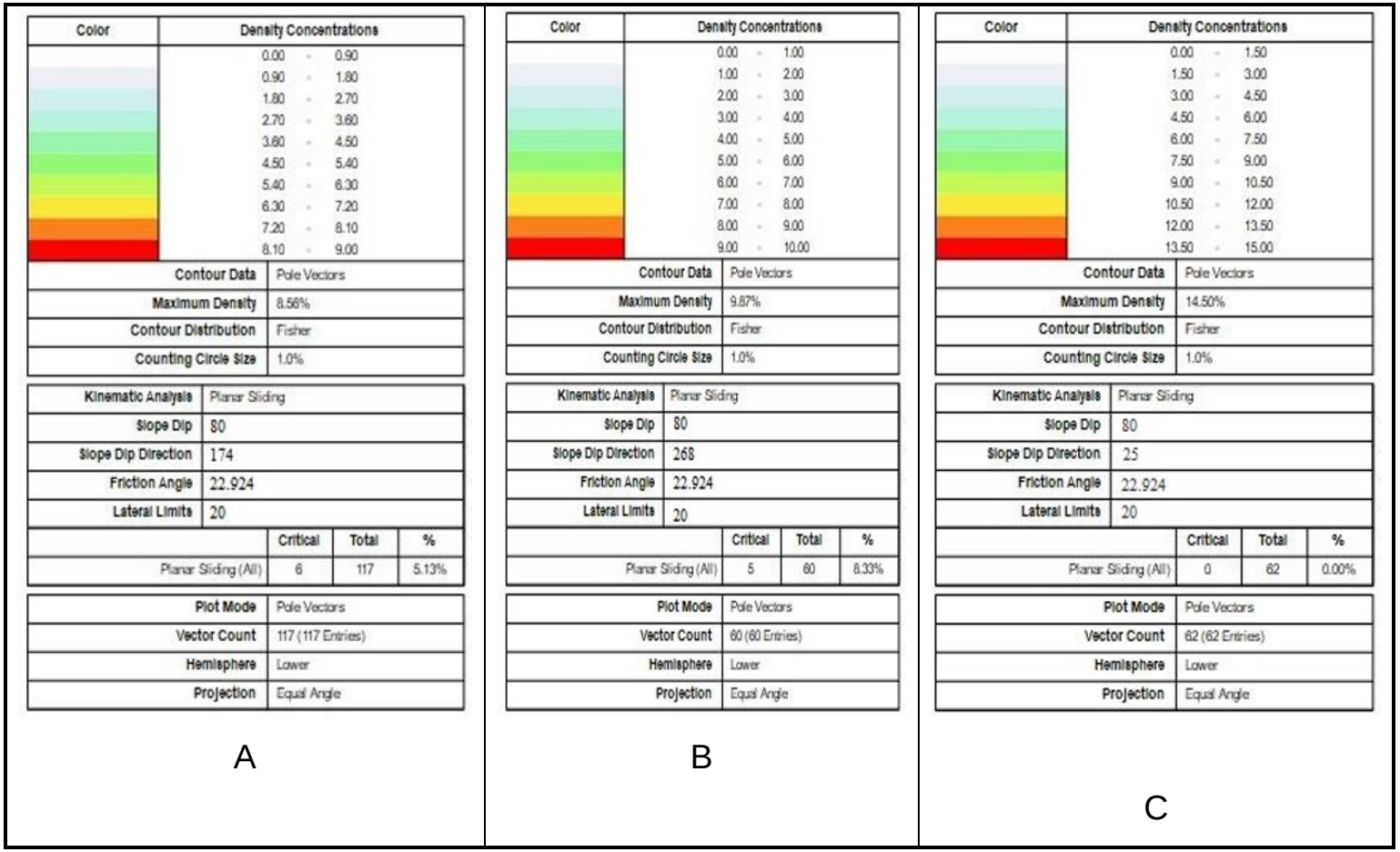

Color	Density Concentrations
	0.00 - 0.90
	0.90 - 1.80
	1.80 - 2.70
	2.70 - 3.60
	3.60 - 4.50
	4.50 - 5.40
	5.40 - 6.30
	6.30 - 7.20
	7.20 - 8.10
	8.10 - 9.00

Contour Data	Pole Vectors
Maximum Density	8.56%
Contour Distribution	Fisher
Counting Circle Size	1.0%

Kinematic Analysis	Planar Sliding
Slope Dip	80
Slope Dip Direction	174
Friction Angle	22.924
Lateral Limits	20

	Critical	Total	%
Planar Sliding (All)	6	117	5.13%

Plot Mode	Pole Vectors
Vector Count	117 (117 Entries)
Hemisphere	Lower
Projection	Equal Angle

A

Color	Density Concentrations
	0.00 - 1.00
	1.00 - 2.00
	2.00 - 3.00
	3.00 - 4.00
	4.00 - 5.00
	5.00 - 6.00
	6.00 - 7.00
	7.00 - 8.00
	8.00 - 9.00
	9.00 - 10.00

Contour Data	Pole Vectors
Maximum Density	9.87%
Contour Distribution	Fisher
Counting Circle Size	1.0%

Kinematic Analysis	Planar Sliding
Slope Dip	80
Slope Dip Direction	268
Friction Angle	22.924
Lateral Limits	20

	Critical	Total	%
Planar Sliding (All)	5	60	8.33%

Plot Mode	Pole Vectors
Vector Count	60 (60 Entries)
Hemisphere	Lower
Projection	Equal Angle

B

Color	Density Concentrations
	0.00 - 1.50
	1.50 - 3.00
	3.00 - 4.50
	4.50 - 6.00
	6.00 - 7.50
	7.50 - 9.00
	9.00 - 10.50
	10.50 - 12.00
	12.00 - 13.50
	13.50 - 15.00

Contour Data	Pole Vectors
Maximum Density	14.50%
Contour Distribution	Fisher
Counting Circle Size	1.0%

Kinematic Analysis	Planar Sliding
Slope Dip	80
Slope Dip Direction	25
Friction Angle	22.924
Lateral Limits	20

	Critical	Total	%
Planar Sliding (All)	0	62	0.00%

Plot Mode	Pole Vectors
Vector Count	62 (62 Entries)
Hemisphere	Lower
Projection	Equal Angle

C

Figure 5.3: Fisher concentration showing more details about the stereonet which include the number of mapped discontinuities, friction angle and the probability of failure.

5.2.3 Wedge failure

Wedge failure occurs when two discontinuities or two sets of discontinuities intersect and form a wedge. Wedge failure can also be investigated using a stereonet. Further to the two discontinuities intersecting, the line of intersection should plunge in the same direction as the slope face at a gentler angle than the slope but greater than the friction angle.

As with the planar failure analysis done in Section 5.2.2, wedge failure was studied separately for each slope or section (i.e., A, B and C). Figure 5.4 provides the stereonets showing the probability of wedge failure for each slope.

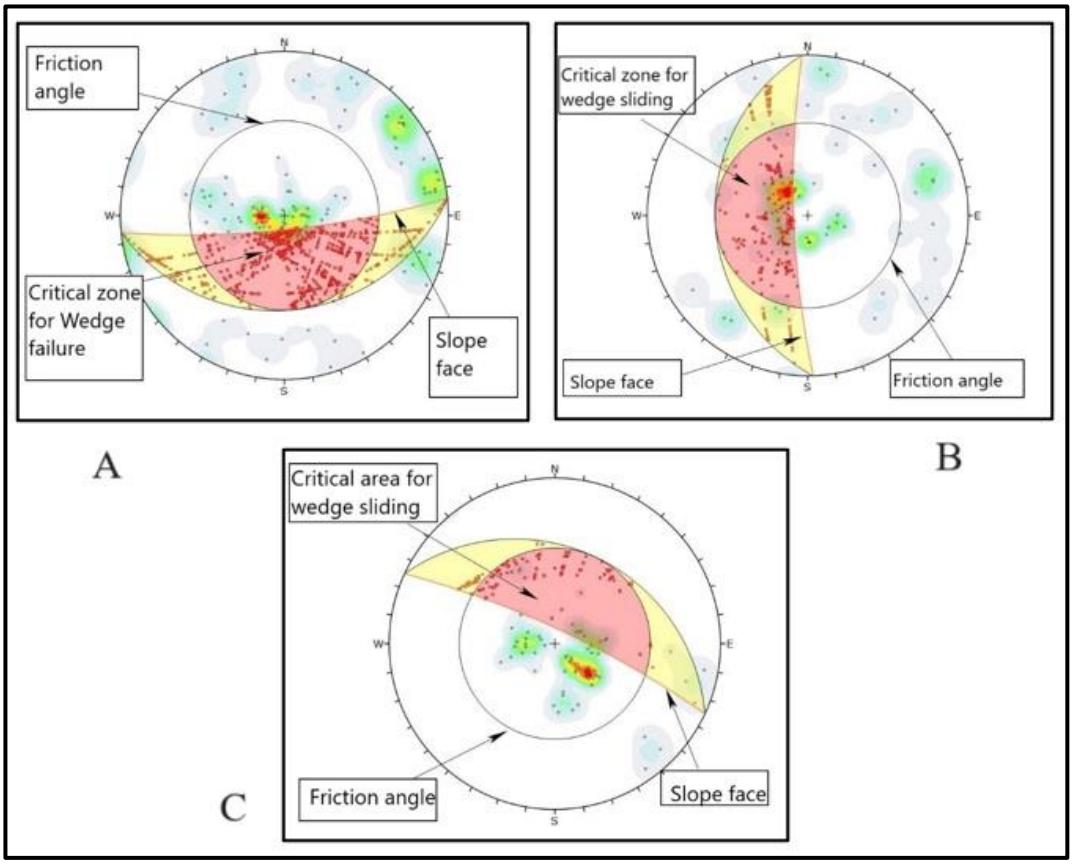

Figure 5.4: Stereonets showing the probabilities of wedge failures for slopes A, B and C.

Note that the stereonets has an area known as the critical zone/area. This is the area shaded in red and between the great circle representing the slope face and the friction angle.

Kimothi et al. (2019) and Rusydy (2019) pointed out that the discontinuities that intersect inside the red-shaded region (critical zone) meet the minimum criteria for wedge failure to occur. Figure 5.4 shows the slope faces for A, B and C and the poles representing the intersection of discontinuities. The interpretation of the stereonets for wedge failure is done in conjunction with the Fisher concentration. The Fisher concentration provides information such as the value of the friction angle, Slope angle, number of the total intersections of discontinuities in the stereonet along with the number of intersecting discontinuities found in the critical zone.

The number of discontinuities in the critical zone against the number of the total number of intersections of discontinuities gives the probability of wedge failure occurring. The fisher concentration diagrams for slopes A, B and C are presented in Figure 5.5.

Upon analysis of the stereonets for slopes A, B and C are presented in Figure 5.4 and the Fisher concentration in section 5.5, the following was discovered:

For slope A, the number of discontinuities that intersect in the stereonet is 6785. Out of the 6785 discontinuities intersecting, only 854 of those are in the critical zone. Therefore, by dividing 854 by 6785 gives the percentage of as 12.59 %. The DIPS software program also computes the probability of wedge failure occurring and present it in the Fisher concentration diagrams.

Slope B on the other hand has 1770 total intersection of discontinuities and only 270 of those are in the critical region. The fisher concentration presents the probability of wedge failure occurring to be at 15.26 %.

Lastly, slope C has 1890 total intersecting discontinuities and only 122 of those are in the critical zone. This brings the probability of failure to be at 6.46 %.

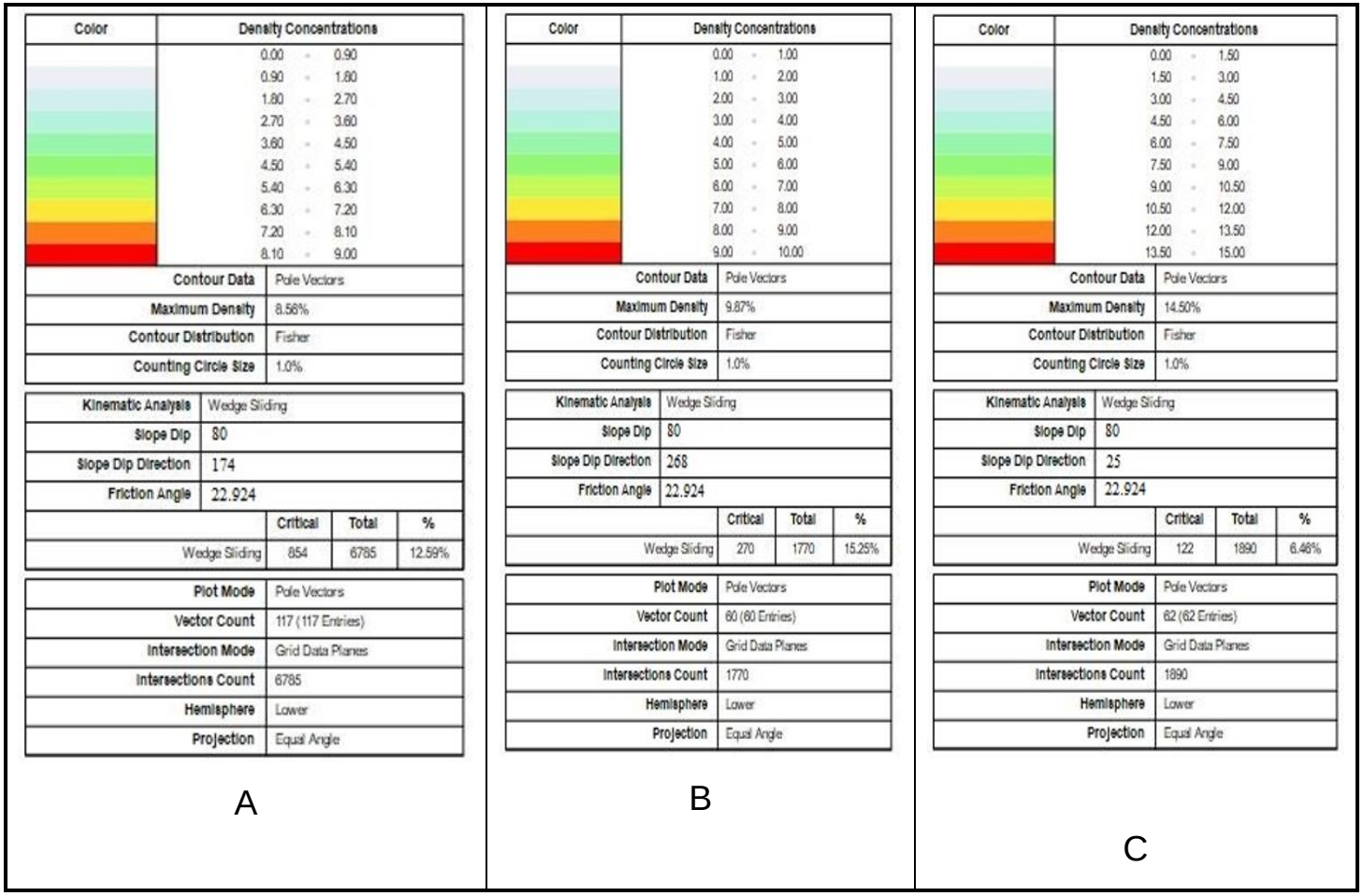

Color	Density Concentrations
	0.00 - 0.90
	0.90 - 1.80
	1.80 - 2.70
	2.70 - 3.60
	3.60 - 4.50
	4.50 - 5.40
	5.40 - 6.30
	6.30 - 7.20
	7.20 - 8.10
	8.10 - 9.00

Contour Data	Pole Vectors
Maximum Density	8.56%
Contour Distribution	Fisher
Counting Circle Size	1.0%

Kinematic Analysis	Wedge Sliding
Slope Dip	80
Slope Dip Direction	174
Friction Angle	22.924

	Critical	Total	%
Wedge Sliding	854	6785	12.59%

Plot Mode	Pole Vectors
Vector Count	117 (117 Entries)
Intersection Mode	Grid Data Planes
Intersections Count	6785
Hemisphere	Lower
Projection	Equal Angle

A

Color	Density Concentrations
	0.00 - 1.00
	1.00 - 2.00
	2.00 - 3.00
	3.00 - 4.00
	4.00 - 5.00
	5.00 - 6.00
	6.00 - 7.00
	7.00 - 8.00
	8.00 - 9.00
	9.00 - 10.00

Contour Data	Pole Vectors
Maximum Density	9.87%
Contour Distribution	Fisher
Counting Circle Size	1.0%

Kinematic Analysis	Wedge Sliding
Slope Dip	80
Slope Dip Direction	268
Friction Angle	22.924

	Critical	Total	%
Wedge Sliding	270	1770	15.25%

Plot Mode	Pole Vectors
Vector Count	60 (60 Entries)
Intersection Mode	Grid Data Planes
Intersections Count	1770
Hemisphere	Lower
Projection	Equal Angle

B

Color	Density Concentrations
	0.00 - 1.50
	1.50 - 3.00
	3.00 - 4.50
	4.50 - 6.00
	6.00 - 7.50
	7.50 - 9.00
	9.00 - 10.50
	10.50 - 12.00
	12.00 - 13.50
	13.50 - 15.00

Contour Data	Pole Vectors
Maximum Density	14.50%
Contour Distribution	Fisher
Counting Circle Size	1.0%

Kinematic Analysis	Wedge Sliding
Slope Dip	80
Slope Dip Direction	25
Friction Angle	22.924

	Critical	Total	%
Wedge Sliding	122	1890	6.46%

Plot Mode	Pole Vectors
Vector Count	62 (62 Entries)
Intersection Mode	Grid Data Planes
Intersections Count	1890
Hemisphere	Lower
Projection	Equal Angle

C

Figure 5.5: Fisher concentration of the wedge failure stereonets showing the total number of intersecting joints and the joints intersecting in the critical region including the probability of failure.

From the three slopes, it can be seen that slope C is the one with the lowest probability of failure at 6.45 %. This was followed by slope A which had the probability of failure of 12.59 %, and lastly, slope B has the highest probability of failure at 15.26 %. It should be noted that the probability of wedge failure occurring is not the probability of the entire slope failing. It is merely a probability of this type (wedge failure) occurring on the slope. The analysis of the stereonets shows that the chances of wedge failure occurring is low to be worried about.

5.2.4 Toppling failure

This study made use of the Direct toppling failure analysis. In this type of failure, two join sets intersect such that the intersection lines dip into the slope and form toppling blocks. The strike of the discontinuities should be nearly parallel to the strike of the slope while dipping at a steep angle in the opposite direction to the slope. The orientation of the strike of the discontinuities in this case should be perpendicular to the dip direction of the slope. Direct toppling is said to be a problem mostly in near vertical slopes.

The dip directions were recorded to be 174°, 268° and 25° for slopes A, B and C respectively. The orientations of the slopes were measured and presented in Table 4.6. Figure 5.6 shows the stereonets that depict the toppling failure of the slopes. As can be seen, the critical area/zone is represented by the red-shaded area. The critical zone is delineated by the use of lateral limits. All the discontinuities that intersect within the red zone represents the risk of blocks forming. The probability of failure for the three slopes (A, B and C) was computed by DIPS computer program. The computed probability of failure for slopes A, B and C was at 17.95 %, 27.67 %, and 37.10 % respectively.

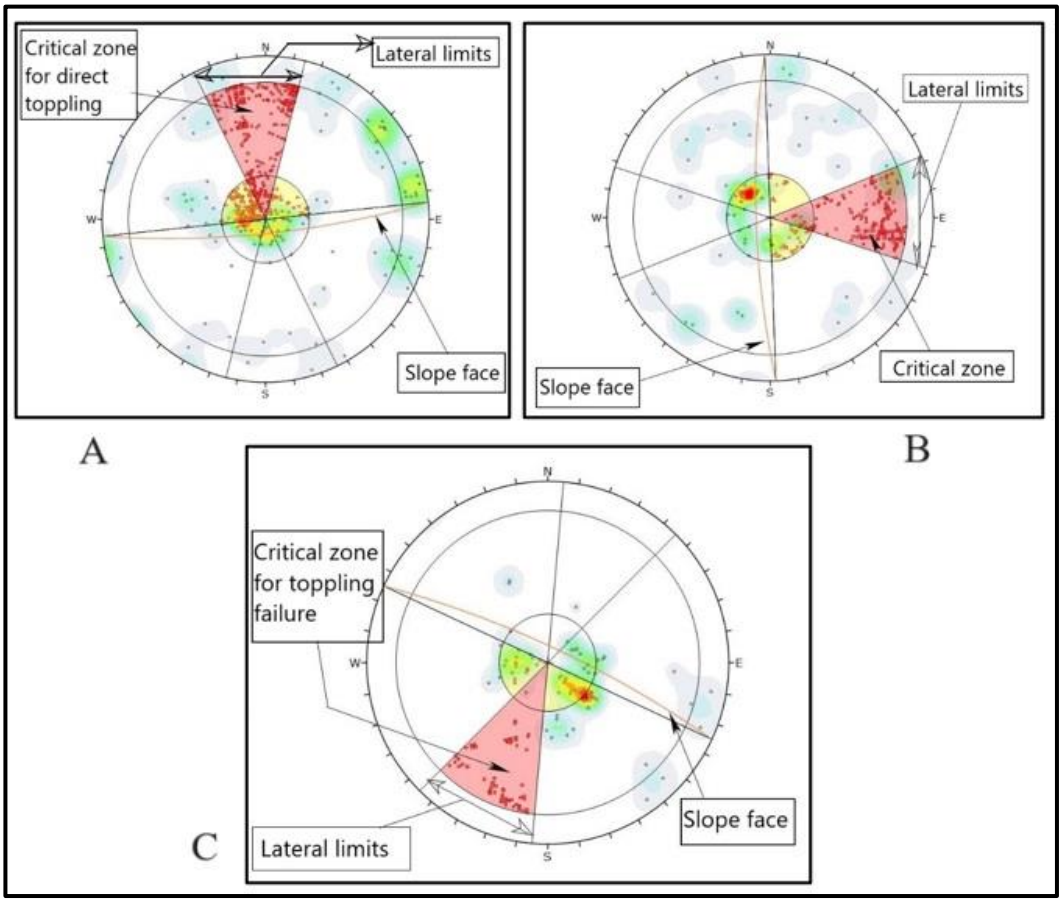

Figure 5.6: Stereonets showing the toppling failures of slopes A, B and C.

Figure 5.7 below shows the fisher concentration for the stereonets representing slopes A, B and C. From the information given on the stereonets, the fisher concentration provides additional information which include the probability of toppling failure occurring on the slopes.

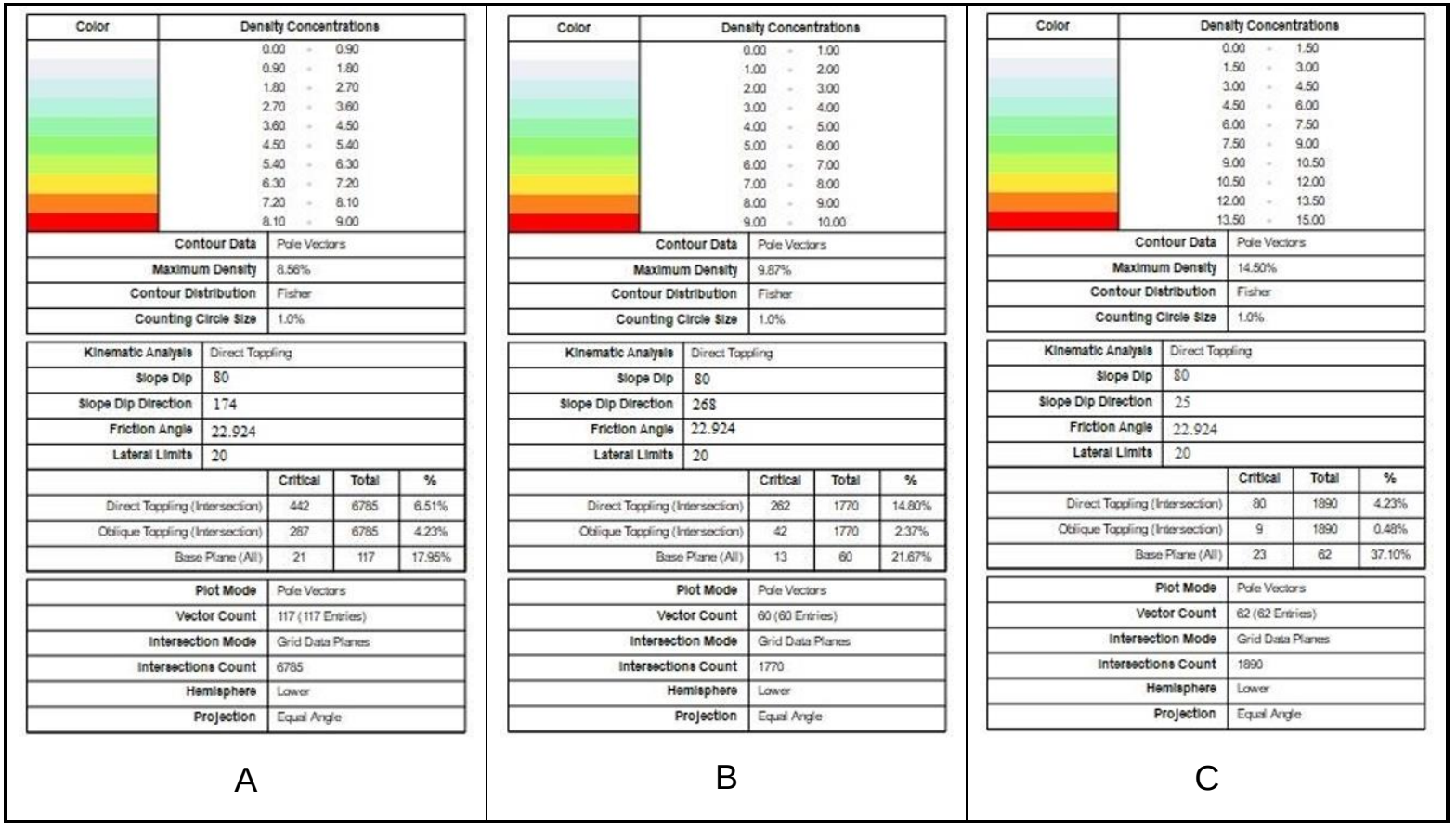

Color	Density Concentrations
	0.00 - 0.90
	0.90 - 1.80
	1.80 - 2.70
	2.70 - 3.60
	3.60 - 4.50
	4.50 - 5.40
	5.40 - 6.30
	6.30 - 7.20
	7.20 - 8.10
	8.10 - 9.00

Contour Data	Pole Vectors
Maximum Density	8.56%
Contour Distribution	Fisher
Counting Circle Size	1.0%

Kinematic Analysis	Direct Toppling
Slope Dip	80
Slope Dip Direction	174
Friction Angle	22.924
Lateral Limits	20

	Critical	Total	%
Direct Toppling (Intersection)	442	6785	6.51%
Oblique Toppling (Intersection)	287	6785	4.23%
Base Plane (All)	21	117	17.95%

Plot Mode	Pole Vectors
Vector Count	117 (117 Entries)
Intersection Mode	Grid Data Planes
Intersections Count	6785
Hemisphere	Lower
Projection	Equal Angle

A

Color	Density Concentrations
	0.00 - 1.00
	1.00 - 2.00
	2.00 - 3.00
	3.00 - 4.00
	4.00 - 5.00
	5.00 - 6.00
	6.00 - 7.00
	7.00 - 8.00
	8.00 - 9.00
	9.00 - 10.00

Contour Data	Pole Vectors
Maximum Density	9.87%
Contour Distribution	Fisher
Counting Circle Size	1.0%

Kinematic Analysis	Direct Toppling
Slope Dip	80
Slope Dip Direction	268
Friction Angle	22.924
Lateral Limits	20

	Critical	Total	%
Direct Toppling (Intersection)	262	1770	14.80%
Oblique Toppling (Intersection)	42	1770	2.37%
Base Plane (All)	13	60	21.67%

Plot Mode	Pole Vectors
Vector Count	60 (60 Entries)
Intersection Mode	Grid Data Planes
Intersections Count	1770
Hemisphere	Lower
Projection	Equal Angle

B

Color	Density Concentrations
	0.00 - 1.50
	1.50 - 3.00
	3.00 - 4.50
	4.50 - 6.00
	6.00 - 7.50
	7.50 - 9.00
	9.00 - 10.50
	10.50 - 12.00
	12.00 - 13.50
	13.50 - 15.00

Contour Data	Pole Vectors
Maximum Density	14.50%
Contour Distribution	Fisher
Counting Circle Size	1.0%

Kinematic Analysis	Direct Toppling
Slope Dip	80
Slope Dip Direction	25
Friction Angle	22.924
Lateral Limits	20

	Critical	Total	%
Direct Toppling (Intersection)	80	1890	4.23%
Oblique Toppling (Intersection)	9	1890	0.48%
Base Plane (All)	23	62	37.10%

Plot Mode	Pole Vectors
Vector Count	62 (62 Entries)
Intersection Mode	Grid Data Planes
Intersections Count	1890
Hemisphere	Lower
Projection	Equal Angle

C

Figure 5.7: Fisher concentration for the toppling failure stereonets.

5.3 Limit equilibrium analysis

This section presents the analytical results of the Limit Equilibrium methods (LEM). As previously stated in Chapter 3, the study area was divided into three sections A, B and C. All three slopes are made up of a similar rock type. The LEM analysis was done utilizing the SLIDE computer program. In theory, the computer program can use all the conventional LEM, however, for this study, only four methods were used. These methods are Bishop's, Janbu's, Morgenstern-price and Spencer's methods. All these four methods are said to consider slip surfaces.

It should be noted that the movements in the mine can cause damage to the rock mass under certain conditions. These conditions are related to the geometry and the geo-material status which determine the behavior and the critical slip surface (Azarafza et al., 2021; Hou et al., 2019; Zhu and Yang, 2018). The damage of the rocks on a slope needs to be investigated and a quantitative assessment is needed in the whole slope stability analysis (Sarma and Tan, 2006). The stability of the slope is determined by the use of the Safety Factor or Factor of Safety (FoS), which is the ratio of the shear strength to the shear stress required for the equilibrium. It is documented that if the FoS is less than 1.5, the slope is deemed unstable (Hoek and Brown, 1981).

5.3.1 Stability analysis of the slopes using SLIDEs models.

The SLIDE program simplifies the process of finding the FoS and the critical slip surface on the strength of LEM. From all the models created from the SLIDE program, a minimum FoS for circular sliding surfaces is considered. With reference to Figures 5.8, 5.9 and 5.10, the FoS values of slopes A, B and C are presented. The FoS values for all three slopes range from 1.739 to 2.271 for all LEMs involved in the computations.

For slope A, the FoS ranges from 2.147 to 2.271. These FoS values rate the slope as safe or stable. Slope B had the FoS which ranges from 1.928 to 2.035. Slope C, on the other hand, had the FoS which ranges from 1.739

to 1.808. Figures 5.8 to 5.10 highlight the LEM modelling with the estimated FoS for slopes A, B and C.

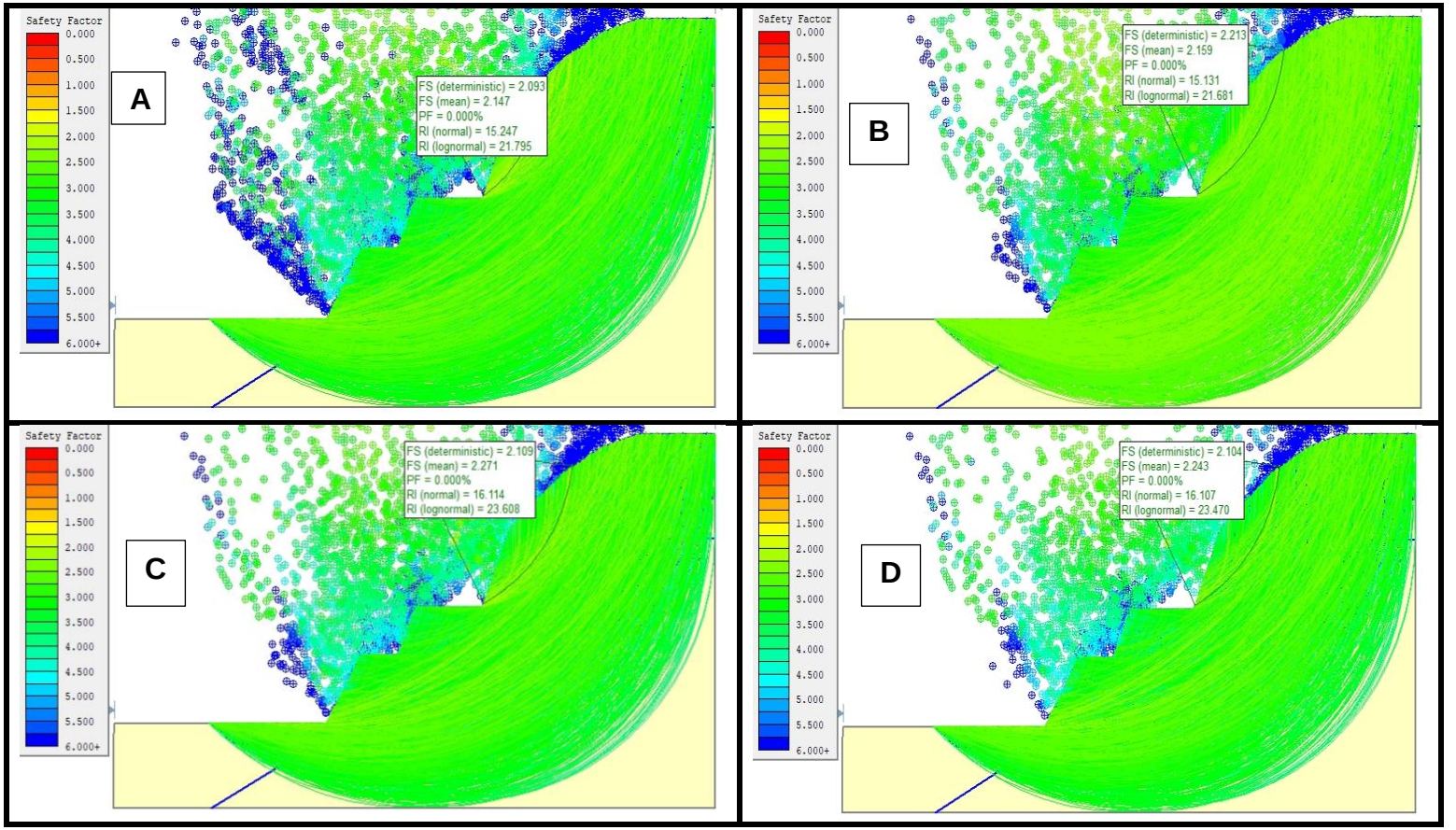

Figure 5.8: Limit Equilibrium models to determine the FoS using (A)Bishop's, (B)Janbu's, (C)Morgenstern-price and (D)Spencer's methods for slope A.

The simulated slopes were supported by field observations and measurements. The results reflect that all three slopes are stable. It can be noted that the results concur with the empirical calculations that the slopes are stable. The empirical results rate the slopes A, B and C as 75, 71 and 71 respectively. In addition to the empirical simulations, it can be noted that the kinematic analysis is also in agreement with the produced results by LEM.

As previously discussed, the LEM determines the critical slip surface. The critical slip surface is the surface with the minimum FoS and it is mostly assumed as the surface where failure is likely to occur on that particular slope. In this study, the critical slip surface on the models was represented by a black line.

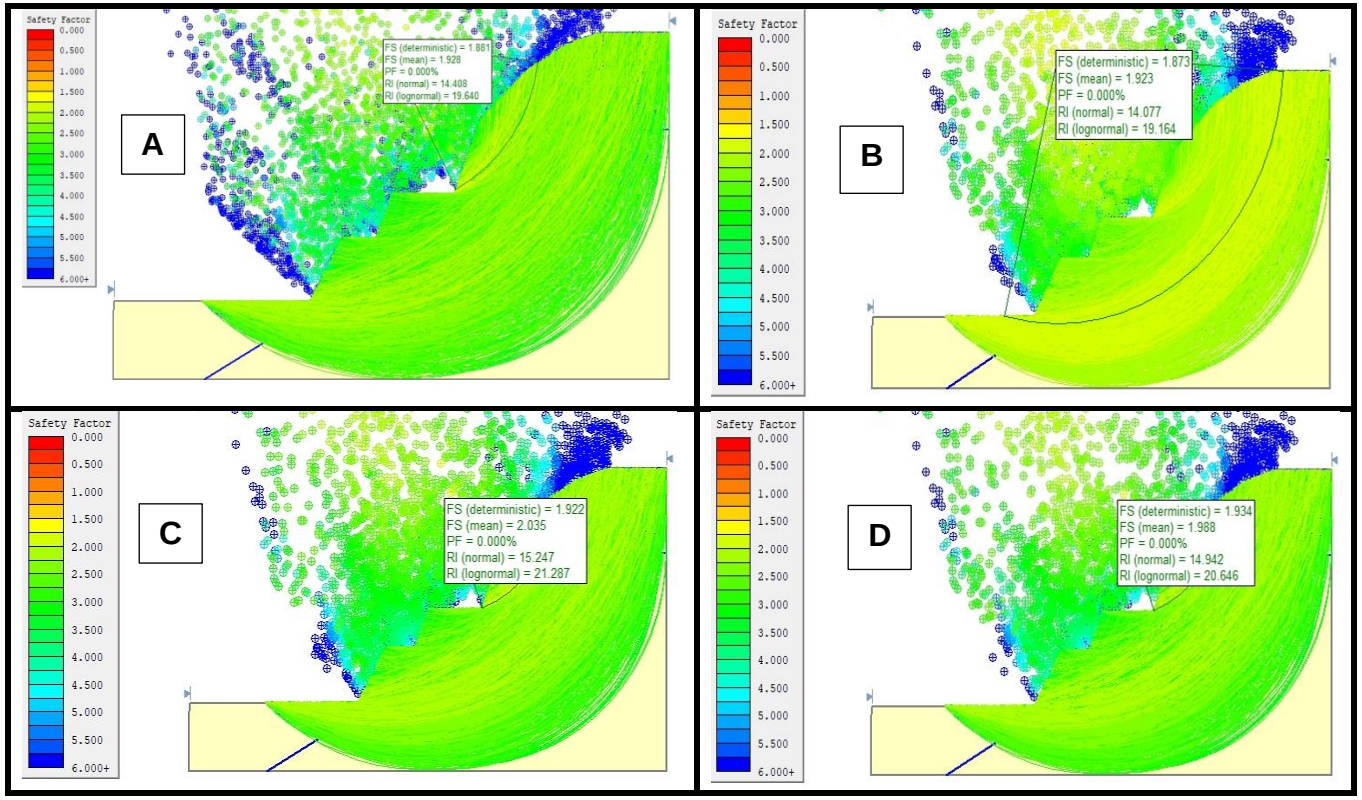

Figure 5.9: Limit Equilibrium models to determine FoS using (A)Bishop's, (B)Janbu's, (C)Morgenstern-price and (D)Spencer's methods for slope B.

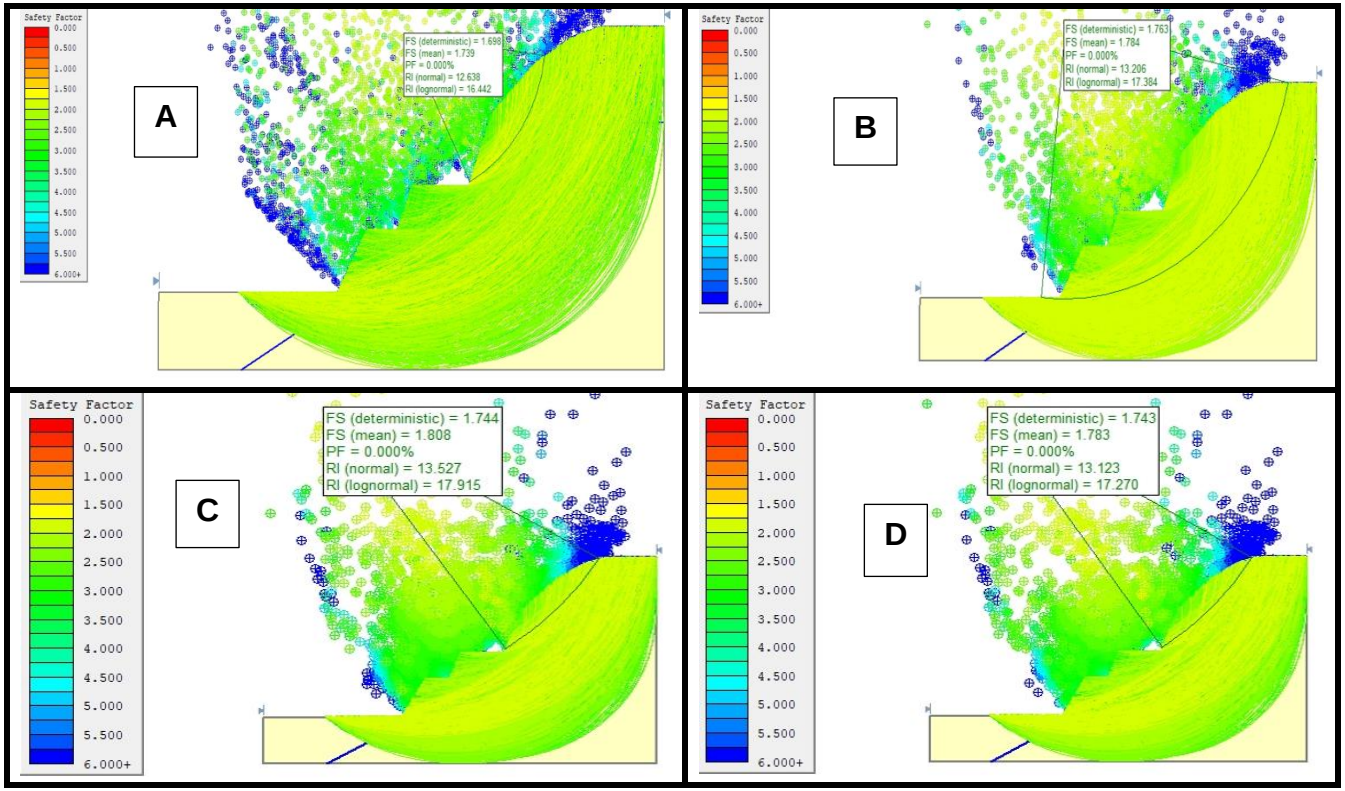

Figure 5.10: Limit Equilibrium models to determine the FoS using (A)Bishop's, (B)Janbu's, (C)Morgenstern-price and (D)Spencer's methods for slope C.

As observed from the simulations, the FoS values are reasonably high. All four methods used produced the FoS value higher than the standard value of 1.5, and this makes the analysis unbiased. The high FoS values of the slope are owed to slope properties, ranging from the bench heights, overall slope angle and material properties. The high values of FoS are proof enough that the slopes are stable and are not prone to immediate failure. Igneous rocks are considered to be stable naturally; hence, the FoS is still considerably high even with the presence of discontinuities.

The kinematic analysis also proves that the probabilities of failures are quite small which shows that the slopes are stable. After the LEM analysis, further investigations of the slopes need to be conducted and, in this instance, numerical analysis was conducted in order to validate the already produced results.

5.4 Numerical analysis of rock behaviour

In Section 3.4.1 of Chapter 3, it was explained that this study made use of a computer program known as OPTUM G2. This program makes use of the FEM principles. FEM is a numerical technique used to simulate complex mining conditions (see Section 2.7.4.1 of Chapter 2). The numerical methods not only simulate but also assist in determining the unstable zones and the potential modes of failure amongst others (Soren et al., 2014). Another program used in this study is the ROCFALL program which assisted in estimating the final deposition location after a rockfall event in the slope.

5.4.1 Long-term stability analysis of the slopes using OPTUM G2

The presence of discontinuities makes the strength of rock mass deteriorate and more complex and difficult to assess. Zhang (2006) indicated that joints are the most common type of discontinuity. With that said, the presence of discontinuities makes the strength behaviour of the rocks to be

compromised. Owing to that, some of the main attributes on the joints that influence the rock strength are joint frequency, orientation and roughness (Zhang, 2006; Tang, 2015; Purwanto, 2020). There have been many researchers who conducted studies on the effect of frequency and orientation on the strength of the rock mass and the slope in general, some of these authors include Jaeger (1960), Lama (1974), Halakatevakis and Sofianos (2010), Maji and Sitharam (2012), Bidgoli and Jing (2014), and Kumar et al. (2017).

These authors reiterated that with an increase in the joint frequency, the rock becomes weak in terms of strength. Therefore, a rock mass with a higher joint frequency will exhibit failure earlier than a rock mass with a lower joint frequency. There is one aspect of discontinuities that is hardly investigated which is the depth at which discontinuities go into the slope from the face or surface of the slope. Mukhlisin and Naam (2015) conducted a study that shows that the depth at which a joint goes in depth has an impact on the stability of the slope. This is a result of the pore water pressure which increases with depth. At the lower parts of the joints, the pore water pressure is high, hence decreasing the safety factor of the slope. This study made use of the OPTUM G2 to investigate the impact of the discontinuity depth on the stability of the slope. As discussed in Chapter 3, one slope is in operation and the other two with no mining activity on them. However, they are being affected by the drilling and blasting that is happening in slope A. In addition to drilling and blasting, the daily operation in the mine also impacts the two slopes not in operation through vibrations.

During drilling and blasting, the energy is released in the form of shock waves into the rock mass. Therefore, during the drilling and blasting, there is a development of joints as well as further elongation of the present joints into the rock mass away from the face of the slope. When the joints continue to increase in depth, the stability of the slope is affected both in the short-term and long-term. The OPTUM G2 program was applied to simulate the slope behaviour and analyse the stability of the slopes in varying depths in the long term.

The methodology of how the investigation was performed was discussed in Section 3.4.1. OPTUM G2 program was able to determine the strength reduction factor. The program calculates the upper and lower strength reduction factors. From the upper and lower strength reduction factors, an average is taken and interpreted as the FoS. This was adopted from a study by Maji (2017) who highlighted the use of the upper and lower bounds of SRF to obtain the final SRF. In order to determine the strength reduction factor, the program runs a series of computations against the model to determine if the best reduction factor. An example of how the program runs the computations of the reduction factor is indicated in Figure 5.11.

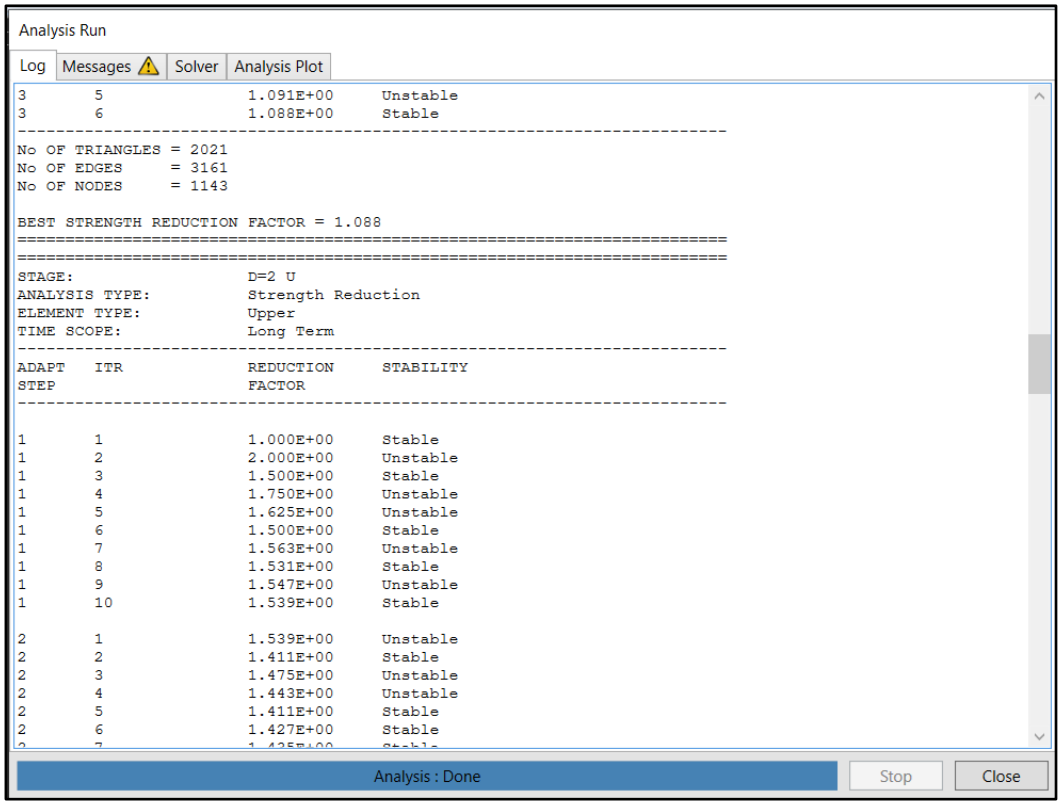

Figure 5.11: Analysis run window on OPTUM G2 which shows how the computations for the SRF were done and the stability verdict if the slope is stable or not.

As observed from Figure 5.11, the program randomly selects a reduction factor and determine if the slope is stable or not. This process is repeated multiple times by the program automatically, thereafter the best reduction factor is then determined. It should be noted that for one model, the upper

and the lower reduction factors are determined. Thereafter, an average between the two reduction factors (Lower and Upper) is taken. This is then recorded as the strength reduction of the slope. Furthermore, the average strength reduction factor determined is interpreted as the FoS of the slope. Once the computations are done, the 'analysis run' window shows the computations that the program did.

After the computation of the reduction factor, the model of how the slope will behave is then generated automatically. It should be noted that the long-term stability analysis was determined for all three slopes (i.e., slopes A, B and C). The stability of the slopes using OPTUM G2 for the three slopes is presented in Sections 5.4.1.1 – 5.4.1.3 below.

5.4.1.1 Stability analysis of Slope A using OPTUM G2

The modelling of failure in slope A was done starting from 1 m length of joints into the slope. This was followed by 2 m, 3 m and lastly 6 m. From all the models, the strength reduction factor was produced by the program. According to Abdellah (2018), the strength reduction factor is used to evaluate the stability of the rock slope and is equivalent to the FoS. The failure at the abovementioned depths will be discussed below.

Let us start by looking at the failure model at 1-m depth. The simulation results of the slope behaviour when joints are at 1-m depth are summarized in Figure 5.12. Indeed, Figure 5.12(a) shows the mine slope prior to failure simulations with the directions of the discontinuities indicated as white lines. On the other hand, Figure 5.12(b) shows the probable failure of the slope. It should be noted that the failure model was conducted under no additional weight or disturbance on the rock mass other than gravity and the weight of the rock mass. The white lines that propagate from the surface of the slope to the inward direction of the slopes represent the discontinuities.

The strength reduction factor (SRF) of the slope at 1m depth was found to be 1.336 and 1.868 for the upper and lower bounds of the slope

respectively. The average SRF was calculated and found to be 1.602. The value was obtained by adding the upper and lower strength reduction factor values and dividing by two. According to Ledesma et al. (2016), the values of the strength reduction method is equivalent to the FoS. The average strength reduction factor of 1.602 was then recorded as the FoS of the slope. According to Stark and Ruffing (2017), a minimum of 1.5 is required to classify a slope as stable. For slope A, the slope can be categorised as stable since its FoS is above 1.5. It should be noted that even if the slope is considered stable according to the FoS set standard, the slope does show fracture propagation which may lead to the instability of the slope in the near future. Therefore, the time-dependent factor of rock mass deterioration is critical in this case.

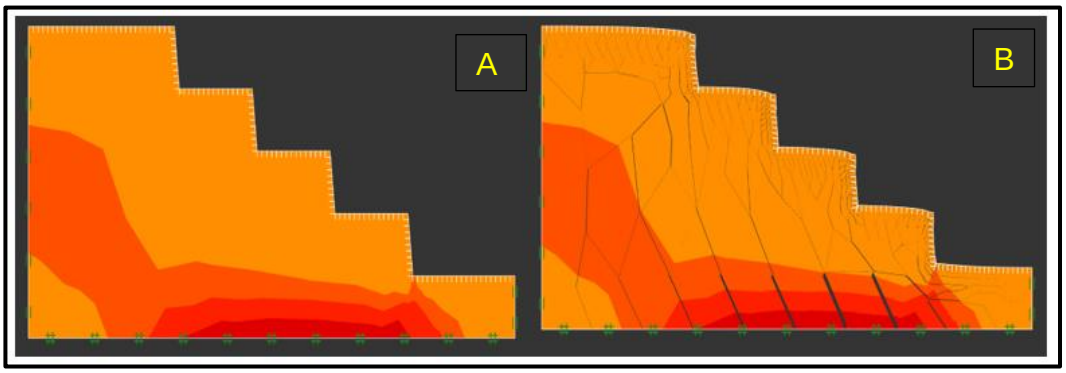

Figure 5.12: Models of slope A with (A) on the left representing the model before failure simulation and (B) represents simulation after failure simulations for 1-m depth.

At 2-m depth of the discontinuities, the lower and upper elements of the SRF were found to be 1.381 and 1.719 respectively (see Figure 5.13). The average SRF was estimated to be 1.55 which meant that the FoS of the slope is at 1.55. From the calculated FoS, it was concluded that the slope can be classified as stable. Since the computed SRF is almost at the minimum limit of 1.5 to deem the slope stable, a little additional stress to the slope can render the slope unstable. WG Wearne is still in operation and the continuous vibrations during the operation of the mine could be sufficient to add stress to the slope leading to instability.

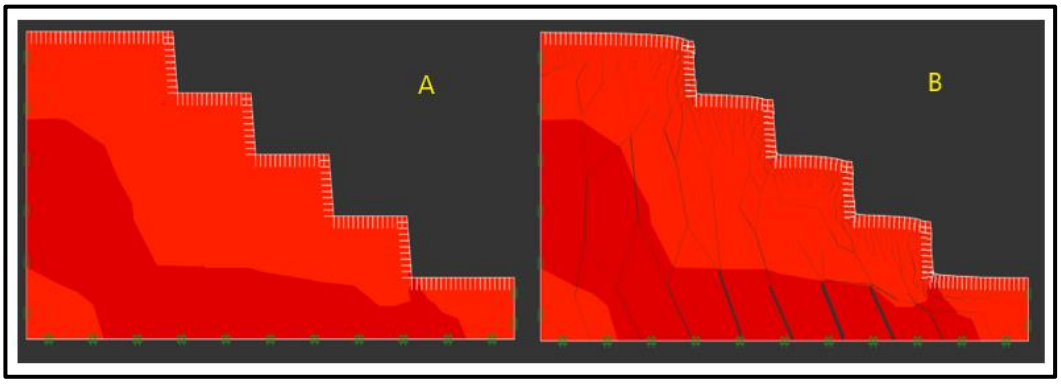

Figure 5.13: Models of slope A before and after failure simulation for 2-m depth.

At a 3-m depth of the discontinuities, the slope showed an increased fracture propagation as shown in Figure 5.14 for an SRF of 1.508. This was calculated as an average value of the slope from 1.207 and 1.809 for lower and upper SRF values respectively. It should be noted that an additional load to the slope may cause instability. Taher et al. (2022) also confirmed that the slopes may collapse under the influence of both the weight and applied loads.

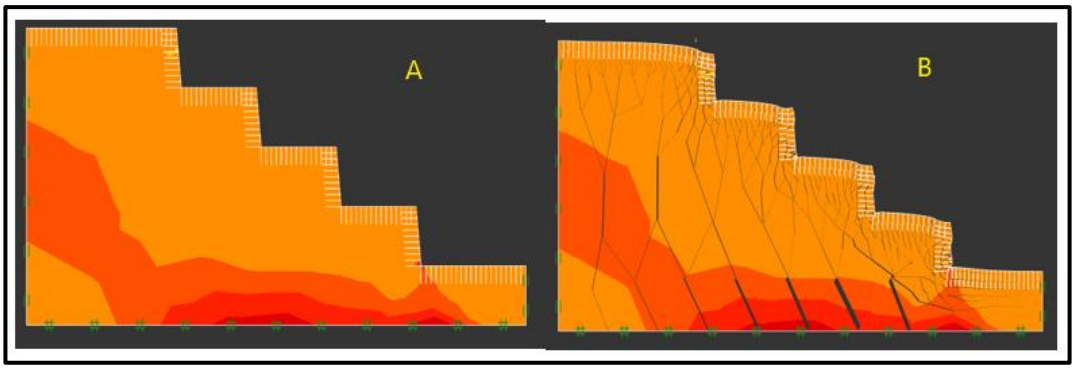

Figure 5.14: Models of slope A before and after failure simulations of discontinuities at 3-m depth.

With the SRF value of 1.508 calculated as an average from lower and upper SRF of 1.207 and 1.809 respectively, the slope is still considered stable. Compared to the failure when discontinuities are 1-m and 2-m deep, there is a noticeable shift at the tips on all benches. Yang et al. (2020) indicated that as the discontinuity length or propagation increases, the stability of the gets compromised. This is because the area of shear is increased with the

increase of discontinuities length. The increase of shear region reduces the cohesion of the slope. The reduction of the cohesion reduces the stability of the slopes. This can be corroborated by the value of the SRF of the slope which has decreased from the two previous models in Figures 5.13 and 5.14. Through analysing the models in Figure 5.16, there is a noticeable increase in the movement of the slope. This is a clear indication that the slope stability is decreasing as the discontinuities deepen.

The failure of the slope when discontinuities are at 6m deep is presented in Figure 5.16 below. The failure when discontinuities are at 6m seems to be severe as compared to when the discontinuities are at 1-m, 2-m and 3-m deep.

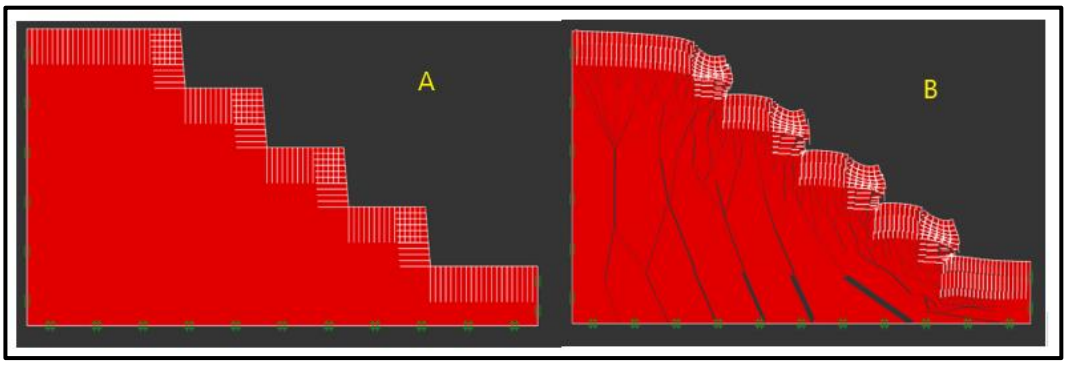

Figure 5.15: Models of slope A before and after failure simulations of discontinuities at 6-m depth.

The increase in fracturing increased based on the intersection of discontinuities. The longer the discontinuities get, the more they intersect with other discontinuities. Zhao et al. (1993) pointed out that the extension of cracks occurs as a result of increased stress in the rock mass. This leads to the formation of smaller rock fragments in the rock mass on the slope.

The smaller fragments of the rocks within the rock mass lead to the reduction of the shear strength of the rock mass. This is due to a decrease in the cohesion of the rock mass caused by the presence of the long discontinuities.

The SRF of the slope with 6-m deep discontinuities is 1.46. This was calculated as an average from the lower and upper SRF of 1.238 and 1.681 respectively. There is a significant decrease in the SRF of the slope with an increase in the fracturing of the rock mass of the slope.

5.4.1.2 Stability analysis of SLOPE B using OPTUM G2

The procedure followed for modelling the failure on slope B is similar to that used on slope A. Like in Section 5.4.1.1, there was no increase in the load factor on the slope, only the gravity and the weight of the rocks were considered. Simulations were run for discontinuities as deep as 1 m, 2 m, 3 m, and 6 m. It is worth noting that the number of benches on slope B was 5 which is not the same as the 4 available on slope A. This intuitively suggests that the SRF should be less than that of slope A due to the increased depth of the slope. Detailed analysis of the stability of slope B is documented in the same chronological order as that presented for slope A.

At first glance, simulation outputs for 1-m deep discontinuities show in Figure 5.16 that the degree of fracturing of slope B is pronounced as compared to Figure 5.12. This was confirmed by the SRF of slope A that was estimated at 1.332 and 1.786 for the lower and upper SRF respectively. The average SRF for this slope was calculated to be 1.51.

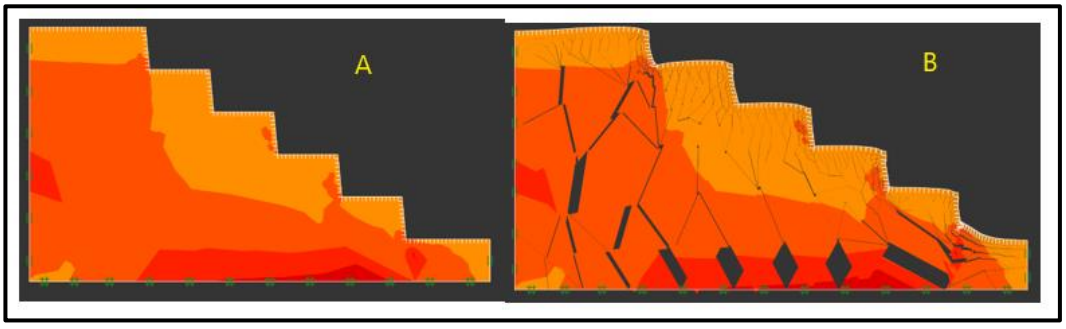

Figure 5.16: Models of slope B before and after failure simulations of discontinuities at 1-m depth.

The calculated SRF for the slope at 1-m depth is a clear indication that the stability of the slope is reduced. This was in comparison to slope A when

the discontinuities were at 1-m depth. Zhang et al. (2021) alluded that the instability of slopes increases as pit gets wider and deeper. The widening and deepening of the pit can be directly linked to the number of benches. As a result, an increase in the number of benches on slope B results in the increase in stress exerted on the slope. The stability of the slope is then reduced. From observation of Figure 5.16, it can be clearly seen that the discontinuities from the model are more projected which is a clear indication of the reduced strength of the slope.

When the discontinuities were at 2-m depth, the SRF of slope B was recorded as 1.281 and 1.719 for upper and lower SRF. The average SRF of slope B at 2-m depth of discontinuities was calculated and found to be 1.5. The prediction of slope behaviour at 2-m depth is shown in Figure 5.17 below.

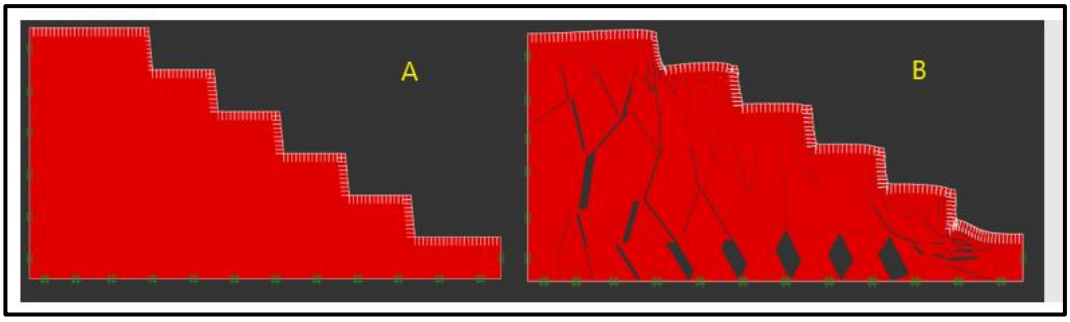

Figure 5.17: Models of slope B before and after failure simulations of discontinuities at 2-m depth.

The discontinuities are more pronounced when the failure is at 2-m depth. This was in comparison to the failure simulation was at 1-m depth. This continues to confirm the point made by Yang et al. (2020) that the length and depth at which discontinuities propagate determines the strength of the rock mass. In this case, it can be seen clearly that the longer the discontinuities deepen, the weaker the rock mass gets.

The calculated SRF of the slope was calculated and found to be exactly 1.5. It should be noted that the calculated SRF is equal to the minimum SRF required to deem a slope stable. Owing to that, the stability of the slope is

at a critical point. An additional load or stress to the slope means that the slope can fail.

At 3-m propagation of the discontinuities, the SRF was found to be 1.258 and 1.722 for lower and upper SRF. The calculated average SRF being 1.49. The joint frequency increases in a more noticeable way. The frequency of the discontinuities is more compared to when the simulation was run for 2 m.

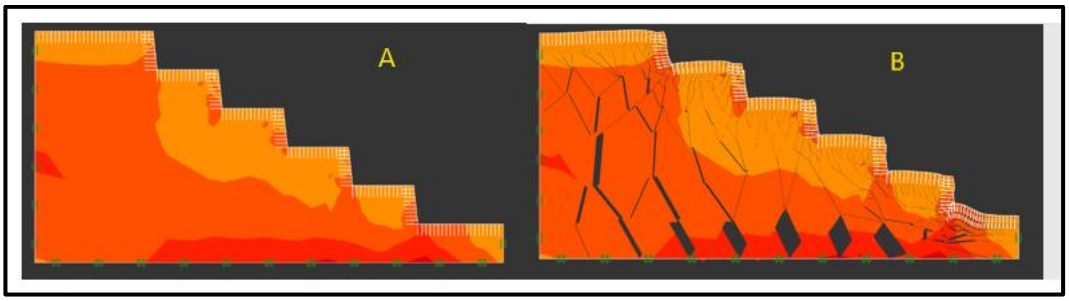

Figure 5.18: Models of slope B before and after failure simulations of discontinuities at 3-m depth.

Zhang et al. (2021) and Li et al. (2022) alluded to the fact that as the pit continues to get deeper, the slope becomes longer and steeper. Slope B has an increased number of benches, and it is longer than slope B. The increase in the length of the slope coupled with an increase of the joint propagation from 2 m to 3 m, there is increase in the area experiencing the stresses. This leads to a reduced SRF on the slope. When assessing the simulation model in Figure 5.21, the simulated propagation of discontinuities becomes more pronounced. This was in comparison to when the discontinuities when the joints were at 1 m and 2 m. This can be further justified by the reduced SRF recorded for the slope. The slope was then be classified as unstable. This is due to the fact that the SRF obtained is below the minimum required to be classified as safe. This means that the average SRF is 1.49. This is below the minimum standard of 1.5 to qualify the slope as stable.

The joints may continue to propagate in the presence of a disturbance factor including the presence of water in the joints (Singh et al., 2016). This study

also conducted a simulation when the discontinuities propagated 6 m into the rock mass. The recorded SRF when the discontinuities were at 6 m was 1.195 and 1.565 for lower and upper elements respectively. The average SRF of the slope was calculated to be 1.38 which according to Gol et al. (2016) is below the minimum acceptable SRF for a stable slope. Therefore, the slope is considered unstable. When the simulation is run with discontinuities at a depth of 6 m, the slope shows a significant difference from when the slope was being modelled for 3-m depth discontinuities. The discontinuities on the rocks are pronounced and the failure of the slope is more visible. The tips of the benches seem to be collapsing and that is due to the increased joint frequency caused by the intersection of the discontinuities. Figure 5.19 shows the modelling of the slope before and after the introduction of 6 m discontinuities.

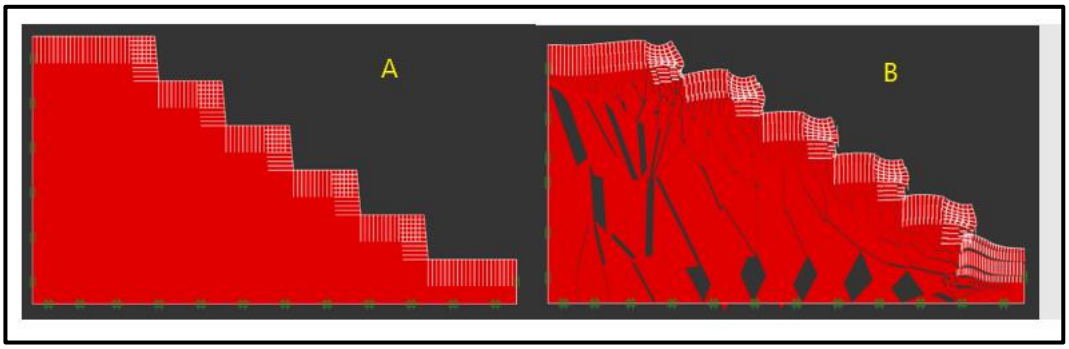

Figure 5.19: Models of slope B before and after failure simulations of discontinuities at 6-m depth.

At 6 m, the fracture propagation is more severe, and this can be confirmed by the SRF which is at 1.38. This renders the slope unstable since the SRF value is below 1.5.

Moradi and Hosseinintoudeshki (2015) conducted a study that led to the conclusion that the more the number of joints, the less the SRF value, which then translates to reduced strength of the slope. When discontinuities propagation is at 6 m, the area of joints intersection increases as compared to when the discontinuities propagation was at 1 m, 2 m, and 3 m. There is a significance difference in the area of intersections when discontinuity

propagation was at 1 m, 2 m, 3 m and 6 m; hence, the reduced strength reduction factor.

5.4.1.3 Stability analysis of SLOPE C using OPTUM G2

The procedure of modelling of slope C was not different from that followed when modelling slopes A and B. The biggest difference observed in the models is that slope C had 3 benches and as a result, the slope is relatively small compared to slopes A and B which have 4 and 5 benches respectively. According to Shiferaw (2021), an increase in the slope height decreases the Factor of safety and the opposite is the case. whereby a decrease in the slope height increases the FoS of the slope. The procedure as discussed in Section 3.4.1 of Chapter 3, 1 m, 2 m, 3 m, and 6 m depth of discontinuities were run.

At 1 m, the slope shows fractures propagating into the slope from the top of the benches going downwards. The SRF of slope C when the discontinuities were propagating only 1 m was found to be 1.344 and 1.896 for the upper and lower elements respectively. The average was calculated to be 1.62. According to Gol et al. (2016), the slope can be classified as stable if the calculated SRF is above the minimum or critical SRF. The minimum required SRF to deem a slope stable is 1.5. The calculated SRF of the slope at 1m depth of discontinuities is above 1.5. This leads to the conclusion that the slope is classified as stable. The SRF of slope C agrees with the conclusion arrived at by Shiferaw (2021). This typifies the fact that slope height plays an important role in the stability of the slope.

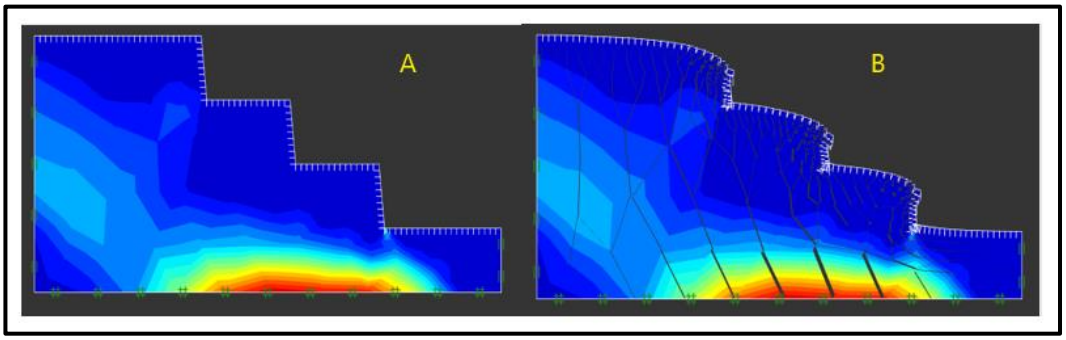

Figure 5.20: Models of slope C before and after failure simulations of discontinuities at 1-m depth.

In this case, slope C has the lowest slope height of the three slopes. Owing to that, slope C has the lowest SRF value between slopes A, B and C. Figure 5.23 shows how the slope is likely to fail under the stated conditions. The simulation output on the left (Figure 5.20A) represents the slope before the failure occurs while on the right, Figure 5.20B) is a representation after the rendering is done after the failure has occurred. It should be noted that the frequency of the discontinuities is great closer to the bench surface and is reduced going deep into the rock mass. The crest of the benches also seems to be experiencing more failure. This is due to the intersection of joints at those points. Moradi and Hosseinintoudeshki (2015) argued that for a slope to fail, a disturbance factor should be present. In the context of this research study, there are crustal stresses acting on the rock mass. As such, when these stresses meet a rock with discontinuities, there is a disturbance on the rock mass such that discontinuities develop and continue to change in size.

Figure 5.21 represents the slope at a 2-m depth of discontinuities simulated before and after failure due to simulated discontinuities. Upon assessment of the simulated model, it can be seen that the difference physically in the models is minimal. However, the calculated SRF tells a different story. There is a slight decrease in the measured SRF. The SRF recorded was 1.367 and 1.813 for the lower and upper SRF of the slope respectively. The average calculated SRF was 1.59. This is a slight decrease from when the discontinuities were at 1-m depth.

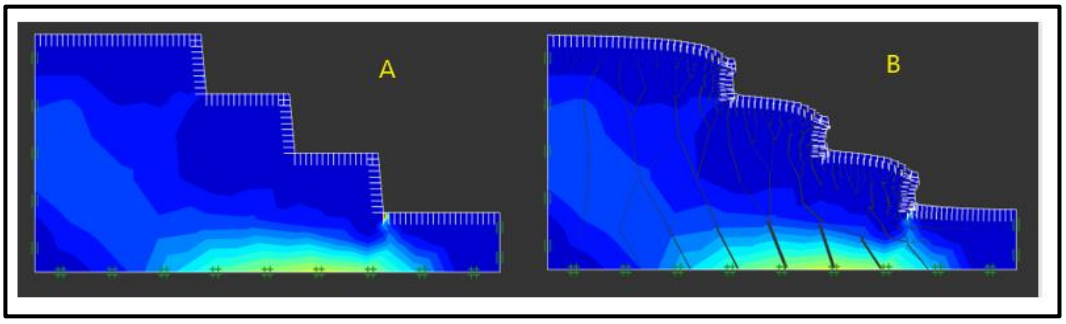

Figure 5.21: Models of slope C before and after failure simulations of discontinuities at 2-m depth.

Moradi and Hosseinintoudeshki (2016) shared that the intersection of the discontinuities reduces the cohesion and consequently reduces the SRF of the rock mass. This is confirmation that the introduction of the discontinuities reduces the cohesion of the rocks. This negatively affects the stability of the slope, which has the potential for failure. Along the crest of the benches is where most differences are seen between the models when the discontinuities were propagating 1 m and 2 m respectively.

At a 3-m depth of discontinuities, the joint frequency closer to the bench surface increases. As indicated by Shiferaw (2021) that the slope height affects the stability of slopes. Slope C has the least number of benches than slopes A and B. Therefore, the initial assumption prior to calculation of the SRF for the slope with discontinuities at 3 m is that it will be higher. This is when comparing it with other slopes (i.e., A and B) when discontinuities were at 3-m depths. Figure 5.22 below shows a model of slope C before and after simulation of discontinuities at 3-m depth.

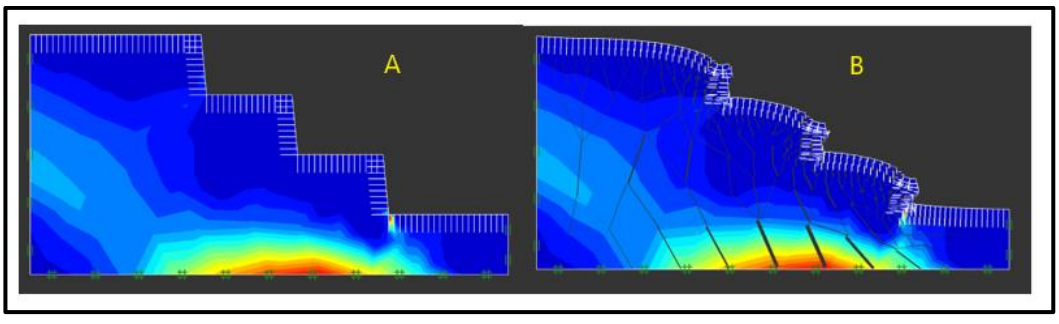

Figure 5.22: Models of slope C before and after failure simulations of discontinuities at 3-m depth.

The recorded SRF for slope C with discontinuities at 3-m depth was 1.248 and 1.792 for the lower and upper SRF. The average was calculated and found to be 1.52. As stated in the previous paragraph, the SRF of slope C with discontinuities at 3 m is higher than that in the same slope C but at similar depth. This confirms the assumption made. According to the minimum standard presented by Stark and Ruffing (2017), the slope can be categorized as stable.

However, the crest of the benches is an indication that the slope is nearing its limit. This simply means that an additional load to the slope can take the SRF to below 1.5. Therefore, a slope can be deemed unstable if the SRF is below 1.5.

At 6-m deep discontinuities, the slope further loses its strength. This can be seen through the computed SRF which was 1.126 and 1.694 for lower and upper SRF. The average SRF of the slope was calculated and the value of the average SRF is 1.41. The value of the average SRF of the slope is well below the minimum required factor of 1.5. Since the slope's SRF is below the minimum required SRF to deem the slope stable, it can be concluded that the slope is unstable. The calculated SRF of slope C with discontinuities at 6m was more than that of slope B, however, it was less than that of slope A when the discontinuities were at 6 m.

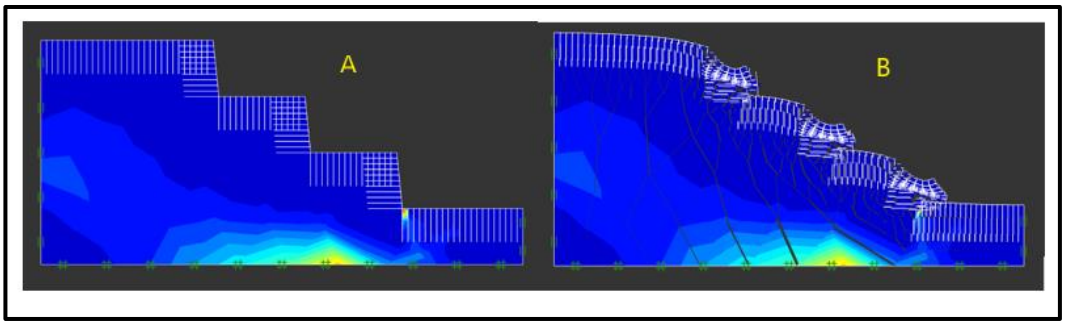

Figure 5.23: Models of slope C before and after failure simulations of discontinuities at 6-m depth.

The models of slopes are presented in Figure 5.23. Figure 5.23A represents slope C prior to failure whereas Figure 5.23B represents the slope after failure. As indicated by Singh et al. (2016), the length and propagation of

discontinuities increase due to the disturbance from the surrounding environments. In an open pit mine, there are certain factors that may affect the stability of the slope. The most common factors include vibrations from blasting, operation of the machinery and presence of water within the discontinuities. The aforementioned factors reduces the cohesion of the rock mass. An increase in the depth at which discontinuities propagate means an increase in the area that loses cohesion in the rock mass. These statements agree with the SRF obtained from the simulation when discontinuities were at 6m. As soon as the discontinuities increase in depth, the SRF reduces. Since the simulation is being done for 6 m joint propagation, the area of intersection increases. Owing to that, the rock along the crest of the benches shows that the slope has lost cohesion, and it is failing. The failure covers the area where the discontinuities propagate.

Note that although the depth of fracturing appears to propagate towards the footwall of the slope this is due to the model block size. If the block was big some of these fractures may propagate further than represented.

5.4.1.4 Summarised findings from the OPTUM G2 simulation results

From the analysis of the slopes using OPTUM G2, it can be observed that when the discontinuities are at a smaller depth, the SRF of the slope is higher. As the depth of discontinuities increases, there is a decrease in the value of the SRF. It can be deduced that fracture propagation weakens the strength of the rock mass as pointed out by Cai et al. (2022). This is because the rocks are continuously being subjected to different stresses which include compressive strength, tensile and shear stresses amongst others. If a rock experiences these stresses and its strength is lower than the experienced stresses, deformation of rock then occurs. As explained in Section 2.3.6 of Chapter 2, the presence of discontinuities reduces the rock strength.

The continuous propagation of discontinuities into the rock mass gradually reduces the rock strength. Similarly, the GSI concurs with this statement. In

Section 3.2.4 (Figure 3.7) of Chapter 3, the increase in the dominance of discontinuities or the discontinuities frequency, this reduces the strength of the rock mass. This can lead to slope instability.

It should be noted that a slope faces multiple stresses and, in this study, the number of benches on a slope also plays a massive role in the stability of the slope. The slopes with more benches were observed exhibit a reduced SRF. An increased number of benches can be translated into an increased slope height. Since the height of the slope is large, the potential for slope instability increases. This is because the weight of the material on the slope increases and as a result, this puts more pressure on the slope and the base as well. An increase in the slope height also affects the angle of repose. The higher the slope height, the shallower the angle of repose. This means that a taller slope will require a flatter angle to remain stable. If the angle of repose is not shallower, the slope can become unstable.

This directly concurs with the obtained results from the OPTUM G2 simulation results. The slopes with a smaller number of benches exhibit a higher strength reduction factor and the ones with an increased number of benches exhibit a reduced SRF (see Table 5.1). Additionally, as the pit continues to get wider and deeper, the stability of the slopes is compromised and most likely to decrease.

From the above models (Figures 5.12 – 5.23), it can be seen that as the depth of discontinuities increases in all the slopes, so does the failure. This is most likely due to the intersection of joints and the increase in principal stress across the excavation. Therefore, the stress distribution will move from the area of weak strength. From all the slopes, it can be observed that when the discontinuities depths are at 1 m, there is a smaller region of joints intersection. This was in comparison to when the discontinuities are at 6 m. There is a larger region of joints intersection when joints are at 6 m. Therefore, when there is an increased depth of discontinuities, the area where the joints intersect forms smaller fragmented rocks which reduces the stability of the slope and an increased chance of failure. It should be

noted that the intersection of discontinuities reduces the shear strength of the rocks. Hence an increased depth of discontinuities shows a larger failure than when discontinuities are at shallow depths.

According to Kolapo et al. (2022), when the joint frequency increases in a slope, so do the probability of failure. In addition to the joint frequency increasing, there is an extension of the discontinuities deep into the rock mass. These discontinuities propagated from the face of the slope deep into the rock mass. Even though the discontinuities are elongating deep into the rock mass, the frequency decreases with depth. However, should the blasting and mining operations continue, the frequency will increase at the lower depths and continue to destabilize the slope. Furthermore, the models only show the elongation of the discontinuities to a certain point and the length at which the discontinuities go further than what the models show cannot certainly be determined and should not be assumed that the discontinuities continue with the same opening.

Table 5.1 and Figure 5.24 show the difference in the SRF of different slopes at different depths of discontinuities. Table 5.1 below should be interpreted in the following way: D=1 L represents the Lower element value of discontinuity depth at 1 m; D=1 U represents the upper element value of discontinuity depth at 1 m; and D=2 L represents the lower element value of discontinuity depth at 2 m.

Table 5.2: Lower, upper and average strength reduction factors for the three slopes investigated at Wearne mine.

SLOPE A			SLOPE B			SLOPE C		
Discontinuity depth and element	Lower and upper SRF	Average SRF	Discontinuity depth and element	Lower and upper SRF	Average SRF	Discontinuity depth and element	Lower and upper SRF	Average SRF
D=1 L	1.336	1.60	D=1 L	1.332	1.56	D=1 L	1.344	1.62
D=1 U	1.868		D=1 U	1.786		D=1 U	1.896	
D=2 L	1.381	1.55	D=2 L	1.293	1.53	D=2 L	1.367	1.59
D=2 U	1.719		D=2 U	1.767		D=2 U	1.813	
D=3 L	1.207	1.51	D=3 L	1.258	1.49	D=3 L	1.248	1.52
D=3 U	1.809		D=3 U	1.722		D=3 U	1.792	
D=6 L	1.238	1.46	D=6 L	1.195	1.38	D=6 L	1.126	1.41
D=6 U	1.681		D=6 U	1.565		D=6 U	1.694	

The line charts were plotted using the average SRF as indicated in Table 5.1 above. The line charts were plotted in order to show the difference in the SRF visually. The line charts of the FoS were plotted using the average SRF value. From the line charts, it can be observed that the slope with more benches has a smaller SRF compared to others. This then confirms that the larger the slope, the more it loses its strength and the more susceptible to failure.

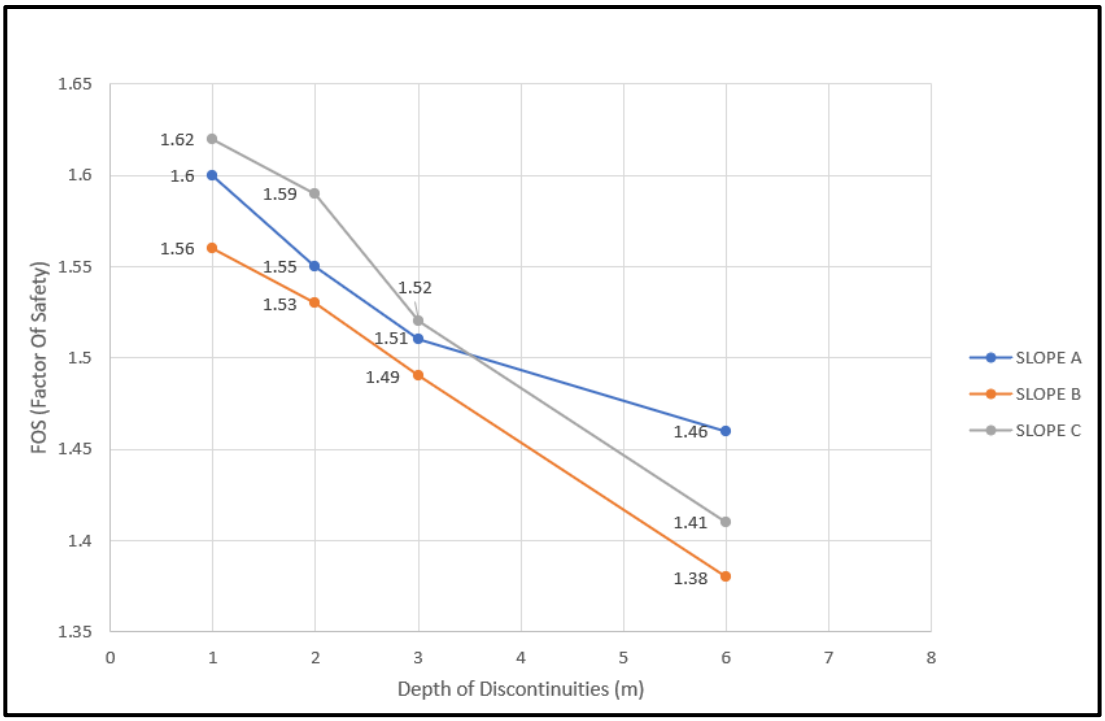

Figure 5.24: Strength reduction factors of different slopes at different depths.

5.5 Numerical simulation of rockfall trajectory using ROCFALL trajectory model

Rockfall analysis is of paramount importance on slopes since it assists in assessing the potential risk of the rocks dislodging or falling from the top of the slope. This analysis helps in determining the measures to implement to reduce the risk posed by falling rocks. The assessment of the rockfalls was conducted primarily to determine the potential area of deposition of rocks that may be

dislodged from the face of the slope. This was done to ensure that the hazard is identified, and remedial actions should be put in place to prevent injuries and property damage. The simulation was run with the assumption that the dislodged rock was from the top bench. There are several parameters that affect the final deposit of the rocks. These parameters include but are not limited to slope geometry (slope height and slope angle) and block size. These parameters are used as input for the simulation.

As indicated in Section 3.4.3 of Chapter 3, slope geometry plays a significant role in the final deposit of the rocks. However, there are other aspects such as the bench height and bench width that also play a similar role. In correspondence with the bench heights is the bench width. It pays a significant role in the rolling distance of the falling rocks. The model presented in Figure 5.25 shows the simulation of rocks from the point when the rocks were dropped from the top of the uppermost bench until the rocks reach the bottom bench. It should be noted that the rocks being dropped are represented by red lines.

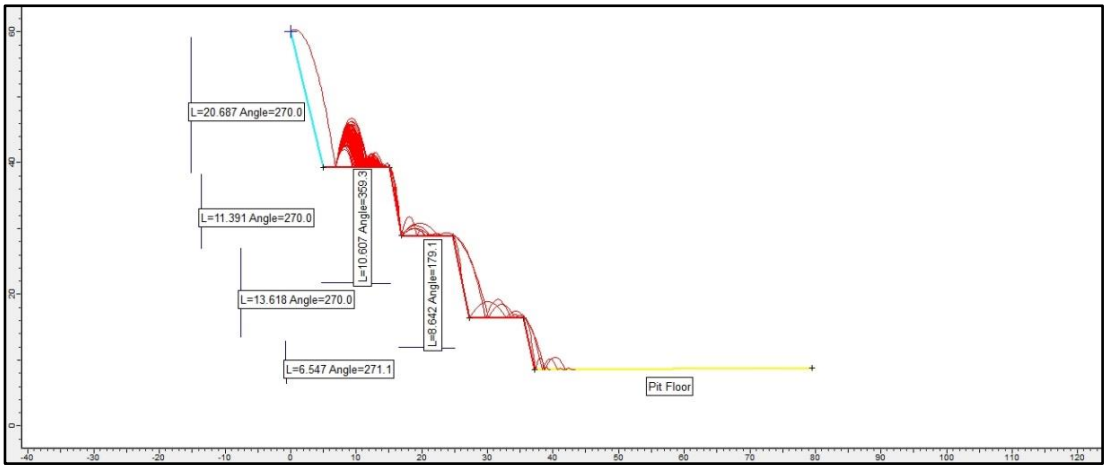

Figure 5.25: Rockfall model of how the rocks move from the high benches to the lower benches.

Sengani (2021) conducted a simulation whereby he concluded that the slope height plays a significant role in the bounce height and the rolling distance of the dislodged rocks. The bench height played a significant role in the bounce

height of the rocks. The bench width influenced whether or not the rocks would roll over to the lower bench. The rock block was simulated to drop from the uppermost bench (bench 5). The weight of the rock along with gravity played a significant role in the velocity of the rock as it reaches the bench below. When the rock block reaches the bench floor, it acts as a projectile whereby it bounces under the influence of kinematic energy. Some simulated rocks reach a height of 5 m above the bench floor, while others have a lesser bounce height and others settle after the bounce (see Figure 5.26).

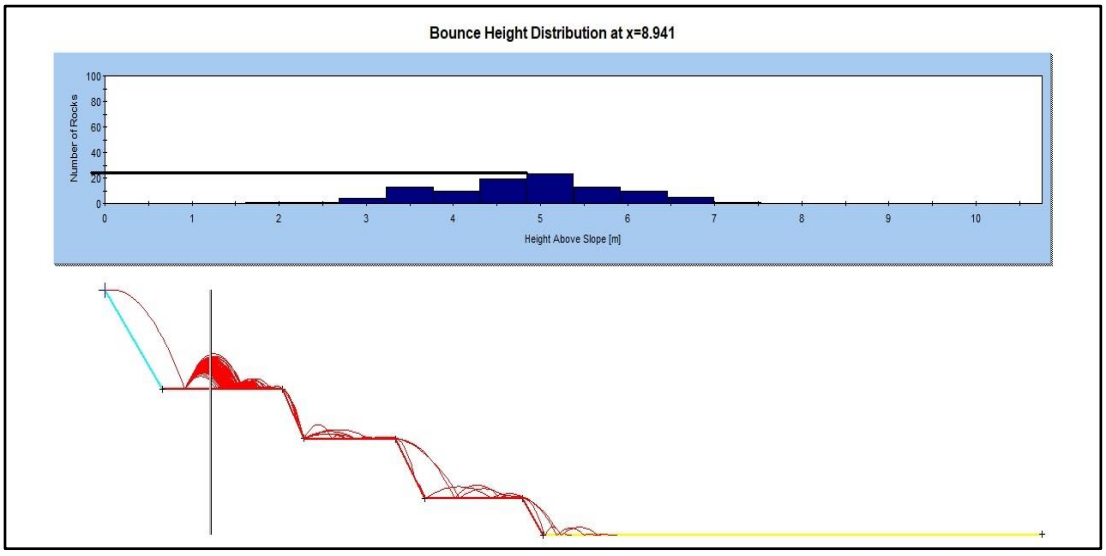

Figure 5.26: Rockfall model and the bounce height distribution along with the number of rocks at different heights at Bench 4.

As indicated in Section 4.2.1 of Chapter 4, some of the rocks rest on the crest of benches on the slope. However, those rocks with enough kinetic energy will roll off to the next bench. Figures 5.26 – 5.29 show the distribution of rocks on all the benches to the bottom bench. The bar chart in each figure above the rockfall simulation depicts the bounce height distribution of rocks and the number of rocks per bounce height.

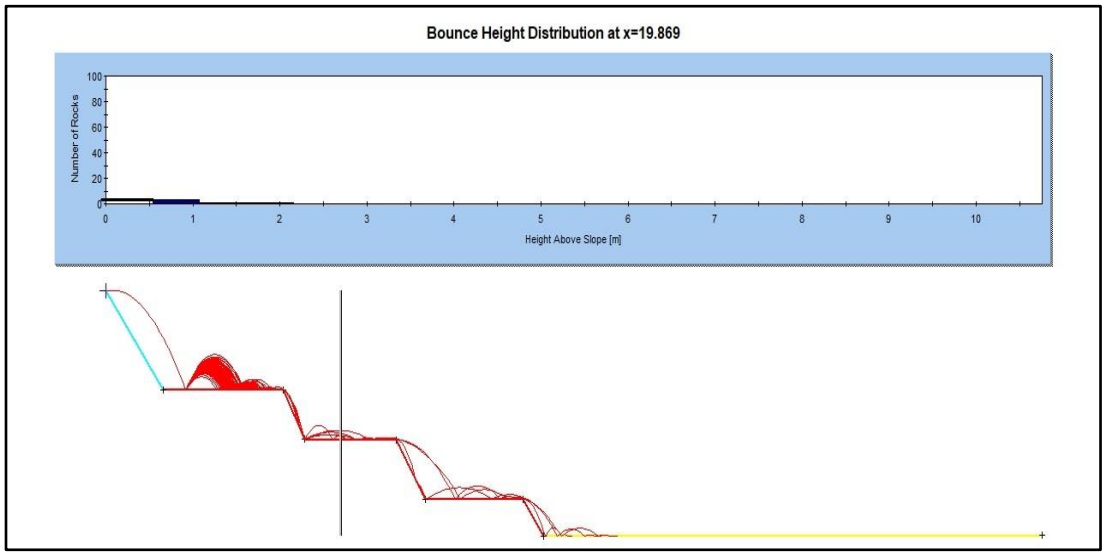

Figure 5.27: Rockfall model, bounce heights distribution along with the number of rocks at bench 3.

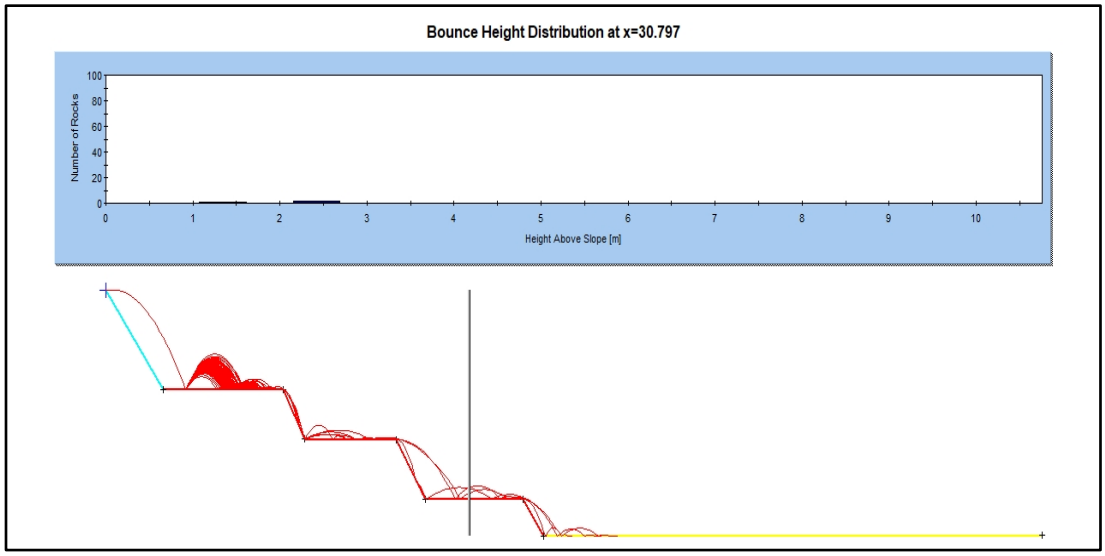

Figure 5.28: Rockfall model, bounce height distribution along with the number of rocks in bench 2.

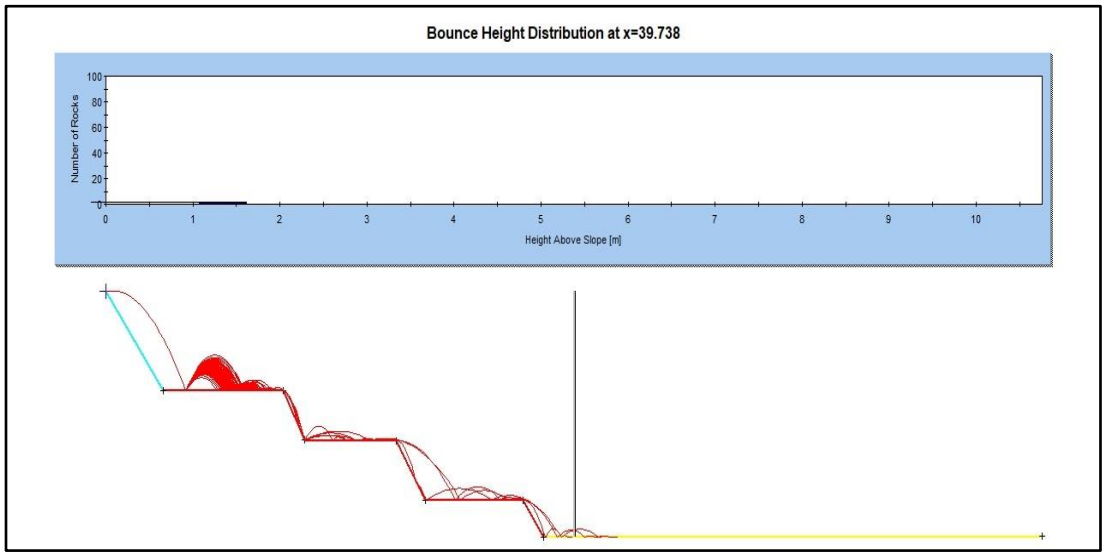

Figure 5.29: rockfall model, bounce height distribution and the number of rocks at the bottom bench (Bench 1).

Through the assessment of Figures 5.26 to 5.29, it can be observed that the frequency of rocks decreases from one bench to the next (bench below). This is due to the fact that as the rocks drop to the bench below, some come to rest and only a few rollovers. As it can be observed that on all the benches, as the rocks move from one bench to the other, they do so in a rolling motion as opposed to bouncing to the slope below. Another parameter that was analysed during rockfall analysis includes the kinetic energy. The kinetic energy measured assists in predicting the potential energy released by the falling rock. In essence, this becomes critical in understanding the extent of the damage that a rockfall may cause. The distribution of the kinetic energy during rockfall can be extracted from the ROCFALL simulation model.

Figure 5.30 shows the simulation of the rockfall along with the kinetic energy. It is noteworthy that the total amount of kinetic energy measured is influenced by the size of the rock mass, velocity, and trajectory rock. The distribution of the kinetic energy of the rock from the top of the slope down to the bottom is presented in Figure 5.30.

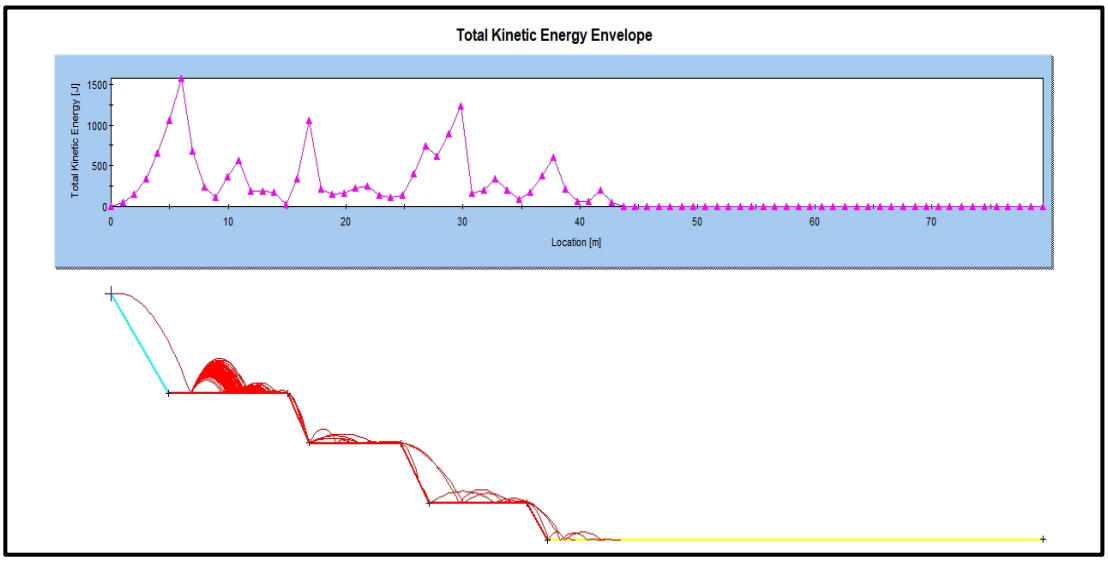

Figure 5.30: Rockfall model of the slope with the kinematic energy distribution from the top bench to the bottom bench.

Through the analysis of the kinetic energy, it can be seen that the kinetic energy of the rocks increases rapidly as the rock hits the floor. At this point, the velocity of the rock mass is at its maximum. The principles of physics stipulates that the kinetic energy is directly proportional to mass and velocity. This means that as the mass or velocity increases, the kinetic energy also increases. This is the reason why the kinetic energy peaks at the point where the rock is hitting the floor. After the rock bounces and reaches the peak height, the kinetic energy approaches zero (0). Subsequently, as the rock rolls from one slope to the one below, the kinematic energy is recorded and as it reaches the maximum velocity, the kinetic energy spikes rise rapidly.

A summarised understanding of the simulation of the rockfall simulations given in Figures 5.26 to 5.29 is that the bounce height of the rocks after they reach the bench floor is primarily dependent on bench height. This is because the velocity a rock reaches at bounce is influenced by the height of the bench. Additionally, the kinetic energy distribution is also dependent on the slope height since it indirectly influences the velocity of the falling rocks. After all the simulations are done, the number of rocks that reach the pit floor is represented

in Figure 5.29. However, it was previously discussed in Section 4.2.1 of Chapter 4 that the benches contain catchment berms and berm walls. It should be noted that the whole rockfall assessment was done to determine the final deposit of the rock as it moves down the slope. Therefore, from the assessment of the models, the rock only rolls from one bench to the one below it. Since the mine has berm walls, it simply means that they would be able to stop the rocks from rolling to the benches below. However, the simulation was run with no berm walls. This was done to show where the rock will be deposited in cases where there is no berm walls. Therefore, the measures put in place as a way of protecting the rockfall from one bench to the next are sufficient and keep the rocks on the same bench.

5.6 Significance of the findings

Yang et al. (2020) explained that when the stress exceeds the rock strength, it leads to reduced rock mass strength. The increased stress produces discontinuities which are the weak zones of the rock mass (Terzaghi, 1962). Therefore, in order to understand the stability of the slope, the discontinuities need to be studied and how they will influence the rock mass stability.

In order to understand the stability of the slopes, several methods were applied, namely: kinematic analysis, Limit equilibrium and numerical simulation. These methods complemented each other in determining if the slopes were stable or not. First off was the Kinematic analysis. This method analysed the orientation of discontinuities against the slope orientation. The analysis was done by making use of the stereonets. The kinematic analysis assisted in determining the probabilities of the three common types of failures from occurring on the slope. It was found that the probabilities of planar and wedge failures occurring is low. However, the probability of toppling failure occurring on the slopes was a bit high. This leads to the conclusion that the three slopes are most likely to face toppling failure above planar and wedge failures.

Secondly, the limit Equilibrium analysis was used to determine the FoS of the slopes using different methods. Four common limit equilibrium analysis methods were selected. These methods are Bishop's, Janbu's, Morgenstern-price and spencer's method. These methods analysed the slopes and the computed FoS by the program showed that the slopes were stable with the least FoS recorded as 1.739 on slope C by Bishop's method.

Thirdly, a numerical based method was used to predict the type of failure under different depths of discontinuities. The simulation was run for discontinuities at 1-m, 2-m, 3-m, and 6-m depth. The results show that the slope was stable when discontinuities were at 1 m, 2 m, and 3 m, with slope B being an exception which was unstable at 3-m depth. This was through the analysis of the SRF of the slopes. At 6m depth, the recorded SRF was below the minimum required for the slope to be classified as stable. Through analysis, this proved a point that the longer the slopes more unstable they become. Additionally, an increase in the depth of the discontinuities reduces the stability of the slopes.

Lastly, rockfall simulation was done in order to determine the location a rock will end if the rock if it falls from the higher benches. The modes showed that a rock can reach the pit floor if there are no barricades put in place to prevent it from rolling to the benches below.

Therefore, the results presented in this chapter were of great significance and do assist in coming to a conclusion if the slopes are stable or not.

Chapter 6: Conclusion and recommendations for future work

6.1 Introduction

The main goal of the study was to employ a variety of techniques to examine the Wearne open pit mine's long-term stability analysis. This chapter offers a summary of the dissertation's results along with suggestions for additional study.

One of the most critical aspects of an open pit mine is slope stability. Furthermore, the stability and structure of the slopes have an impact on the mining operation's success or failure, primarily from an economic and safety perspective. Thus, it is argued that this study is necessary to guarantee the safe and efficient functioning of the mining process.

Specific objectives were established, and various strategies were used to attain them in order to fulfil the primary objective of the study. The primary goal of the research was to examine long-term stability using various techniques. Kinematic analysis, limit equilibrium, and numerical modelling are some of these techniques. These techniques were designed to accomplish particular goals. Finally, a multi-method slope stability study was used to establish the stability of the identified slopes.

6.2 Kinematic analysis

For kinematic analysis, the DIPS computer program was applied. The kinematic analysis was applied to determine the probable failures in the mine slopes. The modes of failure being investigated by the program are planar, wedge and toppling failure modes. From the literature review, it was explained

that there are conditions that lead to the occurrence of a specific mode of failure. These conditions are as follows:

- For planar failure to occur, the discontinuity should be in the same direction as the slope face at an angle gentler (within 20°), but greater than the friction angle along the failure plane.
- Wedge failure occurs when there is an intersection of the two discontinuities forming a wedge-shaped block.
- Toppling failure occurs when the strike of the discontinuity is nearly parallel (at ±20°) to the trend of the slope, but the discontinuities should be dipping in the opposite direction to the slope.

From the stereonets created by the DIPS program, it can be observed that there are only 6 poles in the critical zone out of 117 for slope A, 5 out of 60 for slope B and 0 out of 62 poles of mapped discontinuities. The percentage of the poles in the critical zone versus the total poles of discontinuities mapped is translated to the probability of failure in the slope. For planar failure analysis, the probabilities of failure were 5.13 %, 8.33 % and 0 % for slopes A, B and C respectively.

For wedge failure, slope A had a total of 6785 intersections of discontinuities with only 854 meeting the criteria for wedge failure to occur (meaning they are critical). Slope B had a total of 1770 intersections with only 270 in the critical. The joints intersecting in a critical zone are the ones responsible for failure. Therefore, the number of joints in the critical zone is represented as a percentage of the total intersection of joints on the slope. Slope C had a total of 1890 intersections and only 122 of those are critical. Therefore, the probabilities of failure for all three slopes are 12.59 %, 15.26 % and 6.46 % for slopes A, B and C respectively. With that said, the slope with the highest chance of failure is slope B. However, the probability of failure on all three slopes is not an immediate threat that requires immediate attention.

For toppling failure, base plane results were used which is considered to be a combination of direct and oblique failures. The probability of toppling failures to occur was recorded to be 17.95 %, 21.67 % and 37.10 % for slopes A, B and C respectively. It should be recalled that the toppling failure occurs when the discontinuities are striking in a direction nearly parallel to the strike of the slope and the dip at a steep angle but in an opposite direction. Therefore, the results show that slopes have more discontinuities that may lead to toppling failure as opposed to planar and wedge failures. The probability of toppling failure, therefore, sparked and influenced a further investigation into the rockfall trajectory simulation.

6.3 Limit equilibrium analysis

The limit equilibrium method was applied to determine the FoS of the slopes. This was done using the SLIDES program. This program has the capability of applying multiple Limit equilibrium methods, however, for this study, only four were chosen which are: Bishop's, Janbu's, Morgrnstern-price and Spencer's methods. Each of the mentioned methods has its limitations and the reason for applying multiple methods was because one method counters another method's limitations. This, therefore, added to the credibility of the results produced. Table 6.1 below summarises the FoS for the slopes A, B and C using the different methods as mentioned below.

Table 6.1: Summary of the FoS of the slopes using different methods.

Limit Equilibrium method	Slope A	Slope B	Slope C
Bishop's	2.147	1.928	1.739
Janbu's	2.159	1.923	1.784
Morgenstern-price	2.271	2.035	1.808
Spencer's	2.243	1.988	1.783

The average FoS for the slopes was 2.2050, 1.9685 and 1.7785 for slopes A, B and C respectively. The limit equilibrium method concluded that the slopes were safe based on the FoS. However, authors such as Naeij (2021), Yared (2017), and Hamdah (2013) still have doubts about the limit equilibrium methods; hence, additional methods were applied for this study.

6.4 Numerical modelling

Numerical modelling is a method that uses mathematical tools and principles to solve problems. For this study, two numerical methods were used. These methods are Slope failure simulation using OPTUM G2 and Rockfall simulation using ROCFALL computer program. Both these software packages make use of the Finite element method, which is a technique which quantifies any structural phenomena such as the structural behaviour of the rock mass.

OPTUM G2 was used to develop a predictive model for the slope under varying depths of discontinuities, in addition to this, the model was used to provide the long-term stability analysis of the slope. The OPTUM G2 modelled the slopes as the discontinuities increased in depth. The investigated depths start from 1 m, 2 m, 3 m, and 6 m for all slopes. It should be known that there was a time parameter on the program which enabled the models to run at constant time spacing. For this study, the failure analysis was done after a period of 20 years. After the model was produced, the strength reduction factor was also produced. The strength reduction factor was computed for the slopes when the depth of the discontinuities was at 1 m, 2 m, 3 m, and 6 m. This enabled us to see the effect of the increased depth of discontinuities on the strength reduction factor (SRF) of the slope. The results of the endeavour are summarised in Table 6.2 below.

Table 6. 2 Summary the SRF for slopes A, B and C at different depths.

	Strength reduction factor (SRF)		
Discontinuities depth	Slope A	Slope B	Slope C
1 m	1.60	1.56	1.62
2 m	1.55	1.53	1.59
3 m	1.51	1.49	1.52
6 m	1.46	1.38	1.41

The results imply that the strength of the slope decreases as the joint propagation increases. It can also be observed that the number of benches (which indirectly translates to the size of the slope) plays a significant role in reducing the strength of the slope. The slopes with more benches have a lower SRF compared to the slope with fewer benches at the same length of discontinuity propagation. This is due to an increase in the region of shearing. Furthermore, the cohesion and the friction angle are also affected by the development of the joints.

In terms of ROCFALL trajectory modelling, it should be noted that there are extreme circumstances whereby the rocks come loose from the face. In such cases, the resting location of the rock should be determined. This was achieved through the use of the ROCFALL computer program. The models show that as the rocks were dropped from the uppermost bench, they bounce from the bench floor. Thereafter, some rocks roll over to the lower benches while others come to rest on the very same bench. It should be noted that the number of rocks that reach the bottom of the slope (bottom bench) is less compared to the upper benches. The reason most rocks do not reach the bottom of the slope is due to the decrease in the amount of energy contained within the rock.

Through observation of the models and how the rocks move from one bench to the next, it can be noted that through the use of the berm walls, the rolling of rocks to the lower benches can be prevented.

6.5 Summarised findings

Based on the findings of the research, it was observed that there are several contributing factors associated with rock mass behaviour that can lead to slope instability. The identified contributing factors include slope geometry (angle and height), joints, joints orientation and joints elongation.

In addition to the identification of the contributing factors, the probability of different modes of failures or failure mechanisms occurring on the slopes was also determined using Kinematic analysis through the DIPS program. This program analysed three probable modes of failures which are planar, wedge and toppling failures. It was found that there is a low probability of planar and wedge failures from occurring with toppling being the only one with a relatively high probability of occurring. The FoS of the slopes was then determined by making use of the Limit Equilibrium Method through the SLIDES program. The SLIDES program applied different methods to determine the FoS and an average from those methods was taken for each slope. This method shows that all slopes are stable with their FoS above the minimum required to categorize the slope as stable.

Since it has been proven that blasting, mining activities and other (both natural and artificial activities) influence the elongation of the joints deep into the rock mass, OPTUM G2 program was used to simulate the impact of the deepening discontinuities on the slope, thereafter, the computation of the strength reduction factor of each slope was determined from different depths of discontinuities. Slopes A and C are stable when the depth of discontinuities is at 1 m, 2 m, and 3 m but are unstable at 6 m. Slope B, on the other hand, is only stable when the depths are at 1 m and 2 m; it becomes unstable at 3 m and 6 m. From this, it was deduced that slope B was the least stable of the three cross-sections from the mine.

Finally, the rockfall trajectory simulation was done in order to determine where a rock might end up landing in cases of failure on the slopes. The model shows that the slopes have the height and width properly balanced since the rock can be prevented from rolling off to the bottom benches through the use of berm walls. This is supported by the models produced which show that only a few rocks reach the bottom of the slope following most coming to rest on other benches.

6.6 Recommendations for future work

Based on the scope of the dissertation, several potential areas of research have been identified to further improve the analysis of slope stability. These areas include:

- The application of a 3D model to analyse the effect orientation and change in depth of geological structures have on slope stability.
- Development of appropriate support system for post-mining slope, to reduce slope instability due to rock mass deterioration.
- Apply low-mounted remote sensing sensors to better map the discontinuities and combine them with numerical methods to analyse the stability of slopes.
- The properties of the intact rock should be done at the laboratory to account for variability of the rock mass instead of using a computer program.

References

Abdellah, W.R, Beblawy, M.M., Mohamed, M.T., 2018. Evaluation of open pit slope angles and element types. Mining of mineral deposits, vol. 12, no. 2, pp. 47 – 57

Abramson, L.W., Lee, T.S., Sharma, S., Boyce, G.M, 2002. Slope stability and stabilisation methods, Second Edition. John Willey & Sons, Inc., pp. 378 – 382

Admassu, Y., Shakoor, A., Wells, N.A., 2012. Evaluating selected factors affecting the depth of undercutting in rocks subject to differential weathering. Engineering Geology, vol. 124, pp. 8 – 11

Agam, M.W., Hashim, M.H.M., Murad, M.I., Zabidi, H., 2016. Slope sensitivity analysis using Spencer's method in comparison with general limit equilibrium method. Procedia chemistry, vol.19, pp. 651 – 658

Aki, K., 1988. Local effects in ground motion. Earthquake Engineering and soil dynamics II: Recent advances in ground motion evaluation. Special Publication no. 20, American Association of Civil Engineers, pp. 103 – 155

Aladejare A.E., Akeju, V.O., Wang, Y., 2022. Data-driven characterization of the correlation between uniaxial compressive strength and Youngs' modulus of rock without regression models. Transportation Geotechnics, vol. 32, pp. 1 – 7

Albataineh, N., 2006. Slope stability analysis using 2D and 3D methods. Master's Thesis, University of Akron

Al-E'bayat, M., Sunkpal, M., Sherizadeh, T., 2020. Numerical investigation of rock bridge effect on slope stability using bonded block modelling method. Proceedings of the 54th U.S. Rock Mechanics/Geomechanics Symposium, American Rock Mechanics Association (AMRA)

Alzo'ubi, A., 2016. Rock slopes processes and recommend methods for analysis. International Journal of Geomaterials, vol. 11, pp. 2520 – 2527

Ansari, M.K., Ahmed, M., Singh, T., Ghalayani, I., 2015. Rainfall, a major cause for rockfall hazard along the roadways on hilly terrains in India. Engineering Geology for Society and territory, vol. 1, pp. 457 – 460

Arief, M.Z., Widodo, N.P., Prasseyyo, S.H., 2020. Study of slope geometry effect on 2D and 3D slope stability analysis using equilibrium method. Indonesian Mining Professionals, vol. 2, no. 2, pp. 51 – 56

Aryal, K., 2006. Slope stability evaluation by LE and FE methods. PhD Thesis, Norwegian University of Science and Technology, NTNU

Azarafza, M., Akgün, H., Ghazifard, A., Asghari-Kaljahi, E., Rahnamarad, J., Derakhshani, R., 2021. Discontinuous rock slope stability analysis by limit equilibrium approaches – a review. International Journal of Digital Earth, vol. 14, no. 12, pp. 1918 – 1941

Azarafza, M., Akgün, H., Atkinson, P.M., Derakhshani, R., 2021. Deep learning-based landslide susceptibility mapping. Scientific Reports Nature, vol. 11, no. 1, # 24112

Baba, K., Bahi, L., Ouadif, L., Akhssas, A., 2012. Slope stability evaluations by limit equilibrium and finite element methods applied to a railway in the Moroccan Rif. Open Journal of Civil Engineering, vol. 2, pp. 27 – 32.

Bednarczyk, Z., 2010. Soil-structure interaction on three stabilized flysch landslides in polish carpathians. The First International Conference on Advances in Interaction and Multiscale Mechanics (AIMM'10), pp. 1397 – 1414

Beyene, Y., 2017. Comparison of finite element and limit equilibrium methods for slope stability analysis. Master of Engineering Project, Addis Ababa Science and Technology University

Bidgoli, M.N., Jing, L., 2014. Anisotropy of strength and deformability of fractured rocks. Journal of Rock Mechanics and Geotechnical Engineering, vol. 6, pp. 156 – 164

Bieniawski, Z.T., 1976. Rock mass classification in rock engineering. Proceedings of the Symposium on Exploration for Rock Engineering, vol. 1, Bieniawski, Z.T. (Eds.), Johannesburg, South Africa, 1 – 5 November 1976, pp. 97 – 106

Bieniawski, Z.T., 1989. Engineering rock mass classifications: a complete manual for engineers and geologists in mining, civil, and petroleum engineering. John Wiley and Sons

Budetta, P., 2020. Some remarks on the use of deterministic and probabilistic approaches in the evaluation of rock slope stability. Geosciences, vol. 10, no. 5, pp. 163 – 164

Bye, A.R., Bell, F.G., 2001. Stability assessment and slope design at Sandsloot open pit, South Africa. International Journal of Rock Mechanics and Mining Sciences, vol. 38, no. 3, pp. 449 – 466

Cai, M., Kaiser, P.K., Uno, H., Tasaka, Y., Minami, M., 2004. Estimation of rock mass deformation modulus and strength of jointed hard rock masses using the GSI system. International Journal of Rock Mechanics and Mining Sciences, vol. 41, no. 1, pp. 3 – 19

Cai, J.S., Yeh, T., Yan, E.C., Tang, R., Hao, Y.H., 2021.Design of borehole deployments for slope stability analysis based on a probabilistic approach. Computers and Geotechnics, vol. 133, pp. 2 – 7

Call, R.D., Ryan, T.M., Barkely, R.C., 1993. Geotechnical analysis for open pit mining in areas of large-scale slope instability. In: Innovative Mine Design for the 21st Century, pp. 45 – 56

Chakraborty, A., Goswami, D., 2016. State of the art: three-dimensional (3D) slope-stability analysis. International Journal of Geotechnical Engineering, vol. 10, pp. 493 – 498

Chakraborty, D., Konietzky, H., Walker, K., 2012. A comparative study of different approaches for factor of safety calculations by shear strength reduction technique for non-linear Hoek-Brown failure criterion. Geotechnical and Geological Engineering, vol. 30, pp. 925 – 934

Chaulya, S.K., Prasad, G., 2016. Sensing and monitoring technologies for mines and hazardous areas: Monitoring and prediction technologies. Elsevier

Chen, X., Zhang, L., Chen, L., Li, X., Liu, D., 2019. Slope stability analysis based on the coupled Eulerian-Lagrangian finite element method. Bulletin of Engineering Geology and the Environment, vol. 78, no. 6, pp. 4451 – 4463

Crozier, M.J., 1986. Landslides: causes, consequences and environment. Taylor and Francis, London

Cruden, D.M., Martin, C.D., 2013. Assessing the stability of a natural slope. In: Proceedings of 9th Asian Regional Conference, IAEG, Beijing, China, pp. 46 – 55

Dai, F.C, Lee, C.F., Ngai, Y.Y., 2002. Landslide risk assessment and management: an overview. Engineering Geology, vol. 64, no. 1, pp. 65 – 87

Dawson, E.M., Roth, W.H., Drescher, A., 1999. Stability analysis by strength reduction. Geotechnique, vol. 49, no. 6, pp. 835 – 840

Diamantis, K., Migiros, G., 2018. Estimating the rock mass properties of ultramafic rocks in Central Greece using the triaxial tests of intact rock and the Geological Strength Index. Geotechnical and Geological Engineering, vol. 37, pp. 1839 – 1858

Dykes, A.P., Kirk, K.J., 2006. Slope instability and mass movements in peat deposits. Developments in Earth Surface Processes, vol. 9, pp. 377 – 406

E'bayat, A., Mariam, S., 2017. Assessment of rockfall rollout risk along varying slope geometries using the Rocfall and CRSP software.

Eberhardt, E., 2003. Rock slope stability analysis – Utilization of advanced numerical techniques. Research Report, University British Columbia, Vancouver, Canada, pp. 4 – 38

Eberhardt, E., 2012. The Hoek-Brown Failure criterion. Rock Mechanics and Rock Engineering, vol. 45, pp. 981 – 988

Edelbro, C., 2003. Rock mass strength – A review: Technical Report 2003:16, Lulea University of Technology

Fellenius, W., 1936. Calculation of the stability of earth dams. Transactions of the 2nd Congress on Large Dams, International Commission on Large Dams, Washington, vol. 4, pp. 445 – 459

Ferrari, F., Tiziana, A., Giani, G.P., 2014. Rock Mass Rating spatial estimation by geostatistical analysis. International Journal of Rock Mechanics and Mining Sciences, vol. 70, pp. 162 – 176

Fischer, L., Purves, R.S., Huggel, C., Noetzli, J., Haeberli, W., 2012. On the influence of topographic, geological and cryospheric factors on rock avalanches and rockfalls in high-mountain areas. Natural Hazards and Earth System Sciences, vol. 12, no. 1, pp. 241 – 254

Fredj, M., Hafasaoui, A., Khadri, Y., Boukarm, R., 2018. Influence of the failure surface choice on the safety factor value during slope stability studies. Naukovyi Visnyk Natsionalnoho Hirnychoho Universytetu, no. 3, pp. 3 – 35

Fredj, M., Hafsaoui, A., Boukarm, R., Nakache, R., Saadoun, A., 2019. Numerical modelling of slope stability in open pit phosphate mines, Algeria: A

comparative study. In IOP Conference Series: Earth and Environmental Science, vol. 221, pp. 12 – 20

Fredj, M., Boukarm, R., Saadoun, A., 2021. Influence of blasting activities on slope stability: A case study. Medicon Engineering Themes, vol. 1, no. 2, pp. 12 – 21

Gibson, W., 2011. Probabilistic methods for slope analysis and design. Australian Geomechanics, vol. 46, no. 3, pp. 29 – 39

Goh, A.T.C., 2017. Deterministic and reliability assessment of basal heave stability for braced excavations with jet grout base slab. Engineering Geology, vol. 218, pp. 63 – 69

Goodman, R.E., 1989. Introduction to rock mechanics (vol. 2). Wiley, New York

Goodman, R.E., Kieffer, D.S., 2000. Behaviour of rocks in slopes. Journal of Geotechnical and Geoenvironmental Engineering, vol. 126, pp. 675 – 684

Griffiths, D.V., Lane, P.A., 1999. Slope stability analysis by finite elements. Geotechnique, vol. 49, no. 3, pp. 387 – 403

Griffiths, D.V., Fenton, G.A., 2007. Probabilistic methods in geotechnical engineering. Springer Science and Business Media, vol. 491, pp. 57 – 82

Guadagno, F.M., 2013. Failure analysis of shallow landslides using a three parameter Weibull distribution of slope angle. Rendiconti Online della Societa Geologica Italiana, vol. 24, pp. 110 – 112

Gunther, A., Wienhofer, J., Konietzky, H., 2012. Automated mapping of rock slope geometry, kinematic analysis and with RSS-GIS. Natura Hazards, vol. 61, pp. 29 – 49

Guzzetti, F., Reichenbach, P., Wieczorek, G.F., 2003. Rockfall hazard and risk assessment in the Yosemite Valley, California, USA. Natural Hazards and Earth System Sciences, vol. 3, no. 6, pp. 491 – 503

Habil, H., Yuliza, E., Munir, M.M., Irsyam, M., Khairurrijal, K., 2016. Instrumentation system design and laboratory scale simulation of landslide disaster mitigation. Journal of Physics, vol. 739, no. 1, # 012056

Halakatevakis, N., Sofianos, A.I., 2010. Correlation of the Hoek-Brown failure criterion for a sparsely jointed rock mass with an extended plane of weakness theory. International Journal of Rock Mechanics and Mining Sciences, vol. 47, no. 7, pp. 1166 – 1179

Hamdan, H., Vafidis, A., Agioutantis, Z., Sharif, E., 2013. Contribution of electrical tomography methods in estimating slope stability at Mavropigi Lignite open pit mine, Northern Greece. Second International Conference on Engineering Geophysics, European Association of Geoscientists and Engineers

He, M.C., Feng, J.L., Sun, X.M., 2008. Stability evaluation and optimal excavated design of rock slope at Antaibao open pit coal mine, China. International Journal of Rock Mechanics and Mining Sciences, vol. 45, pp. 289 – 302

Helsdingen, P., 2017. Assessing the stability of Road cuttings on the Zuuberg pass using Romana's Slope mass rating. Proceedings of the 9th South African Young Geotechnical Engineers conference, Dolphin Coast

Hocking, G., 1976. A method for distinguishing between single and double plane sliding of tetrahedral wedges. International Journal of Rock Mechanics and Mining Sciences and Geomechanics Abstract, vol. 13, no. 7, pp. 225 – 226

Hoek, E., Bray, J.W., 1981. Rock slope engineering, 3rd Edition. Institution of Mining and Metallurgy, London, pp.55 – 70

Hoek, E., Carranza-Torres, C., Corkum, B., 2002. Hoek-Brown failure criterion, 2002 Edition. In Proceedings of the 5th North American Rock Mechanics Society Meeting, Toronto, ON, Canada, pp. 7 – 10

Hoek, E., Diederichs, M.S., 2006. Empirical estimation of rock mass modulus. International Journal of Rock Mechanics and Mining Sciences, vol. 43, no. 2, pp. 203 – 215

Hoek, E., 2007. Rock mass properties – Practical rock engineering. Rocscience, Available at URL: http://www.Rocscience.com/hoek/corner/11_Rock_mass_properties.pdf. pp.1-7

Hou, X., Li, T., Qi, S., Guo, S., Li, P., Xi, Y., Xing, X., 2021. Investigation of cumulative influence of infiltration on the slope stability with a thick unsaturated zone. Bulletin of Engineering Geology and the Environment, vol. 80, pp. 5467 – 5480

Huang, A.B., Lee, J.T., Ho, Y.T., Chui, Y.F., Cheng, S.Y., 2012. Soils and foundation, vol. 52, pp. 737 – 747

Huang, C.C., Yeh, S.H., 2012. Predicting periodic rainfall-induced slope displacement using force-equilibrium-based finite displacement method. Journal of GeoEngineering, vol. 10, pp. 83 – 89

Huang, C., Radi, B., El Hami, A., 2016. Uncertainty analysis of deep drawing using surrogate model based probabilistic method. The International Journal of Advanced Manufacturing Technology, vol. 86, no. 9 – 12, pp. 3229 – 3240

Humphrey, C.M., Adams, J.A., 2008. Compass visualizations for human-robotic interaction. In: Proceedings of the 3rd International Conference on Human-Robot Interactions

Huo, Y.X., Zhai, H.F., 2012. The study on slope stability analysis based on finite element method. Advanced Materials Research, vol. 575, pp. 70 – 74

Hussain, S., Rehman, Z.U., Khan, N.M., Ahmed, I., Raza, S., Tahir, M., Ullah, A., Afzel, D., Khan, A., Salman, M., Sherin, S., 2021. Proposing a viable stabilization method for slope in a weak rock mass environment using

numerical modelling: A case study from cut slopes. Journal of Mining and Environment (JME), vol. 4, pp. 2 – 11.

Jaeger, J., 1960. Shear fracture of anisotropic rocks. Geological Magazine, vol. 97, pp. 65 – 72

Janbu, N., 1954. Stability analysis of slopes with dimensionless parameters. Doctor of Science Thesis, Harvard University.

Janbu, N., 1973. Slope stability computations. Wiley (John) and Sons, Inc.

Jin, L., Wei, J., Luo, C and Qin, T., 2023. Slope stability analysis based on improved radial movement optimization considering seepage effect. Alexandra Engineering Journal, Vol. 79, pp. 591-607.

Juang, C.H., Zhang, J., Shen, M., Hu, J., 2019. Probabilistic methods for unified treatment of geotechnical and geological uncertainties in a geotechnical analysis. Engineering Geology, vol. 249, pp. 148 – 161

Kaur, A., Sharma, R.K. Slope stability analysis techniques: A review. International Journal of Engineering Applied Sciences and Technology, vol. 1, no. 4, pp. 52 – 57

Karam, K.S., 2005. Landslide risk assessment and uncertainties. Doctor of Philosophy Thesis, Massachusetts Institute of Technology

Karam, K., He, M., Soussa, L., 2015. Slope stability risk management in open pit mines. In Proceedings of the 7th GiT4NDM and 5th EOGL International Conference, Abu Dhabi, United Arab Emirates, 14 – 16 March, UAE University, Al-Ain, United Arab Emirates, pp. 1 – 10

Keefer, D.V., 2000. Statistical analysis of an earthquake-induced landslide distribution – The 1989 Loma Prieta, California event, Engineering Geology, vol. 58, pp. 231 – 249

Khabbaz, H., Fatahi, B., Nucifora, C., 2012. Finite element methods against limit equilibrium approaches for slope stability analysis. In Proceedings of the Australia New Zealand Conference on Geomechanics, pp. 1293 – 1298

Kolapo, P., Oniyide, G.O., Said, K.O., Lawal, A.I., Onifade, M., Munemo, P., 2022. Overview of slope failure in mining operations. Mining, vol. 2, pp. 350 – 384

Kong, T.B., 2017. Engineering Geology in Malaysia – some case studies. Bulletin of the Geological society of Malaysia, vol. 64, pp. 65 – 79

Kumar, V., Parkash, V., 2015. A model study of slope stability in mines situated in south India Pelagia research library. Advances in Applied Research, vol. 6, pp. 82 – 90

Kumar, M., Rana, S., Pant, P.D., Patel, R.C., 2017. Slope stability analysis of Balia Nala landslide, Kumaun Lesser Himalaya, Nainital, Uttarakhand, India. Journal of Rock Mechanics and Geotechnical Engineering, vol. 9, pp. 150 – 158

Kumar, N.S.H., Choudhary, R.P., Murthy, Ch.S.N., 2020. Model based reliability analysis of shovel-dumper system's mechanical failures used in the surface coal mine: A case study. Safety and Reliability, vol. 39, no. 3 – 4, pp. 1 – 15

Lama, R.D., 1974. The Uniaxial compressive strength of a jointed rock mass Festschrift-Leopold Muller-Salzburg zum 65 Geburtstag, Institut fur Felsmechanik und Bodenmechanik, Universitat Karlsruhe, pp. 67 – 78

Lee, M., Morris, W., Harris, J., Leblanc, G., 2012. A network extraction tool for mineral exploration: A case study from the Wopmay origin, Northwest territories. Exploration Geophysics, vol. 43, no. 2, pp. 116 – 124

Li, K.S., Lo, S.C.R., 1993. Probabilistic methods in geotechnical engineering. Proceedings of the Conference on Probabilistic Methods in Geotechnical Engineering, Canberra

Liu, X., Li, D.Q., Cao, Z.J., Wang, Y., 2020. Adaptive Monte Carlo simulation method for system reliability analysis of slope stability based on limit equilibrium methods. Engineering Geology, vol. 264, pp. 105384

Llano-Serna, M.A., Williams, D.J., Ruest, M.R., 2016. Analysis of Kennecott Utah Copper's Biggham Canyon Mine Pit Wall slides. Proceedings of Tailings and Mine Waste 2016, Keystone, Colorado state University, pp. 787 – 794

Lowell, S.M., 1990. The KM mountain Landslide near Skamokawa, Washington. Washington Geologic Newsletter, vol. 18, no. 4, pp. 3 – 7

Lu, Y., 2015. Deformation and failure mechanism of slope in three dimensions. Journal of Rock mechanics and Geotechnical Engineering., vol. 7, no. 2, pp. 109 – 119

Lu, C.W., Lai, S.C., 2011. Application of finite element method for safety factor analysis of slope stability. International Conference on Consumer Electronics, Communications and Networks (CECNET), pp. 3954 – 3957.

Madun, A., Omar, H., 2001. Influence of discontinuity sets on slope failures at Pos Selim Highway, Malaysia. In Geological Society of Malaysia. pp. 237 – 242

Maerz, N.H., Youssef, A., Fennessey, T.W., 2005. New risk consequence rockfall hazard rating system for Missouri highways using digital image analysis. Environmental and Engineering Geoscience, vol. 103, pp. 13 – 16

Maji, V.B., Sitharam, T.G., 2008. Prediction of elastic modulus of jointed rock mass using artificial neural networks. Geotechnical and Geological Engineering, vol. 26, no. 4, pp. 443 – 452

Maji, V.B., Sitharam, T.G., 2012. Testing and evaluation of strength deformation behaviour of jointed rocks. Geomechanics and Geoengineering, vol. 7, no. 2, pp. 149 – 158.

Maji, V.B., 2017. An insight into slope stability using strength reduction technique. Journal of the geological society of India, vol. 89, no. 1, pp. 77-81

Markland, J.T., 1972. A useful technique for estimating the stability of rock slopes when the rigid wedge slide type of failure is expected. Rock Mechanics Research, Imperial College, London, 20 p

Matsui, T., San, K.C., 1992. Finite element slope stability analysis by shear strength reduction technique. Soils and Foundations, vol. 32, no. 1, pp. 59 – 70

McColl, S.T., 2015. Landslide causes and triggers. In: Schroder, J.F., Davis, T. (Eds.), Landslide Hazards, Risk and Disasters, pp. 17 – 42

McQuillan, A., Canbulat, I., Oh, J., Gale, S., Yacoub, T., 2018. Geotechnical review of an open cut coal mine slope using 3D LEM and new empirical run out chart predictions. Proceedings of the 2018 International Symposium on Slope Stability in Open Pit Mining and Civil Engineering, BCO Congress, Barcelona

Mehranpour, M.H., Kulatilake, P.H., 2016.Comparison of six major intact rock failure criteria using a particle flow approach under true-triaxial stress condition. Geomechanics and Geophysics for Geo-Energy and Geo-Resources, vol. 2, no. 4, pp. 203 – 229

Ming, D.W., Mittlefehldt, D.W., Morris., R.V., Golden, D.C., Gellert, R., Yen, A., Clark, B.C., Squyres, W., Farrand, W.H., Ruff, S.W., Arvidson, R.E., Klingelhofer, G., McSween, H.Y., Radionov, D.S., Schroder, C., De Souza Jr, P.A., Wang, A., 2006. Geochemical and mineralogical indicators for aqueous processes in the Columbia hills of Gusev Crater, Mars. Journal of Geophysical Research, vol. 111, no. E2, pp. 1 – 23

Mohamad, E.T., Kassim, K.A., Komoo, I., Gafar, N., 2009. The effect of moisture content to the strength of weathered sandstone. Malaysian Journal of Civil Engineering, vol. 20, no. 1, pp. 137 – 144

Mohamad, E.T., Kassim, K.A., Komoo, I., 2005. An overview of existing rock excavability assessment techniques. Journal Kejuruteraan Awam, vol. 17, no. 2, pp. 46 – 59

Moloi, M., Zvarivadza, T., 2016. Investigating slope failure and rockfall controls at a south African coal mine. 6th International Conference on Computer Applications in the Mineral Industries, Turkey, pp. 5 – 7

Moses, D., Shimada, H., Sasaoka, T., Hamanaka, A., Dintwe, T.K., Wahyudi, S., 2020. Slope stability analysis by using integrated approach. World Journal of Engineering and Technology, vol. 8, pp. 405 – 428

Mote, T., Morley, D., Keusher, T., Crampton, T., 2004. GIS-based kinematic stability analysis. The ESRI User Conference in Proceedings 24th Annual ESRI International User Conference, August, pp. 9 – 13

Muhedin, D.A., Qadir, S.J., Hamakareem, M.I., Rash, A.J.H., 2020. Effect of sawdust as partial replacement of sand in concrete. Journal of University of Duhok, vol. 23, no. 2, pp. 658 – 664

Mukhlisin, M., Naam, S.I., 2015. Effect of rock fragments on pure water pressure and slope stability at a hill slope. Journal of Geological Society, India, vol. 86, pp. 337 – 343

Naeij, M., Soroush, A., 2021. Comprehensive 3D Numerical Study on interaction between structure and dip-side faulting. Soil Dynamics and Earthquake Engineering, vol. 140, #106285

Nash, D.,1987. Comprehensive review of limit equilibrium methods of stability analysis. In: Andersen, M.G. and Richards, K.S., Eds., Slope Stability, Wiley, New York, pp. 11 – 75

Norrish, N.I., Wyllie, D.L., 1996. Stabilization of rock slopes: Landslide investigation and mitigation. National Academy Press, Washington vol. 247, pp. 391 – 425

Noroozi, A.G., Hajiannia, A., 2015. The effects of various factors on slope stability. International Journal of Science Engineering Investigations, vol. 4, no. 46, pp. 44 – 48

Palmstrom, A., 1982. The volumetric joint count – A useful and simple measure of the degree of jointing. Proceedings of 4th international congress. International Association for Engineering Geology and the Environment. New Delhi, pp. 221 – 228

Palmstrom, A., 1985. Application of the volumetric joint count as a measure of rock mass jointing. Proceedings of the International Symposium on fundamentals of rock joints, Bjorkliden, pp.103 – 110

Palmstrom, A., 1986. The volumetric joint count as a measure of rock mass jointing. Annals of the Israel Physical Society, Fragmentation and Flow, Jerusalem, vol. 8, pp.1 – 18

Park, H.-J., Lee, J.-H., Kim, K.-M., Um, J.-G., 2016. Assessment of rock slope stability using GIS-based probabilistic kinematic analysis. Engineering Geology, vol. 203, pp. 56 – 69

Pincus, H.J., 2003. Goodness-of-fit of six probability functions to some commonly used properties of rock. Proceedings of the 39th U.S. Rock Mechanics Symposium, vol. 2, pp. 2757– 2764.

Potgieter, J.T., 2016. Finite Element versus Limit Equilibrium stability analysis for surface excavations. Master's dissertation, University of Pretoria

Prakash, B., 2009. Design of stable slope for open cast mines. National Institute of Technology: Rourkela, India

Priest, S.D., 1993a. Discontinuity analysis for rock engineering. Chapman and Hall, London

Priest, S.D., 1993b. The collection and analysis of discontinuity orientation data for engineering design with examples. In Comprehensive Rock Engineering. Principles, practice and projects. Volume 3: Rock testing and site characterization, Pergamon press, Oxford, pp. 167 – 192

Purwanto, D., Sabrianto, A., Dedi, E.W., Nirmana, F.Q., Hideaki, Y., 2020. Study on influence of joint orientation on rock engineering properties for mining and infrastructure design. IOP Conference Series no. 589, Earth and Environmental Science

Rabie, M., 2013. Comparison study between traditional and finite element methods for slopes under heavy rainfall. Housing and Building National Research Center, vol. 10, pp. 160 – 168

Read, J.R.L., 2019. The geotechnical engineer in metalliferous open pit mines, keynote lecture, Proceedings of the 14th International Congress on Rock Mechanics and Rock Engineering, International Society for Rock Mechanics and Rock Engineering

Read, J., Stacey, P., 2010. Guidelines for open pit slope design. CSIRO Publishing, Collingwood, Australia

Raghuvanshi, T.K., 2019. Plane failure in rock slopes. A review on stability analysis techniques. Journal of King Saud University Sciences, vol. 31, pp. 101 – 109

Rocscience, 2021a. Slide3: 3D slope stability analysis, pp. 3

Rocscience, 2021b. RS3:3D finite element analysis, pp. 2

Rocscience, 2021. Estimating joint stiffness, pp. 14

Rowland, S., Duebendorfer, E., Schiefelbein, I., 2007. Structural analysis and synthesis – A laboratory course in structural geology, 3rd Edition. Blackwell Publishing

Russel, E.A., MacLaughin, M.M., Turner, R.M., 2018. UAV-based geotechnical modelling and mapping of an inaccessible underground site. 52nd US Rock Mechanics/Geomechanics symposium, Seattle, Washington, USA, OnePetro

Rusydy, I., Al-Huda, N., Fahmi, M., Effendi, N., 2019. Kinematic analysis and rock mass classifications for rock slope failure at USAID highways, Structural Durability and Health Monitoring, vol. 13, no. 4, pp. 379 – 398

Ryan, T.M., Call, R.D., 1992. Applications of rock mass monitoring for stability assessment of pit slope failure. In Proceedings of the 33rd U.S. Symposium on Rock Mechanics, American Rock Mechanics Association, ARMA, pp. 221 – 229

Saha, A., 2010. Genetic algorithm-based search coupled with Boltzmann selection in locating the critical surface in slope stability. Hong Kong Geotechnical Society (HKGES), The 14th Asian Regional Conference on Soil Mechanics and Geotechnical Engineering, The Hong Kong Polytechnic University, pp. 34

Salmanfarsi, A.F., Awang, H., Ali, M.I., 2020. Rock mass classification for rock slope stability assessment in Malaysia: a review. Institute of Physics Conference Series 903, Materials Science and Engineering, vol. 712, no. 1, pp. 1 – 9

Salunkhe, D., Chvan, G., Bartakke, R.N., Kothavale, P.R., 2017. An overview on methods for slope stability analysis. International Journal of Engineering Research and Technology (IJERT), vol. 6, no. 3, pp. 528 – 535

Sarma, S.K., 1979. Stability analysis of embankments and slopes. Journal of Geotechnical and Geoenvironmental Engineering, vol. 105, ASCE 15068

Sari, M., 2019. Stability analysis of cut slopes using empirical, Kinetical, Numerical and Limit Equilibrium methods: case of old Jeddah-Mecca road (Saudi Arabia). Environmental Earth Sciences, vol. 78, no. 21, # 621

Sari, M., 2021. Secondary toppling failure analysis and optimal support design for ignimbrites in the Ihlara Valley (Cappadocia, Turkey) by finite element method (FEM). Geotechnical and Geological Engineering, vol. 39, no. 7, pp. 5135 – 5160

Sari, M., 2021. Determination of representative elementary volume (REV) for jointed rock masses exhibiting scale-dependent behavior: a numerical investigation. International Journal of Geo-Engineering, vol. 12, no. 1, # 34

Sarkar, S., Kanungo, D.P., Kumar, S., 2012. Rock mass classification and slope stability assessment of road cut slopes in Garhwal Himalaya, India. Geotechnical and Geological Engineering, vol. 30, no. 4, pp. 827 – 840

Sarkar, S., Pandit, K., Dahiya, N., Chandna, P., 2021. Quantified landslide hazard assessment based on finite element slope stability analysis for Uttarkashi-Gangnani Highway in Indian Himalayas. Natural Hazards, vol. 106, pp. 1895 – 1914

Sarma, S.K., Tan, D., 2006. Determination of critical slip surface in slope analysis. Geotechnique, vol. 56, pp. 539 – 550

Savely, J.P., 1993. Slope management strategies for successful mining. In Proceeding of Innovative Mine Design for the 21st Century, AIME Arizona Section, Doubletree, pp. 13

Sengani, F., Mulenga, F., 2020. Application of limit equilibrium analysis and numerical modeling in a case of slope instability. Sustainability, vol. 12, no. 21, pp. 8870 – 8871

Sengani, F., 2021. Investigation of rockfall and slope instability with advanced geotechnical methods and ASTER images. PhD Thesis, University of South Africa

Selby, M.G., 1993. Hillslope materials and processes, 2nd Edition. Oxford University Press, 451 p.

Sha, L., 2016. Analysis of slope instability factors and protection. International Journal of Multidisciplinary Research and Development, vol. 3, no. 4, pp. 181 – 182

Shiferaw, H.M., 2021. Study on the influence of slope height and angle on the factor of safety and shape of failure of slopes based on method of analysis. Journal of Basic Applies Sciences, vol. 10, # 31

Sigdel, A., Adhikari, R.K., 2020. Engineering geological and geotechnical studies of Taprang Landslide, West-central Nepal: An approach for slope stability analysis. Journal of Geological Research, vol. 2, pp. 22 – 35

Simataa, E., 2019. Investigating slope stability in open pit mine – A case study of phyllites wall at Sentinel pit. University of the Witwatersrand

Singh, B, Goel, R.K., 2012. Engineering rock mass classification: Tunneling, foundations and landslides. Butterworth-Heinemann, Elsevier

Singh, P.K., Singh, K.K., Singh T.N., 2017. Slope failure in stratified rocks: A case from NE Himalaya, India. Landslides, vol. 14, pp. 1319 – 1331

Soren, K., Budi, G., Sen, P., 2014. Stability analysis of open pit slope by finite difference method. International Journal of Research in Engineering and Technology (IJRET), vol. 3, no. 5, pp. 326 – 334

Spencer, E., 1967. A method of analysis for stability of embarkments assuming parallel inter-slice forces. Geotechnique, vol. 17, pp. 11 – 26

Stead, D., Eberhardt, E., Coggan, J.S., 2006. Developments in the characterization of complex rock slope deformation and failure using numerical modelling techniques. Engineering Geology, vol. 83, pp. 217 – 235

Suchomel, R., Mašı, D., 2010. Comparison of different probabilistic methods for predicting stability of a slope in spatially variable c–φ soil. Computers and Geotechnics, vol. 37, no. 1 – 2, pp. 132 – 140

Suman, S., 2015. Slope stability analysis using numerical modelling. Bachelor of Technology report, National Institute of Technology

Sun, L., Grasseli, G., Liu, Q., Tang, X., Abdelaziz, A., 2022. The role of discontinuities on rock slope stability: insights from a combined finite-discrete element simulation. Computers and Geotechnics, vol.147, # 104788

Sun, X., Miao, L., Wang, H., Wu, L., Fan, G., Xia, J., 2022. Sand foreshore slope stability and erosion mitigation based on microbiota and enzyme mix-induced carbonate precipitation. Journal of Geotechnical and Geoenvironmental Engineering, vol. 148, no. 8, pp. 4 – 7

Suppe, J., 1985. Principles of structural geology. Prentice Hall

Sutejo, Y., Gofar, N., 2015. Effect of area development on the stability of cut slopes. In Proceedings of the 5th International Conference of Euro Asia Civil Engineering Forum (EACEF-5), Procedia Engineering, vol. 125, pp. 331 – 337

Taher, N.R., Gor, M., Aksoy, H.S., Awlla, H.A., 2022. Numerical investigation of the effect of slope angle and height on the stability of a slope composed of sandy soil. Journal of Science and Technology, vol. 12, pp. 664 – 675

Tang, X.S., Li, D.Q., Zhou, C.B, Phoon, K-K., 2015. Copula-based approaches for evaluating slope reliability under incomplete probability information. Structural Safety, vol. 52, pp. 90 – 99

Tarun, S., Rao, K.S., 2016. Kinematic stability analysis of multi-faced rock slopes in the Himalayas. Proceedings of the Conference on Recent Advances in Rock Engineering (RARE 2016). Advances in Engineering Research, pp. 281 – 284

Tatone, B.S., Grasselli, G., 2010. ROCKTOPPLE: A spreadsheet-based program for probabilistic block-toppling analysis. Computers and Geosciences, vol. 36, no. 1, pp. 98 – 114

Terzaghi, K., 1962. Stability of steep slopes on hard unweathered rock. Géotechnique, vol. 12, no. 4, pp. 251 – 270

Ullah, R., Abdullah, R., Kassim, A., Yanus, N.Z.M., Sendo, H., 2021. Assessment of residual soil properties for slope stability analysis. International of Journal of Geomate, vol. 21, no. 86, pp. 72 – 80

Wanstreet, P., 2007. Finite element analysis of slope stability. Master's Thesis, West Virginia University

Wei, L., Koutnik, T., Woodward, M., 2010. A slope stability case study by limit equilibrium and finite elements methods. Geoflorida 2010: Advances in Analysis, Modelling and Design (GSP199), pp. 3090 – 3099

Wines, D.R., Lilly, P.A., 2003. Estimates of rock joint shear strength in part of the Fimiston open pit operation in Western Australia. International Journal of Rock Mechanics and Mineral Sciences, vol. 40, pp. 929 – 937

Wines, D.A., 2016. A comparison of slope stability analysis in two and three dimensions. Journal of Southern African Institute of Mining and Metallurgy, vol. 116, no. 5, pp. 399 – 406

Wyllie, D.C., 2014. Calibration of rock fall modelling parameters. International Journal of Rock Mechanics and Mining Sciences, vol. 67, pp. 170 – 180

Wyllie D.C., Mah C.W., 2004. Rock slope engineering: civil and mining. CRC Press

Wyllie, D.C., Mah, C.W., 2005. Rock slope engineering: civil and mining, Taylor and Francis

Xiong, X., Huang, D.X., 2022. Cross-sectional empirical studies on the personal report of intercultural communication awareness and intercultural communication apprehension for English majors in vocational college. Journal of Hunan Industry Polytechnic, vol. 5, pp. 110 – 114

Yang, H., 2005. Slope stability investigation and analysis in Iowa. Doctor of Philosophy Thesis, Iowa State University

Yang, Y., Xu, D., Liu, F., Zheng, H., 2020. Modeling the entire progressive failure process of rock slopes using a strength-based criterion. Computers and Geotechnics, vol. 126, pp. 1 – 6

Yang, Y., Wu, W., Zheng, H., 2020. Searching for critical slip surfaces of slopes using stress fields by numerical manifold method. Journal of Rock Mechanics and Geotechnical Engineering, vol. 12, pp.1313 – 1325

Yousseff, A., Maerz, N.H., 2009. Slope stability hazard assessment and mitigation methodology along eastern desert Aswan-Cairo highway, Egypt. Journal of King Abdulaziz University: Earth Sciences, vol. 20, pp. 161 – 189

Yin, Z.Q., Hu, Z.X., Wei, Z.D., Zhao, G.M., Hai-Feng, M., Z; Feng, R.M., 2018. Assessment of Blasting induced Ground vibration in an open-pit mine under different rock properties. Advances in Civil Engineering, vol. 2018, no. 6, pp. 1 – 10

Yuke, S., 1999. Research on stability analysis for China open pits, Beijing. Science and Technology Press

Zhang, C., 2006. Using multivariate analysis and GIS to identify pollutants and their spatial patterns in urban soils in Galway, Ireland. Environmental Pollution, vol. 142, no. 3, pp. 501 – 511

Zhang, X., Krabbenhoft, K., Pedroso, D.M.., Lyamin, A.V., Sheng, D., Da Silva M.V., 2013. Particle finite element analysis of large deformation and granular flow problems. Computer Geotechnics, vol. 54, pp.133 – 142

Zhang, X., Sheng, D., Sloan, S.W., Bleyer, J., 2017. Lagrangian modelling of large deformation induced by progressive failure of sensitive clays with elastoviscoplasticity. International Journal for Numerical Methods in Engineering, vol. 112, pp. 963 – 989.

Zhang, X., Lin, H., Wang, Y., Yong, R., Zhao, R., Du, S., 2021. Damage evolution characteristics of saw-tooth joint under sheer creep condition. International Journal of Damage Mechanics, vol. 30, no. 3, pp. 453 – 480

Zhu, B., Pei, H., Yang, Q., 2018. Probability analysis of submarine landslides based on the Response Surface Method: A case study from the South China Sea. Applied Ocean Research, vol. 78, pp. 167 – 179

Zondo, S., 2023. Review of the waste slope stability design of a landfill site in Gauteng. 4th African Regional Conference on Geosynthetics (GeoAfrica 2023), vol. 368, # 02004